



Imaging of retinoblastoma patients: advanced MRI techniques and associated morbidity

Firazia Rodjan

**IMAGING OF RETINOBLASTOMA PATIENTS: ADVANCED
MRI TECHNIQUES AND ASSOCIATED MORBIDITY**

Firazia Rodjan
2014

The studies presented in this thesis were performed at the Department of Radiology in collaboration with the department of Ophthalmology and Pathology, VU University Medical Center, Amsterdam, The Netherlands, Department of Radiology, Institut Curie, Paris, France, Department of Diagnostic and Interventional Radiology and Neuroradiology, University Hospital, Essen, Germany, Department of Radiology, University Hospital, Lausanne, Switzerland, Department of Neuroimaging and Neurointerventional (NINT), Azienda Ospedaliera e Universitaria Santa Maria alle Scotte, Siena, Italy.

The research project was financially supported by the ODAS foundation (Delft, The Netherlands), ZonMw AGIKO-Stipendium (Den Haag, The Netherlands), the National Foundation for the Blind and Visually Impaired (Utrecht, The Netherlands), Blindenhulp Foundation (The Hague, The Netherlands) and the Dutch Eye Fund (Utrecht, The Netherlands), Department of Radiology VU University Medical Center (Amsterdam, The Netherlands).

Printing of this thesis was sponsored by:

Landelijke stichting voor blinden en slechtzienden, Toshiba medical systems Nederland, Angiocare BV, Sectra Benelux, Rockmed, Stichting Blindenhulp, Chipsoft BV and the Department of Radiology VU University Medical Center.

Cover design: Martijn Steenwijk

Layout and printed by: Gildeprint - Enschede

ISBN: 978-94-6108-804-8

Copyright © 2014 F. Rodjan, The Netherlands

All rights reserved. No part of this publication may be reproduced, stored in a retrieval system, or transmitted in any form or by any means, electronic, mechanical, photocopying, recording or otherwise, without the prior permission of the author.

VRIJE UNIVERSITEIT

IMAGING OF RETINOBLASTOMA PATIENTS: ADVANCED
MRI TECHNIQUES AND ASSOCIATED MORBIDITY

ACADEMISCH PROEFSCHRIFT

ter verkrijging van de graad Doctor aan
de Vrije Universiteit Amsterdam,
op gezag van de rector magnificus
prof.dr. F.A. van der Duyn Schouten,
in het openbaar te verdedigen
ten overstaan van de promotiecommissie
van de Faculteit der Geneeskunde
op maandag 1 december 2014 om 11.45 uur
in de aula van de universiteit,
De Boelelaan 1105

door

Firazia Rodjan

geboren te Zwolle

promotoren: prof. dr. J.A. Castelijns
prof. dr. A.C. Moll

copromotoren: dr. P. de Graaf

Voor mama

CONTENTS

List of Abbreviations

<i>Chapter 1</i>	General introduction	11
<i>Chapter 2</i>	Guidelines for imaging retinoblastoma: imaging principles and MRI standardization (<i>Ped Radiol 2011</i>)	27
<i>Chapter 3</i>	Retinoblastoma: Value of dynamic contrast-enhanced MR imaging and correlation with tumor angiogenesis (<i>Am J Neuroradiol 2012</i>)	49
<i>Chapter 4</i>	Detection of calcifications in retinoblastoma using gradient-echo MR imaging sequences: comparative study between in-vivo MR imaging and ex-vivo high resolution CT (<i>accepted for Am J Neuroradiol 2014</i>)	65
<i>Chapter 5</i>	Brain abnormalities on MR imaging in retinoblastoma patients (<i>Am J Neuroradiol 2010</i>)	79
<i>Chapter 6</i>	Trilateral retinoblastoma: neuroimaging characteristics and value of routine brain screening on admission (<i>J Neuro-oncology 2012</i>)	91
<i>Chapter 7</i>	Second cranio-facial malignancies in hereditary retinoblastoma survivors previously treated with radiation therapy: clinic and radiologic characteristics and survival outcomes (<i>Eur J Cancer. 2013</i>)	107
<i>Chapter 8</i>	General discussion and future perspectives	123
<i>Chapter 9</i>	Summary in Dutch/ Nederlandse samenvatting	135
<i>Chapter 10</i>	Dankwoord	147
	List of publications	151
	Curriculum Vitae	153

LIST OF ABBREVIATIONS

3D	3-dimensional
$\kappa_5\text{min}$	curve pattern analysis first DCE time series
$\kappa_{17}\text{min}$	curve pattern analysis for the full dataset
AES	anterior eye segment
CSF	cerebrospinal fluid
CT	computed tomography
DCE MRI	dynamic contrast enhanced magnetic resonance imaging
FLASH	fast low-angle shot
FLT-1	vascular endothelial growth factor receptor 1
GRE	gradient-echo
HE	hematoxylin-eosin
ICC	intraclass correlation coefficient
k_{ep}	rate constant k_{ep}
K^{trans}	transfer constant
MR	magnetic resonance
MRI	magnetic resonance imaging
MVD	microvessel density
PFV	persistent fetal vasculature
PHPV	persistent hyperplastic primary vitreous
PNET	primitive neuroectodermal tumor
ROI	region of interest
SE	spin-echo
SI	signal intensity
T1W	T1-weighted
T2W	T2-weighted
T2*WI	T2*-weighted imaging
TE	echo-time
TR	repetition-time
v_e	extravascular extracellular space per unit volume of tissue
VEGF	vascular endothelial growth factor
US	ultrasound

Chapter 1

General introduction

INTRODUCTION

Retinoblastoma is rare but also the most common malignant intra-ocular tumor in young children. The incidence is one in 17,000 births in the Netherlands, comparable to incidences in other countries such as the United States, United Kingdom, Northern Europe and Singapore^{1,2}. In 90%-95% of patients with retinoblastoma, the tumor is diagnosed before the age of 5 years, and rarely in utero³ as the immature retina is still developing in these young patients. Retinoblastoma has very rarely been reported in older children or young adults^{4,5}. The disease could involve one eye (unilateral retinoblastoma) or both eyes (bilateral retinoblastoma). The age at diagnosis is younger for patients with bilateral retinoblastoma as explained below. The mean age at presentation for bilateral tumors is 12 months, while that for unilateral tumors is 24 months⁶.

Genetics

Retinoblastoma shows a hereditary and non-hereditary form. In 1971, Knudson proposed the two-hit hypothesis that retinoblastoma is a neoplasm caused by loss or mutation of both alleles of the Rb1-gene, localized on chromosome 13q14⁷. In the heritable form, the first hit is a germ cell mutation. Every cell in the body already has the first hit. The second hit occurs in a particular retinal cell. When only one more hit is necessary to cause neoplastic transformation, it is likely that more than one cell, out of millions of cells in the developing retina, will become capable of neoplastic growth. In these hereditary patients indeed, more often multiple tumors are seen. In contrast, no germline mutation is present in non-hereditary retinoblastoma (60% of all retinoblastoma cases) and two independent mutations or hits must occur in the same retinal cell to develop a neoplasm. Because it is less likely that two hits in the same cell occur, non-hereditary retinoblastoma more often presents at a later age and as a solitary tumor and always unilateral. Approximately 40% of patients with retinoblastoma have the hereditary form, which can be divided into a familial and sporadic hereditary form. The familial hereditary form involves a parent or family member with retinoblastoma, proving that one of the parents was the carrier of the Rb1 gene. In the sporadic form of hereditary retinoblastoma, the patient is the first person in the first generation in the family with retinoblastoma. All bilateral cases of retinoblastoma and 15% of the unilateral cases are related to a constitutional (hereditary or de novo) mutation of the Rb-1 gene⁸. In hereditary retinoblastoma, the germline mutation is highly penetrant (90%) and shows an autosomal dominant transmission with a 45% risk of retinoblastoma in the offspring. In patients with 13q deletion syndrome with loss of parts of chromosome 13q14 carrying Rb1 genetic material, retinoblastoma could also develop. Recently, a new form of non-hereditary retinoblastoma was discovered. These patients present with unilateral retinoblastoma at a very young age. This particular form of retinoblastoma develops by amplifications in the MYCN-oncogene in the presence of non-mutated RB1-genes⁹.

Clinical features and diagnosis

Clinical symptoms of retinoblastoma depend on tumor size, the site of origin and on its growth pattern. The most frequent presenting sign of retinoblastoma is a white pupil reflex (leukocoria). Strabismus could be a very early sign when a small tumor arises in the macula. Red eye, orbital cellulitis, hazy cornea, hyphema (blood in the anterior chamber), discolorization of the iris and glaucoma are less common symptoms¹⁰ and are associated with a poor prognosis for globe salvage and vision¹¹. In some cases however, other conditions could cause confusion in retinoblastoma diagnosis, like Coats' disease, congenital cataract, persistent hyperplastic primary vitreous, retinal detachment, retinopathy or prematurity, toxocariosis, and other¹². In most cases, careful clinical examination can differentiate these conditions from retinoblastoma. The diagnosis of retinoblastoma is made on clinical grounds with fundoscopy and ultrasound examination, which detect the majority of the cases. On fundoscopy, retinoblastoma appears as a white mass. Ocular ultrasound demonstrates a echogenic mass in contrast to vitreous, with fine calcifications¹². In addition, detailed history, physical examination, imaging, DNA analyses and sometimes fluorescein angiography are obtained to complete the diagnosis.

Biopsy should be avoided in retinoblastoma because of the risk for extraocular disease dissemination¹³.

Staging

Two classifications are used to stage retinoblastoma; 1) The Reese-Ellsworth classification (REC) and 2) the International Classification of Retinoblastoma (ICRB). The REC (table 1) was designed to predict outcome from treatment with external beam radiation therapy (EBRT), used internationally as the primary eye salvage treatment in the 1980s until introduction of chemotherapy¹⁴. The ICRB system (table 2) was developed to predict outcome from combination chemotherapy and focal therapy. This system is more relevant to modern therapies than the REC and became the standard staging system globally in the early 2000 for tumors contained in the eye(s)¹⁵.

Table 1: Reese-Ellsworth Classification for Retinoblastoma

Group 1: Very favourable for maintenance of sight:
a Solitary tumour, smaller than 4 disc diameters (DD), at or behind the equator
b Multiple tumours, none larger than 4 DD, all at or behind the equator
Group 2: Favourable for maintenance of sight:
a Solitary tumour, 4 to 10 DD at or behind the equator
b Multiple tumours, 4 to 10 DD behind the equator
Group 3: Possible for maintenance of sight:
a Any lesion anterior to the equator
b Solitary tumour, larger than 10 DD behind the equator
Group 4: Unfavourable for maintenance of sight:
a Multiple tumours, some larger than 10 DD
b Any lesion extending anteriorly to the ora serrata
Group 5: Very unfavourable for maintenance of sight:
a Massive tumours involving more than one half the retina
b Vitreous seeding

DD = disc diameter

Table 2: International Classification of Intraocular Retinoblastoma

Group	Characteristics
A	Very low risk Small tumors away from macula and optic disc Tumors < 3 mm in greatest dimension confined to the retina and Located at least 3 mm from macula and 1.5 mm from the optic disc
B	Low risk All remaining tumors confined to the retina All other tumors confined to retina not in group A Subretinal fluid (without seeding) < 3 mm from the base of tumor
C	Moderate risk Local subretinal fluid or vitreous seeding Local subretinal fluid alone > 3 to < 6 mm from tumor Vitreous seeding or subretinal seeding < 3 mm from the tumor
D	High risk Diffuse subretinal fluid or seeding Subretinal fluid alone > 6 mm from tumor Vitreous seeding or subretinal seeding > 3 mm from the tumor
E	Very high risk Presence of any one or more of poor prognostic features More than two thirds of globe filled with tumor Tumor in anterior segment or ciliary body Iris neovascularization, neovascular glaucoma Tumor necrosis, phthisis bulbi

Histopathology

Retinoblastoma appears macroscopically as single or multiple white nodules within the retina. The tumor may grow endophytically from the inner retinal surface, through the internal limiting membrane of the retina towards the center of the globe and spread into the vitreous. Retinoblastoma can shed vitreous seedings, which are characterized by clumps of tumor cells

floating within the vitreous cavity. Alternatively, the tumor may grow exophytically behind the retina and in some cases even results in retinal detachment or subretinal hemorrhage. In advanced stages, the tumor may breach the Bruch membrane to invade the choroid. In rare cases, retinoblastoma can present as diffuse infiltration of the retina without a specific tumor mass¹⁶. This form of retinoblastoma, which is more common in older patients can pretend to be an intraocular infection of inflammation because of the absence of a mass and the low incidence of characteristic calcifications¹⁷.

Microscopically, retinoblastoma shows a monomorphous mass of small tumor cells with a high nuclear-to-cytoplasmic ratio imparting a blue color quality on histologic sections stained with hematoxylin and eosin. This sea of small blue cells is sometimes interrupted by strands of fibrous ensheathed blood vessels and doughnutlike structures formed by the tumor cells with a central lumen, the so-called Flexner-Wintersteiner rosettes (or retinoblastomatous rosettes). Although characteristic for retinoblastoma, this cell is also seen in pineoblastomas and medulloepitheliomas¹⁸. A second specialized structure found within retinoblastoma is the fleurette in few retinoblastoma tumors¹⁷. A minority of retinoblastoma may also contain Homer-Wright rosettes, similar to the Flexner-Wintersteiner rosettes but without a central lumen. The frequent presence of Flexner-Wintersteiner rosettes characterizes well-differentiated tumors, whereas Homer-Wright rosettes may occur in both well- and poor-differentiated retinoblastoma.

Prognostic risk factors and local recurrences

Retinoblastoma spreads either by haematogenous metastases or by direct extension through the optic nerve and in its meningeal sheath to cerebrospinal fluid¹⁹. Pathology is the golden standard to evaluate metastatic risk factors in retinoblastoma. Current pathological risk factors include invasion of the anterior eye segment, choroid, sclera and optic nerve behind the lamina cribrosa (post-laminar optic nerve invasion, furthermore tumor angiogenesis, extensive tumor necrosis and massive choroidal invasion^{9,19-23}. Children with postlaminar optic nerve invasion and massive choroidal invasion require adjuvant chemotherapy to reduce the risk of metastatic spread⁸. Because currently possibilities in non-operative management of retinoblastoma are increasing, non-invasive evaluation of these risk factors by imaging is becoming more and more important.

Diagnostic imaging

Fundoscopy under general anesthesia in combination with ultrasound examinations, enables detection of more than 91%-95% of the retinoblastomas and are the most important sources for diagnosis²⁴. Only in cases with unclear ocular medium, such as corneal haze, anterior chamber hemorrhage or vitreous hemorrhage, the ability of ultrasound to detect small calcifications is limited. CT used to be the standard imaging technique to detect calcifications in retinoblastoma in about 81%-96% of the tumors²⁴⁻²⁶. Owing to the suspected raised radiosensitivity of patients with the hereditary form of the disease, CT has been progressively replaced by MRI in

detection of tumor extent and tumor staging and is not recommended anymore ²⁷. In suspected retinoblastomas, MRI however could be a technique to confirm the diagnosis by detection of calcification with T2*-WI. Although this technique seems promising, its diagnostic accuracy must be determined ²⁸.

For evaluation of tumor risk factors, in particular invasion in ocular coats and optic nerve and extraocular extension, MRI with its superior contrast resolution is generally recommended as diagnostic method in retinoblastoma ^{24;26}.

Imaging of risk factors

Pre-treatment staging is important to guide conservative treatment options and determine the surgical approach for enucleation in order to prevent postoperative residual intraorbital tumor tissue. Children with histopathological risk factors need adjuvant chemotherapy to reduce the risk for metastatic spread ^{13;19;29;30}. Despite the fact that pathology is the golden standard for evaluation of metastatic risk factors, MRI showed its potential in detecting these tumor parameters in vivo ^{8;31-35}. The use of orbital surface coils during imaging instead of head coils is generally recommended on 1.5T MR machines, since it increases both the signal-to-noise ratio and the spatial resolution ^{19;22;24;26;36}.

Evaluation of post-laminar optic nerve invasion, massive choroidal invasion, tumor angiogenesis and extensive tumor necrosis on MRI, has shown promising results ^{19;25;31;32;37}. Interruption of the normal linear enhancement at the optic nerve disc on MRI is suggestive for optic onerve invasion ³². Histopathological proven optic nerve invasion is associated with a significant increase of metastatic disease and mortality rate ^{19;22;38}. In retinoblastoma with post-laminar optic nerve invasion, leptomeningeal metastases should be suspected ⁸. Focal choroidal thickening on MRI is a sign of massive choroidal invasion which in itself is a significant predictor of metastases ³⁸.

Tumor angiogenesis is a histopathological risk factor that helps to identify retinoblastoma patients at high risk for disease dissemination after enucleation ²¹. Currently, the degree of angiogenesis can only be assessed in vitro on histopathological angiogenic markers, such as microvessel density or VEGF expression and its receptors ^{21;39}. Angiogenesis-related risk for tumor progression on MRI in retinoblastoma is only described as anterior eye segment enhancement, which reflects angiogenesis in the iris and correlates with tumor volume and optic nerve invasion ³³. So far, no evidence for in-vivo evaluation on MRI of angiogenesis in the tumor itself is available. A potential MRI application to evaluate tumor angiogenesis non-invasively is dynamic contrast enhanced MR imaging (DCE-MRI). The change of signal intensity (SI) over time reflects the delivery of the contrast into the tumor interstitial space. The rates of contrast washin and subsequent washout from the tumor are related to tissue vascularization and perfusion, capillary permeability and composition of the interstitial space and could be a potential non-invasive method to evaluate angiogenesis in retinoblastoma ⁴⁰.

Extensive tumor necrosis in vitro is significantly associated with high risk prognostic factors post-laminar optic nerve invasion and choroidal invasion ²⁰. Although recently, the diffusion weighted MRI technique showed adequate differentiation between viable and necrotic tissue ³⁴, no imaging method has been described to evaluate the degree of tumor necrosis.

Depiction of these histopathological risk factors with MRI is not optimal yet. Despite relatively high values of specificity for optic nerve and choroidal invasion, variable values for sensitivity were assessed due to differences in MRI protocols and rather small patient populations with secondarily low incidences of risk factors^{8;13;23;25;31;33;41}.

Retinoblastoma associated intracranial abnormalities

Trilateral retinoblastoma is a primary intra-cranial primitive neuro-ectodermal tumor in a patient with intra-ocular retinoblastoma occurring in the pineal gland or suprasellar region. Pineal tissue has the same origin as the retina, resulting in histological similar tumors ⁴². The risk of trilateral retinoblastoma depends on the hereditary aspect of the disease and varies from 0,5% - 15% ⁴³. Trilateral retinoblastoma usually presents with symptoms of intracranial hypertension and prognosis is very poor ⁴⁴⁻⁴⁶. Therefore, in every new retinoblastoma patient the brain is imaged for analysis of the midline structures to depict trilateral retinoblastoma. The incidence of trilateral retinoblastoma at diagnosis of retinoblastoma is unknown, because in the majority of cases described in literature no imaging of the brain was performed.

Besides malignant tumors, benign intracranial abnormalities are also reported in retinoblastoma patients. Benign pineal cysts are possibly associated with retinoblastoma although the presence of these cysts is quite common in the general population ⁴⁷⁻⁵⁰.

Treatment

The aims of the treatment of retinoblastoma are curing the disease and preservation of life, vision and eye. The most radical approach is surgical treatment and is preferred in unilateral retinoblastoma diagnosed in an advanced stage with an eye full of tumor and without functional vision.

For a long time radiotherapy (external beam radiation therapy (EBRT) and radioactive plaque therapy) was the main conservative treatment as the tumor was rarely reachable for laser ablation therapy ⁵¹. The late complications of EBRT however were a major concern in the treatment of especially hereditary retinoblastoma patients because of its long-term risks ⁵²⁻⁵⁴. The increased use of focal treatment and chemotherapy was mainly developed to avoid the use of EBRT. Numerous conservative treatment options are now available for intraocular retinoblastoma: laser ablation, systemic chemotherapy with or without a combination with laser photocoagulation or radioactive plaque therapy and in lesser extent EBRT for advanced forms or after failure of other treatments ⁵⁵⁻⁶³. Recently the use of intra-arterial and intra-vitreous chemotherapy, a technique with infusion of small doses (but locally very high concentrations) of chemotherapy via the ophthalmic artery,

seems promising in retinoblastoma treatment with minimal systemic effect^{64;65}. In most cases, the current treatment strategy need a combination of several of the therapeutic modalities indicated above.

Whereas small tumors without extensive vitreous seedings are generally effectively treated with focal treatment strategies such as laser ablation, large advanced tumors require tumor reduction with intravenous chemotherapy and to a lesser extent radiation or both, to avoid enucleation⁶⁶. Intra-arterial chemotherapy can be performed repeatedly in young children without significant systemic or local side effects and is effective in preventing progression to clinical metastases in >95% of the cases⁶⁷⁻⁶⁹. Intravitreal chemotherapy is a recent upcoming treatment strategy for retinoblastoma with extensive vitreous seedings⁷⁰. Preliminary studies show that intravitreal melphalan injection for persistent or recurrent vitreous seedings can provide tumor control with minimal toxicity and complications⁷¹. Therefore, non-invasive tumor characterization and monitoring of treatment response must be evaluated.

Follow-up of retinoblastoma survivors

Hereditary retinoblastoma survivors have an increased risk for developing second primary tumors (SPT)⁷². Radiation therapy increases this risk with a cumulative incidence of 28% to 36% in irradiated patients at 30 to 40 years after diagnosis of retinoblastoma^{73;74}. In non-hereditary retinoblastoma, no increased risk for SPT was found. Chemotherapy containing alkylating agents, alone or in combination with radiotherapy, also seems to be involved in the development of SPT⁷⁵. Osteosarcomas and soft tissue sarcomas are the most well-known SPTs in retinoblastoma survivors, particularly in younger individuals^{76;77}. Radical resection remains the main primary therapeutic method for optimal tumor control and cure, but despite aggressive treatment, mortality is still very high.

Other complications from radiation include damage to the optic nerve, cataract (radiation damage to the lens of the eye causes a cataract), chronic keratitis and photophobia because of dryness due to irradiation of the lacrimal gland, abnormal orbital bone development (midfacial hypoplasia) and vitreous hemorrhage, due to radiation retinopathy^{52;53;63;78}.

European Retinoblastoma Imaging Collaboration (ERIC)

Retinoblastoma is a very rare disease. All retinoblastoma patients in the Netherlands are referred to the VU University Medical Center with an incidence of 12 – 15 new patients a year. Because of the infrequency of retinoblastoma, we started a European retinoblastoma imaging collaboration in 2008 with 4 other participating retinoblastoma reference centers from Paris, Essen, Siena and Lausanne. In this collaboration experienced radiologists come to an agreement regarding research questions, imaging protocols, and data management for a larger retinoblastoma population to stimulate retinoblastoma research. Part of the studies in this thesis were initiated from this collaboration.

PURPOSE AND OUTLINE OF THE THESIS

The aim of this thesis is firstly to evaluate the potential of different advanced MRI techniques to evaluate imaging features involving prognostic factors and treatment response such as angiogenesis and tumor necrosis. Secondly, this thesis focused on broader aspects related to imaging of retinoblastoma patients. Imaging of potentially related structural brain abnormalities, trilateral retinoblastoma and radiation induced second cancers in retinoblastoma survivors.

Imaging is becoming more and more important in the diagnosis of retinoblastoma and is a significant factor in the choice of treatment nowadays. Because of the lack of standardization it is important to formulate minimal required sequences in retinoblastoma imaging. Due to the low incidence of the disease, uniformity of retinoblastoma imaging protocols is also necessary in order to stimulate research by multi-institutional international imaging collaboration. In chapter 2 the minimal protocol requirements formulated by the European Retinoblastoma Imaging Collaboration (ERIC) are discussed for retinoblastoma diagnosis, tumor extent and the detection of associated neoplasms.

Advanced MRI techniques

In chapter 3 and 4 the role of advanced imaging techniques for lesion characterization with T2*WI and noninvasive evaluation of treatment response and prognostic factors by dynamic contrast enhanced imaging are discussed. Calcifications are characteristic for retinoblastoma. Chapter 3 describes the ability of T2*WI in visualization of retinoblastoma calcifications. This advanced technique is compared with ex-vivo CT scans of enucleated eyes. Although imaging with CT is the golden standard in detecting calcifications, avoiding radiation risk by replacing CT with MRI is preferable in hereditary retinoblastoma.

Upcoming conservative treatment options require additional non-invasive imaging parameters for assessment of treatment response and prognosis. Histopathological parameters as tumor angiogenesis and necrosis are well known parameters in ex-vivo eyes. Chapter 4 describes the necessity of noninvasive evaluation of these parameters. The role of dynamic contrast enhanced imaging is discussed.

Retinoblastoma associated abnormalities and neoplasms

Chapter 5 describes structural brain abnormalities and pineal gland lesions associated with retinoblastoma in a large group of patients. The results of this study led to the question whether specific morphologic characteristics in the brain could be indicative for the development of trilateral retinoblastoma. Because trilateral retinoblastoma is very rare, this research question could only be answered within the multicenter ERIC collaboration. Chapter 6 discusses the clinical findings and MRI characteristics of associated intracranial tumors in retinoblastoma patients.

Second primary tumors are the leading cause of death in hereditary retinoblastoma survivors in the western world. External beam radiation therapy increases this risk. To obtain more insight in the presentation and outcomes, imaging characteristics of cranio-facial second primary tumors in irradiated hereditary retinoblastoma survivors will be discussed in chapter 7.

GENERAL DISCUSSION AND CONCLUSION

Chapter 8 summarizes the results of the studies presented in this thesis and discusses the clinical implications and suggestions for future research.

REFERENCES

1. Moll AC, Kuik DJ, Bouter LM, et al. Incidence and survival of retinoblastoma in The Netherlands: a register based study 1862-1995. *Br J Ophthalmol* 1997;81:559-62
2. Broaddus E, Topham A, Singh AD. Survival with retinoblastoma in the USA: 1975-2004. *Br J Ophthalmol* 2009;93:24-27
3. Singh AD, Black SH, Shields CL, et al. Prenatal diagnosis of retinoblastoma. *J Pediatr Ophthalmol Strabismus* 2003;40:222-24
4. MacCarthy A, Draper GJ, Steliarova-Foucher E, et al. Retinoblastoma incidence and survival in European children (1978-1997). Report from the Automated Childhood Cancer Information System project. *Eur J Cancer* 2006;42:2092-102
5. Mietz H, Hutton WL, Font RL. Unilateral retinoblastoma in an adult: report of a case and review of the literature. *Ophthalmology* 1997;104:43-47
6. Chung EM, Specht CS, Schroeder JW. From the archives of the AFIP: Pediatric orbit tumors and tumorlike lesions: neuroepithelial lesions of the ocular globe and optic nerve. *Radiographics* 2007;27:1159-86
7. Knudson AG, Jr. Mutation and cancer: statistical study of retinoblastoma. *Proc Natl Acad Sci U S A* 1971;68:820-23
8. de Graaf P, Goricke S, Rodjan F, et al. Guidelines for imaging retinoblastoma: imaging principles and MRI standardization. *Pediatr Radiol* 2011;
9. Rushlow DE, Mol BM, Kennett JY, et al. Characterisation of retinoblastomas without RB1 mutations: genomic, gene expression, and clinical studies. *Lancet Oncol* 2013;14:327-34
10. Abramson DH, Frank CM, Susman M, et al. Presenting signs of retinoblastoma. *J Pediatr* 1998;132:505-08
11. Abramson DH, Beaverson K, Sangani P, et al. Screening for retinoblastoma: presenting signs as prognosticators of patient and ocular survival. *Pediatrics* 2003;112:1248-55
12. Shields JA, Shields CL, Parsons HM. Differential diagnosis of retinoblastoma. *Retina* 1991;11:232-43
13. Uusitalo MS, Van Quill KR, Scott IU, et al. Evaluation of chemoprophylaxis in patients with unilateral retinoblastoma with high-risk features on histopathologic examination. *Arch Ophthalmol* 2001;119:41-48
14. Reese AB, Ellsworth RM. The evaluation and current concept of retinoblastoma therapy. *Trans Am Acad Ophthalmol Otolaryngol* 1963;67:164-72
15. Linn MA. Intraocular retinoblastoma: the case for a new group classification. *Ophthalmol Clin North Am* 2005;18:41-53, viii
16. Brisse HJ, Lumbroso L, Freneaux PC, et al. Sonographic, CT, and MR imaging findings in diffuse infiltrative retinoblastoma: report of two cases with histologic comparison. *AJNR Am J Neuroradiol* 2001;22:499-504
17. Materin MA, Shields CL, Shields JA, et al. Diffuse infiltrating retinoblastoma simulating uveitis in a 7-year-old boy. *Arch Ophthalmol* 2000;118:442-43
18. Hirato J, Nakazato Y. Pathology of pineal region tumors. *J Neurooncol* 2001;54:239-49
19. Khelifaoui F, Validire P, Auperin A, et al. Histopathologic risk factors in retinoblastoma: a retrospective study of 172 patients treated in a single institution. *Cancer* 1996;77:1206-13
20. Chong EM, Coffee RE, Chintagumpala M, et al. Extensively necrotic retinoblastoma is associated with high-risk prognostic factors. *Arch Pathol Lab Med* 2006;130:1669-72
21. Marback EF, Arias VE, Paranhos A, Jr., et al. Tumour angiogenesis as a prognostic factor for disease dissemination in retinoblastoma. *Br J Ophthalmol* 2003;87:1224-28
22. Shields CL, Shields JA, Baez K, et al. Optic nerve invasion of retinoblastoma. Metastatic potential and clinical risk factors. *Cancer* 1994;73:692-98
23. Chantada GL, Dunkel IJ, Antoneli CB, et al. Risk factors for extraocular relapse following enucleation after failure of chemoreduction in retinoblastoma. *Pediatr Blood Cancer* 2007;49:256-60
24. Beets-Tan RG, Hendriks MJ, Ramos LM, et al. Retinoblastoma: CT and MRI. *Neuroradiology* 1994;36:59-62

25. Lemke AJ, Kazi I, Mergner U, et al. Retinoblastoma - MR appearance using a surface coil in comparison with histopathological results. *Eur Radiol* 2007;17:49-60
26. Weber AL, Mafee MF. Evaluation of the globe using computed tomography and magnetic resonance imaging. *Isr J Med Sci* 1992;28:145-52
27. de Jong MC, de Graaf P, Noij DP, et al. Diagnostic Performance of Magnetic Resonance Imaging and Computed Tomography for Advanced Retinoblastoma: A Systematic Review and Meta-analysis. *Ophthalmology* 2014;
28. Galluzzi P, Hadjistilianou T, Cerase A, et al. Is CT still useful in the study protocol of retinoblastoma? *AJNR Am J Neuroradiol* 2009;30:1760-65
29. Honavar SG, Singh AD, Shields CL, et al. Postenucleation adjuvant therapy in high-risk retinoblastoma. *Arch Ophthalmol* 2002;120:923-31
30. Chantada GL, Dunkel IJ, de Davila MT, et al. Retinoblastoma patients with high risk ocular pathological features: who needs adjuvant therapy? *Br J Ophthalmol* 2004;88:1069-73
31. Brisse HJ, Guesmi M, Aerts I, et al. Relevance of CT and MRI in retinoblastoma for the diagnosis of postlaminar invasion with normal-size optic nerve: a retrospective study of 150 patients with histological comparison. *Pediatr Radiol* 2007;37:649-56
32. de Graaf P, Barkhof F, Moll AC, et al. Retinoblastoma: MR imaging parameters in detection of tumor extent. *Radiology* 2005;235:197-207
33. de Graaf P, van der Valk P, Moll AC, et al. Contrast-enhancement of the anterior eye segment in patients with retinoblastoma: correlation between clinical, MR imaging, and histopathologic findings. *AJNR Am J Neuroradiol* 2010;31:237-45
34. de Graaf P, Pouwels PJ, Rodjan F, et al. Single-shot turbo spin-echo diffusion-weighted imaging for retinoblastoma: initial experience. *AJNR Am J Neuroradiol* 2012;33:110-18
35. Gizewski ER, Wanke I, Jurklics C, et al. T1 Gd-enhanced compared with CISS sequences in retinoblastoma: superiority of T1 sequences in evaluation of tumour extension. *Neuroradiology* 2005;47:56-61
36. Messmer EP, Heinrich T, Hopping W, et al. Risk factors for metastases in patients with retinoblastoma. *Ophthalmology* 1991;98:136-41
37. Schueler AO, Hosten N, Bechrakis NE, et al. High resolution magnetic resonance imaging of retinoblastoma. *Br J Ophthalmol* 2003;87:330-35
38. Shields CL, Shields JA, Baez KA, et al. Choroidal invasion of retinoblastoma: metastatic potential and clinical risk factors. *Br J Ophthalmol* 1993;77:544-48
39. Rossler J, Dietrich T, Pavlakovic H, et al. Higher vessel densities in retinoblastoma with local invasive growth and metastasis. *Am J Pathol* 2004;164:391-94
40. Guo JY, Reddick WE. DCE-MRI pixel-by-pixel quantitative curve pattern analysis and its application to osteosarcoma. *J Magn Reson Imaging* 2009;30:177-84
41. Chantada GL, Casco F, Fandino AC, et al. Outcome of patients with retinoblastoma and postlaminar optic nerve invasion. *Ophthalmology* 2007;114:2083-89
42. Bader JL, Miller RW, Meadows AT, et al. Trilateral retinoblastoma. *Lancet* 1980;2:582-83
43. Kivela T. Trilateral retinoblastoma: a meta-analysis of hereditary retinoblastoma associated with primary ectopic intracranial retinoblastoma. *J Clin Oncol* 1999;17:1829-37
44. Michaud J, Jacob JL, Demers J, et al. Trilateral retinoblastoma: bilateral retinoblastoma with pinealoblastoma. *Can J Ophthalmol* 1984;19:36-39
45. Whittle IR, McClellan K, Martin FJ, et al. Concurrent pineoblastoma and unilateral retinoblastoma: a forme fruste of trilateral retinoblastoma? *Neurosurgery* 1985;17:500-05
46. de Potter P, Shields CL, Shields JA. Clinical variations of trilateral retinoblastoma: a report of 13 cases. *J Pediatr Ophthalmol Strabismus* 1994;31:26-31
47. Fleege MA, Miller GM, Fletcher GP, et al. Benign glial cysts of the pineal gland: unusual imaging characteristics with histologic correlation. *AJNR Am J Neuroradiol* 1994;15:161-66
48. Sener RN. The pineal gland: a comparative MR imaging study in children and adults with respect to normal anatomical variations and pineal cysts. *Pediatr Radiol* 1995;25:245-48
49. Karatza EC, Shields CL, Flanders AE, et al. Pineal cyst simulating pinealoblastoma in 11 children with retinoblastoma. *Arch Ophthalmol* 2006;124:595-97

50. Beck PM, Balmer A, Maeder P, et al. Benign pineal cysts in children with bilateral retinoblastoma: a new variant of trilateral retinoblastoma? *Pediatr Blood Cancer* 2006;46:755-61
51. Lumbroso-Le RL, Aerts I, Levy-Gabriel C, et al. Conservative treatments of intraocular retinoblastoma. *Ophthalmology* 2008;115:1405-10, 1410
52. Imhof SM, Mourits MP, Hofman P, et al. Quantification of orbital and mid-facial growth retardation after megavoltage external beam irradiation in children with retinoblastoma. *Ophthalmology* 1996;103:263-68
53. Imhof SM, Moll AC, Hofman P, et al. Second primary tumours in hereditary- and nonhereditary retinoblastoma patients treated with megavoltage external beam irradiation. *Doc Ophthalmol* 1997;93:337-44
54. Kleinerman RA, Tucker MA, Tarone RE, et al. Risk of new cancers after radiotherapy in long-term survivors of retinoblastoma: an extended follow-up. *J Clin Oncol* 2005;23:2272-79
55. Abramson DH, Scheffer AC. Transpupillary thermotherapy as initial treatment for small intraocular retinoblastoma: technique and predictors of success. *Ophthalmology* 2004;111:984-91
56. Murphree AL, Villablanca JG, Deegan WF, III, et al. Chemotherapy plus local treatment in the management of intraocular retinoblastoma. *Arch Ophthalmol* 1996;114:1348-56
57. Lumbroso L, Doz F, Urbietta M, et al. Chemothermotherapy in the management of retinoblastoma. *Ophthalmology* 2002;109:1130-36
58. Levy C, Doz F, Quintana E, et al. Role of chemotherapy alone or in combination with hyperthermia in the primary treatment of intraocular retinoblastoma: preliminary results. *Br J Ophthalmol* 1998;82:1154-58
59. Schueler AO, Jurklies C, Heimann H, et al. Thermochemotherapy in hereditary retinoblastoma. *Br J Ophthalmol* 2003;87:90-95
60. Shields CL, Mashayekhi A, Cater J, et al. Chemoreduction for retinoblastoma. Analysis of tumor control and risks for recurrence in 457 tumors. *Am J Ophthalmol* 2004;138:329-37
61. Beck MN, Balmer A, Dessing C, et al. First-line chemotherapy with local treatment can prevent external-beam irradiation and enucleation in low-stage intraocular retinoblastoma. *J Clin Oncol* 2000;18:2881-87
62. Brichard B, De Bruycker JJ, De PP, et al. Combined chemotherapy and local treatment in the management of intraocular retinoblastoma. *Med Pediatr Oncol* 2002;38:411-15
63. Abramson DH, Beaverson KL, Chang ST, et al. Outcome following initial external beam radiotherapy in patients with Reese-Ellsworth group Vb retinoblastoma. *Arch Ophthalmol* 2004;122:1316-23
64. Brodie SE, Munier FL, Francis JH, et al. Persistence of retinal function after intravitreal melphalan injection for retinoblastoma. *Doc Ophthalmol* 2013;126:79-84
65. Munier FL, Gaillard MC, Balmer A, et al. Intravitreal chemotherapy for vitreous seeding in retinoblastoma: Recent advances and perspectives. *Saudi J Ophthalmol* 2013;27:147-50
66. Gobin YP, Dunkel IJ, Marr BP, et al. Intra-arterial chemotherapy for the management of retinoblastoma: four-year experience. *Arch Ophthalmol* 2011;129:732-37
67. Abramson DH, Dunkel IJ, Brodie SE, et al. A phase I/II study of direct intraarterial (ophthalmic artery) chemotherapy with melphalan for intraocular retinoblastoma initial results. *Ophthalmology* 2008;115:1398-404, 1404
68. Abramson DH, Dunkel IJ, Brodie SE, et al. Superselective ophthalmic artery chemotherapy as primary treatment for retinoblastoma (chemosurgery). *Ophthalmology* 2010;117:1623-29
69. Shields CL, Kaliki S, Al Dahmash S, et al. Management of advanced retinoblastoma with intravenous chemotherapy then intra-arterial chemotherapy as alternative to enucleation. *Retina* 2013;33:2103-09
70. Munier FL, Soliman S, Moulin AP, et al. Profiling safety of intravitreal injections for retinoblastoma using an anti-reflux procedure and sterilisation of the needle track. *Br J Ophthalmol* 2012;96:1084-87
71. Shields CL, Manjandavida FP, Arepalli S, et al. Intravitreal melphalan for persistent or recurrent retinoblastoma vitreous seeds: preliminary results. *JAMA Ophthalmol* 2014;132:319-25
72. Marees T, Moll AC, Imhof SM, et al. Risk of second malignancies in survivors of retinoblastoma: more than 40 years of follow-up. *J Natl Cancer Inst* 2008;100:1771-79

73. Wong FL, Boice JD, Jr., Abramson DH, et al. Cancer incidence after retinoblastoma. Radiation dose and sarcoma risk. *JAMA* 1997;278:1262-67
74. Shinohara ET, DeWees T, Perkins SM. Subsequent malignancies and their effect on survival in patients with retinoblastoma. *Pediatr Blood Cancer* 2014;61:116-19
75. Aerts I, Pacquement H, Doz F, et al. Outcome of second malignancies after retinoblastoma: a retrospective analysis of 25 patients treated at the Institut Curie. *Eur J Cancer* 2004;40:1522-29
76. Woo KI, Harbour JW. Review of 676 second primary tumors in patients with retinoblastoma: association between age at onset and tumor type. *Arch Ophthalmol* 2010;128:865-70
77. Turaka K, Shields CL, Meadows AT, et al. Second malignant neoplasms following chemoreduction with carboplatin, etoposide, and vincristine in 245 patients with intraocular retinoblastoma. *Pediatr Blood Cancer* 2012;59:121-25
78. Tawansy KA, Samuel MA, Shammas M, et al. Vitreoretinal complications of retinoblastoma treatment. *Retina* 2006;26:S47-S52

Chapter 2

*Guidelines for imaging retinoblastoma: imaging
principles and MRI standardization*

Pim de Graaf
Sophia Göricke
Firazia Rodjan
Paolo Galluzzi
Philippe Maeder
Jonas A. Castelijns
Hervé J. Brisse

on behalf of the European Retinoblastoma Imaging Collaboration (ERIC)

ABSTRACT

Retinoblastoma is the most common intraocular tumor in children. The diagnosis is usually established by the ophthalmologist on the basis of fundoscopy and US. Together with US, high-resolution MRI has emerged as an important imaging modality for pretreatment assessment, i.e. for diagnostic confirmation, detection of local tumor extent, detection of associated developmental malformation of the brain and detection of associated intracranial primitive neuroectodermal tumor (trilateral retinoblastoma). Minimum requirements for pretreatment diagnostic evaluation of retinoblastoma or mimicking lesions are presented, based on consensus among members of the European Retinoblastoma Imaging Collaboration (ERIC). The most appropriate techniques for imaging in a child with leukocoria are reviewed. CT is no longer recommended. Implementation of a standardized MRI protocol for retinoblastoma in clinical practice may benefit children worldwide, especially those with hereditary retinoblastoma, since a decreased use of CT reduces the exposure to ionizing radiation.

INTRODUCTION

Retinoblastoma is the most common intraocular tumor in children. The incidence is one in 17,000 births. Mean age at clinical presentation is 2 years in unilateral forms (60% of cases) and 1 year in bilateral forms [1, 2]. All bilateral forms, as well as 15% of unilateral forms are related to a constitutional (hereditary or de novo) mutation of the RB-1 gene, localized on chromosome 13q14 [2]. Usually the patients present with leukocoria (white pupil reflection) or a squint.

Retinoblastoma is curable. If detected while still confined to the globe and if there are no metastatic risk factors, the child will nearly always survive following appropriate treatment [3,4]. The preservation of visual function depends on ocular preservation, initial tumor volume, the anatomical relationships of the tumors to the macula and optic disk and the adverse effects of the treatments (cataracts, vitreous hemorrhage) [5]. In the presence of metastatic risk factors, adjuvant treatment regimens are usually applied to prevent life-threatening relapse [6,7].

Diagnosis of retinoblastoma is usually made by fundoscopy (Fig. 1) (under general anesthesia) and US. The ophthalmologist usually performs both investigations. In almost all cases classic intratumoral calcifications can be detected by US providing high confidence rate regarding diagnosis. Various tumor parameters (laterality; number, location and size of tumors; tumor seeding to vitreous, subretinal space or anterior segment) can be evaluated with these techniques. These are important for grouping the retinoblastoma and to guide therapeutic decisions. Further diagnostic imaging plays a crucial role in determining the local extent and for detecting associated brain abnormalities, i.e. intracranial tumor extension, possible midline intracranial primitive neuroectodermal tumor (PNET) and brain malformations in patients with 13q deletion syndrome [8–10].

PNETs are associated with hereditary retinoblastoma, a combination known as trilateral retinoblastoma, which occurs in 5–15% of children in the hereditary subgroup [10,11]. Besides the pineal region (pineoblastoma), tumors may also occur in the suprasellar or parasellar regions. Trilateral retinoblastoma has been lethal in virtually all cases reported in literature; however, early detection and intensive (chemo-)therapy may be lifesaving for some patients [10,12,13].

Conservative treatment strategies (avoidance of enucleation and external beam radiation therapy) can be successful in the early stages of retinoblastoma and in some patients with advanced intraocular disease [14]. The options for eye-preserving therapy have significantly improved during recent years and are mainly based on tumor reduction with chemotherapy, and are usually combined with laser coagulation, cryotherapy or radioactive plaque. Recently, selective ophthalmic artery infusion of a chemotherapeutic agent became available as an additional treatment option for locally advanced disease [15]. As a consequence, more children are treated without histopathological confirmation and, what is more important, without assessment of risk factors for disease dissemination and prognosis. Therefore, imaging is very important in local staging.

Whereas imaging is increasingly used for diagnosis and as a basis for treatment decisions in retinoblastoma, there is a lack of standardization for choosing among modalities and for the minimum quality of MRI. The purpose of this report is to present a guideline for diagnostic imaging of retinoblastoma including a standardized MRI protocol using conventional pulse sequences. The potential role of advanced imaging techniques for lesion characterization and detection of tumor extent (such as 3D T1W sequences, diffusion-weighted imaging, diffusion tensor imaging and MR-spectroscopy) is beyond the scope of this guideline.

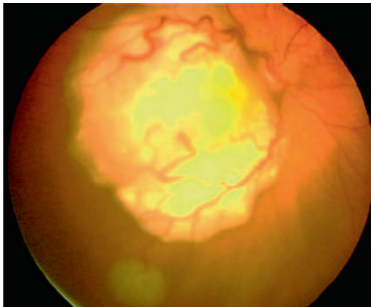


Fig. 1 Fundus photograph shows two tumors. The large white mass with prominent feeder vessels is located at the macula causing reduced visual acuity. A smaller tumor is located in the inferolateral part of the retina. Image courtesy Annette C. Moll, Amsterdam

Risk factors for metastasis and local recurrence

Retinoblastoma may spread either by hematogenous dissemination or by direct extension either through the bulbar wall into the orbit or via the optic nerve and its meningeal sheath [16]. Therefore, current risk factors for metastasis and local recurrence include invasion of the optic nerve posterior to the lamina cribrosa (in particular if there is tumor at the surgical resection margin), anterior eye segment (AES), or extensive invasion of the ocular coats (massive choroidal and scleral invasion) [17–20]. Pathology remains the gold standard to assess high-risk features of retinoblastoma. The rate of postlaminar optic nerve invasion in patients treated by primary enucleation has been estimated at 7–8% [21,22]. Choroidal invasion is present in 23–42% of enucleated eyes, out of which the invasion is massive in about 9–11% [19,23–25]. The exact incidence of massive choroidal invasion is unknown, especially since the definition of “massive” differs among pathologists. Recently, new consensus criteria were proposed by a worldwide collaboration of pathologists and pediatric oncologists [26]. Tumor invasion into the AES is very rare, being present in approximately 2% of primary enucleated eyes [24,27–30]. Children with histopathological risk factors for metastatic disease require adjuvant chemotherapy to reduce the risk of relapse [18–20,31].

Radiation exposure and second primary malignancies in hereditary retinoblastoma

Unlike survivors of non-hereditary retinoblastoma, survivors of hereditary retinoblastoma have an elevated risk of developing second (or even more) malignancies with a cumulative mortality rate of 17% [32–34]. In patients with hereditary retinoblastoma, the cumulative incidence of a second

primary malignancy within 40 years of the initial retinoblastoma is 28% [34]. Chemotherapy has been reported to increase the risk of leukemia in survivors of retinoblastoma [35]. Radiotherapy is associated with an increased risk of soft-tissue sarcomas in survivors of hereditary retinoblastoma, with a reported significant association of radiation dose with the risk of second primary (or more) cancers [34,36]. Assuming a linear relation between radiation dose and stochastic risk, several studies have demonstrated a theoretical increased risk of CT-associated radiation-induced fatal cancers in children [37]. Although low, this risk is likely to be further increased in patients with hereditary retinoblastoma, who are known to be genetically unstable, due to the inherited germ cell mutation in the RB-1 tumor-suppressor gene. To minimize the development of subsequent cancers, survivors of retinoblastoma are advised to avoid unnecessary radiation. Furthermore, children undergoing radiotherapy for retinoblastoma may experience abnormalities in the growth and maturation of their craniofacial skeleton, resulting in mid-face deformities [38]. For these reasons, external beam radiotherapy was dramatically reduced for the conservative treatment options, and the principle of minimizing the exposure to ionizing radiation should also be applied to imaging. US and MRI should be used instead of CT. The radiation from interventional procedures, e.g., selective ophthalmic artery chemotherapy infusion, is also important [39]. The radiation dose should be optimized, precisely measured and clearly reported in future publications to facilitate balancing risks and benefits both in imaging and therapy.

CHOICE OF IMAGING MODALITY

US, CT and MRI are the mainstay for imaging of head and neck tumors in children. US is particularly useful for examining superficial masses, such as retinoblastoma, whereas CT and MRI are used to delineate deeper lesions, particularly those involving the skull base and the central nervous system. Nowadays, diagnostic evaluation of retinoblastoma consists primarily of US and MRI. Positron emission tomography has become an important modality for cancer imaging in general; however, its value in retinoblastoma imaging is currently limited [40].

US

The human eye, with its superficial position and its fluid-filled structures, is ideally suited for US. Ocular US is usually performed by the ophthalmologist while the child is under general anesthesia, but can also quite easily be performed without sedation. In retinoblastoma, US demonstrates an irregular mass, more echogenic than the vitreous body, with fine calcifications (highly reflective foci mostly with characteristic acoustic shadowing) [41] (Fig. 2). Histologically, there is calcification present in approximately 95% of tumors [42]. Calcification is key to differentiating retinoblastoma from other mass lesions in a young child. US detects calcifications in 92–95% of cases where it is present histopathologically [42, 43]. Retinal detachment may also

be observed, which is an important feature to define tumor growth pattern, either endophytic or exophytic, or a combination of both. Endophytic tumors arise from the inner layers of the retina and grow into the vitreous body. Frequently, small clusters of tumor cells detach from an endophytic mass, producing multiple floating tumor islands; this process is known as vitreous seeding. Exophytic tumors originate in the outer layers and grow in the subretinal space, which causes retinal detachment with subretinal exudate and possible subretinal tumor seeding. Tumors with exophytic growth more frequently have choroidal infiltration compared to endophytic tumors [44]. Diffusely infiltrating retinoblastoma is a rare histological form characterized by diffuse infiltration of the retina without a tumor mass [45]. Tumor height and diameter are usually measured at US, as these measurements are used for choice of treatment. Color Doppler can be useful for differentiating a vascularized tumor mass from echogenic effusions and for differentiation against developmental abnormalities such as persistent hyperplastic primary vitreous (PHPV; also known as persistent fetal vasculature, PFV), with the characteristic persisting hyaloid artery.

US is not the imaging modality of choice for direct evaluation of metastatic risk factors. Tumoral calcifications commonly obscure visualization of the optic nerve [41]. Indirect detection of optic nerve invasion by measurement of optic nerve diameter with a 3D-US technique has been reported in a single case report [46], hence its value remains unknown.

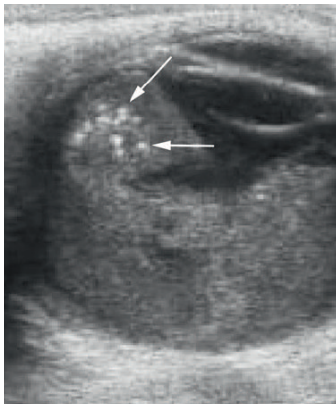


Fig. 2 US reveals a hyperechoic tumor occupying the posterior segment of the globe. Calcium deposits, seen as highly reflective foci (arrows), are pathognomonic for retinoblastoma in a young child

CT

On CT, retinoblastoma is typically a mass of high density compared with the vitreous body, usually calcified and moderately enhancing after iodinated contrast medium administration. CT detection of calcifications in retinoblastoma has a sensitivity of 81–96%, and an even higher specificity [47]. However, delineation of intraocular soft-tissue detail is limited. The evidence from surveys suggests that CT is still regarded an obligatory imaging tool for evaluation of

leukocoria, primarily because CT is supposed to be the best imaging modality for detection of intraocular calcifications [47–49]. However, justification of the irradiation of a large group of retinoblastoma patients requires a base of evidence of the procedure’s clinical effectiveness and possibly also radiation-effectiveness [50] for supplying (1) valuable additional information leading toward the diagnosis of retinoblastoma and (2) valuable additional information, compared to non-ionizing radiation modalities in detection of tumor extent.

CT was the first imaging modality used to detect optic nerve invasion [51–53] and is historically assumed to be precise in detection of tumor extent [54–56]. However, this assumption is based on conflicting outdated literature, without thorough evidence by radiologic-pathologic correlation studies. The sensitivity of CT in detection of optic nerve invasion is actually very low, even in patients with extensive optic nerve invasion (length of invaded nerve segment > 2 mm) [21, 51, 53]. The specificity, accuracy and negative predictive value of CT remain artificially high because of the relatively low incidence of optic nerve invasion in normal-size nerves. An enlarged nerve due to massive tumor infiltration is rare in developed countries. Assuming retinoblastoma invasion into the optic nerve produces distortion of the anastomotic vascular network in the anterior optic nerve region, Jacquemin and Karcioğlu [52] considered that non-visualization of the central retinal vessels is a reliable indicator of optic nerve invasion. However, these results were not confirmed by other studies [21].

MRI

Diagnostic MRI evaluation of a suspected retinoblastoma requires much more than performing a routine MR imaging examination of the orbit. High-resolution contrast-enhanced MRI is the technique of choice and should be used whenever possible to answer the key clinical questions (to evaluate an intraocular mass and to determine disease extent; Fig. 3). MRI has proved to be the most sensitive technique for evaluating retinoblastoma, especially regarding tumor infiltration of the optic nerve, extraocular extension and intracranial disease [21,22,44,57,58]. A major factor influencing the success of MRI is the use of appropriate hardware and optimized pulse sequences with appropriate spatial resolution for ocular MRI [21, 22, 44, 57–61].

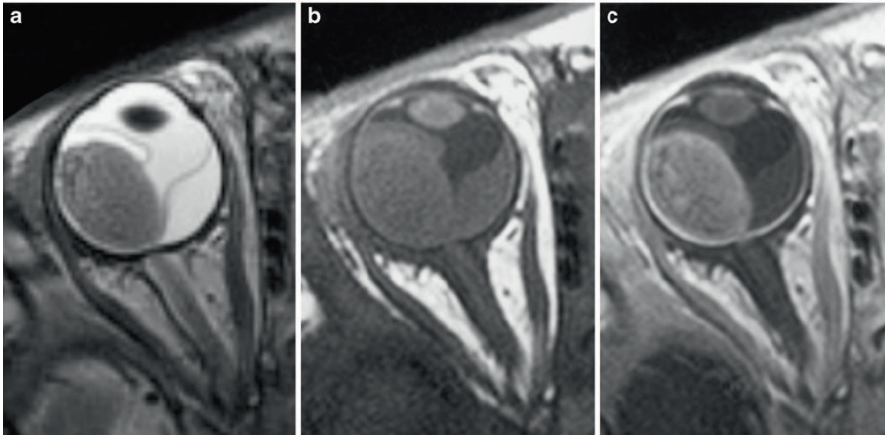


Fig. 3 Transaxial T2-weighted (TR/TE, 3,460/116 ms) (a) and T1-weighted (TR/TE, 374/14 ms) Precontrast (b) and postcontrast (c) MRI of exophytically growing retinoblastoma with secondary retinal detachment. Retinoblastoma typically has low signal intensity Fig. 3 Transaxial T2-weighted (TR/TE, 3,460/116 ms) (a) and T1-weighted (TR/TE, 374/14 ms) precontrast (b) and postcontrast (c) MRI of exophytically growing retinoblastoma with secondary retinal detachment. Retinoblastoma typically has low signal intensity

IMAGING STRATEGY

Diagnosis of retinoblastoma

Examination under general anesthesia with funduscopy and US almost inevitably leads to the diagnosis. As US detects foci of calcification in almost all retinoblastomas, there is now little benefit of routine CT for detection of calcifications in suspected retinoblastoma. Due to technical development, US and MRI are currently almost as accurate as CT for detection of calcifications. Recently, Galluzzi et al. [42] showed that when data from ophthalmoscopy, US and MRI are put together, no calcifications detected on CT were missed. A high-resolution gradient-echo T2W sequence showed promising results regarding detection of calcifications and has been shown to be more effective than spin-echo techniques [42, 44].

The differential diagnosis of retinoblastoma includes several non-neoplastic lesions that also cause leukocoria. After retinoblastoma, which accounts for 47–58% of cases of leukocoria in children, other causes in decreasing order of frequency include PHPV, Coats disease, larval granulomatosis (*Toxocara canis*), retinopathy of prematurity, and retinal astrocytic hamartoma [48]. Calcification is the most important differentiating feature of retinoblastoma. However, when clinical diagnosis remains uncertain, US and MRI help characterize and differentiate intraocular abnormalities, especially when ophthalmological evaluation is limited due to opaque ocular refractive media, as may occur in all of these conditions. The role of CT in the detection of (sometimes subtle) characteristic findings is limited due to its low soft-tissue contrast [48, 55].

Detection of tumor extent

In the past, CT was used to determine tumor size, retro-orbital spread and intracranial growth; however, spread within the optic nerve past the cribriform lamina, and infiltration of choroid and sclera, which are important prognostic factors, are not reliably assessed with CT [51, 53]. Because of its superior soft-tissue contrast, MRI is more sensitive and specific than CT in detection of tumor extent and metastatic risk factors. MR imaging using high-resolution protocols is currently considered to be the most accurate and valuable tool in pretreatment staging of retinoblastoma, without known biological side effects.

Standardized retinoblastoma MRI protocol

Although individual examinations should always be tailored to the specific queries in individual patients (laterality, disease extent, therapy options), there are general recommendations for MRI in retinoblastoma. In the following paragraphs we discuss the minimum requirements for diagnostic evaluation of retinoblastoma or mimicking lesions according to the consensus reached among members of the European Retinoblastoma Imaging Collaboration (ERIC). If these recommendations cannot be followed because of technical limitation, ERIC members recommend to refer the patient to the nearest (or national) reference center for retinoblastoma, where a multidisciplinary team of specialized physicians (ophthalmology, pediatric oncology, radiology, pathology, radiotherapy, clinical genetics, psychology) and specialized nurses will ensure that practice conforms to the best standards of care.

Patient handling

Although the technical success of MRI usually depends on the cooperation of the patient, in retinoblastoma appropriate sedation techniques or general anesthesia are nowadays widely used, with a high yield of diagnostic scans. Nevertheless, in our experience the success rate of intravenous sedation is highly dependent on the presence of trained anesthetists and of the choice of radiofrequency coils. Especially, the use of small surface coils decreases the success rate, because these coils need to be accurately positioned close to the eye. The depth of sedation may be insufficient for accurate patient positioning. Therefore, general anesthesia is recommended for MRI in children with retinoblastoma. Another advantage of general anesthesia is the possibility to ensure that the eyelids are fully closed and to avoid uncontrolled eye movements by putting pads (fixed with tape) on the closed eyelids. Thereby susceptibility artifacts caused by air-tissue interface or by air bubbles under the eyelids is avoided, which is favorable for the image quality in the anterior eye segment. If possible, the MR examination can be combined with fundoscopy and US under the same general anesthetic.

Hardware

Clinical MRI of orbit and eyes is mostly acquired using the current standard field strengths up to 1.5 T. Since adequate imaging of retinoblastoma requires high spatial resolution, the field strength of the MR system should be at least 1.5 T. The performance of scans at 1.5 T using a head coil is the most practical approach for evaluation of retinoblastoma. However, this combination usually gives insufficient signal-to-noise ratio (SNR) at required in-plane image resolution and section thickness. Therefore, scanning at 1.5 T should always be performed with one or two small surface coils (diameter ≤ 5 cm) to reliably detect small lesions and metastatic risk factors (Fig. 4). Indeed, the use of surface coils in ocular tumors has been reported to increase the diagnostic accuracy [44, 62]. The main advantage of higher field strengths (3 T) is the increased SNR. Publications on ocular 3-T MRI are still limited [63, 64]. At 3 T with multi-channel head coil or surface coils one can achieve high-resolution images similar to those obtained at 1.5 T with surface coils (Fig. 5). We think the diagnostic accuracy for detection of tumor extent might improve, but there is currently no published evidence for this.



Fig. 4 High-resolution MRI in retinoblastoma. The child is under general anesthesia. A small circular surface coil (arrow) is accurately positioned close to the affected eye

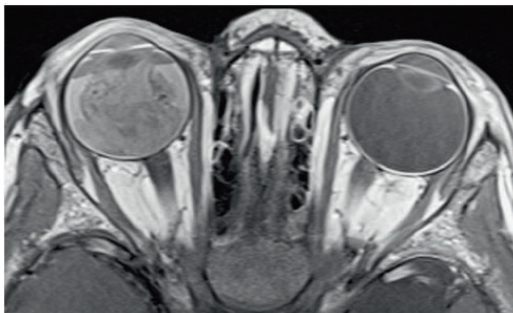


Fig. 5 Transaxial contrast-enhanced T1-weighted (TR/TE, 722/14 ms) image obtained at 3.0 T using a 32-channel head coil shows an exophytic retinoblastoma with secondary total retinal detachment and proteinaceous subretinal effusion

Imaging protocol

MRI protocols vary because of differences in available equipment and individual preferences. However, despite differences, certain basic elements are common to most imaging protocols for retinoblastoma. The minimal requirements for diagnostic evaluation of retinoblastoma or mimicking lesions according to the consensus reached among members of the European Retinoblastoma Imaging Collaboration (ERIC) are presented below and summarized in Table 1. A typical MR imaging protocol for retinoblastoma should always include high-resolution imaging of the affected eye(s) and imaging of the entire brain.

Table 1 MRI protocol in Retinoblastoma*

Requirements	
Scanner and coils	Field strength above 1 T 1.5 T system combined with one or two small surface coils (< 5 cm diameter) 3.0 T system combined with multichannel head coil
Sequences (minimal requirements)	
Orbits	Transverse T2-W (slice thickness ≤ 2 mm) Optional: Transverse CISS (Siemens) / FIESTA (GE) / DRIVE (Philips)
Eye(s) and optic nerve(s)	Inplane pixel size < 0.5 x 0.5 mm; slice thickness ≤ 2 mm Unilateral disease (or bilateral disease with only one eye strongly affected) Precontrast T1-W; at least one plane (transverse or oblique-sagittal) T2-W; at least one plane (transverse or oblique-sagittal) Postcontrast T1-W, no FS; two planes (transverse and oblique-sagittal) Bilateral disease (both eyes strongly affected) Precontrast T1-W (transverse) T2-W (transverse) Postcontrast T1-W, no FS; two planes (oblique-sagittal on both eyes and transverse)
Brain	Transverse T2-W (slice thickness ≤ 4 mm) Postcontrast T1-W (2D SE with slice thickness ≤ 3 mm or 3D GRE ≤ 1 mm)

FS fat-saturation, *SE* spin-echo, *GRE* gradient-echo

* consensus among members of the European Retinoblastoma Imaging Collaboration (ERIC)

Orbits

Regardless of laterality, at least one transaxial thin-slice (≤ 2 mm) T2W sequence should cover both orbits. For T2W imaging based on a (fast) spin-echo technique, it is recommended to use a long TE (heavily T2-weighted; TE ≥ 120 ms) for generating the image contrast necessary to

provide an optimal differentiation of retinoblastoma and surrounding vitreous or subretinal fluid (Fig. 6). Fat saturation combined with T2W imaging is not recommended. When fat suppression is used, the resulting loss in SNR should be compensated (e.g., by increasing the number of acquisitions).

T2W spin-echo may be replaced by gradient-echo T2W sequences such as 3D steady-state free precession sequences with slice thickness ≤ 1 mm (Fig. 6; vendor-specific acronyms: CISS [Constructive Interference in Steady State, Siemens], FIESTA [Fast Imaging Employing Steady State Acquisition, GE Healthcare]; DRIVE [Driven Equilibrium, Philips]) (slice thickness, ≤ 1 mm). These pulse sequences provide detailed images of both orbits and eyes, and allow accurate comparison of eye size, anterior chamber depth and laterality. Very small tumors can be depicted with these techniques.

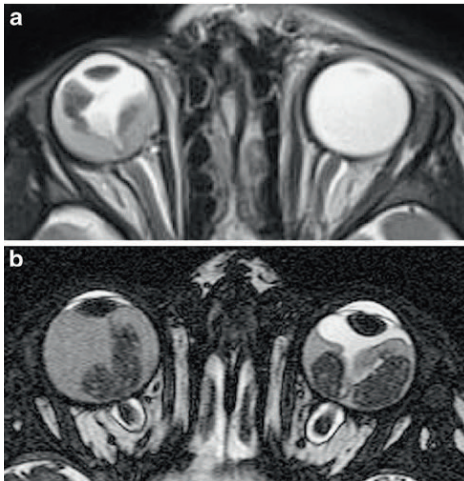


Fig. 6 a Thin-slice transaxial T2-weighted (TR/TE, 4,430/102 ms; section thickness, 2 mm) image demonstrates retinoblastoma of the right eye with secondary retinal detachment. b Transaxial constructive interference steady-state (TR/TE, 14/7 ms) image of bilateral retinoblastoma with secondary retinal detachment. Notice the shallow anterior chamber of the right eye, a sign of increased intraocular pressure

Eye and distal optic nerve

Increased spatial resolution will improve the accuracy of MRI in assessing the anatomical details of the papilla, lamina cribrosa and pre- and postlaminar segments of the optic nerve [65]. The continuous improvement of MR units and the use of small fields-of-view with either multi-channel head coils or surface coils now allows much higher image resolution. High spatial resolution means section thickness ≤ 2 mm and in-plane pixel size $\leq 0.5 \times 0.5$ mm. For optimal detection of optic nerve invasion, the image plane through the orbit (transaxial and sagittal oblique) should align with the orientation of the distal (1 cm) end of the nerve, just posterior to the lamina cribrosa (Fig. 7). One section in each of these sequences should be precisely aligned within the distal part of the optic nerve at the level of the middle of the optic disk. Although the use of the fat-saturation technique is highly recommended for contrast-enhanced MR imaging in orbital pathology, its use in high-resolution contrast-enhanced T1W MRI in retinoblastoma is

declining [44, 58]. In the minimal requirements for diagnostic evaluation of retinoblastoma or mimicking lesions according to the consensus reached among members of the ERIC, the use of fat saturation in contrast-enhanced T1W sequences is no longer recommended.

- Transaxial or sagittal oblique T1W spin-echo helps detection of intraocular blood and subretinal fluid with high protein content. Retinoblastoma is slightly hyperintense with respect to the vitreous body.
- Transaxial or sagittal oblique heavily T2W spin-echo provides detailed information about the classic low signal intensity of retinoblastoma and presence of retinal detachment.
- Transaxial and sagittal oblique contrast-enhanced T1W spin-echo provides information about the enhancement of lesions, optic nerve- and ocular wall invasion, and anterior eye segment enhancement.

The recommended protocol for high-resolution MR imaging of the eye(s) and distal optic nerve(s) differs slightly between unilateral or bilateral disease (Table 1, Figs. 8-9). Incidence of metastatic risk factors is highly dependent on tumor location and tumor size. Therefore, a distinction is made between bilateral disease with only one eye strongly affected (high-resolution MRI can be performed in the worst affected eye only) and extensive disease in both eyes (high-resolution MRI of both eyes).

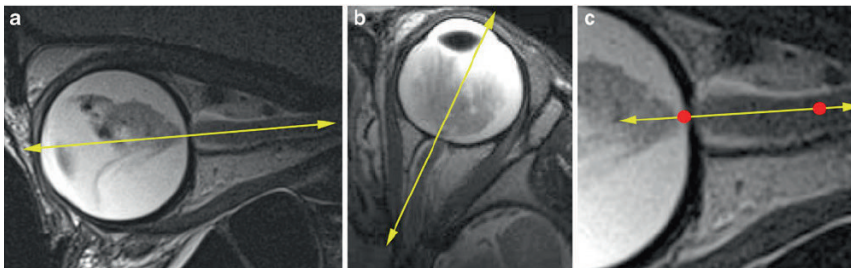


Fig. 7 Recommended slice positions. One T2-weighted section in the sagittal oblique plane and one in the transaxial plane should be precisely aligned at the middle of the optic disk and the distal (at least 1 cm) end of the optic nerve. a Correct alignment of transaxial sections. b Correct alignment of sagittal oblique sections. c Detailed view of the distal optic nerve (line segment: imaging axis; distal 1 cm of the optic nerve between red dots)

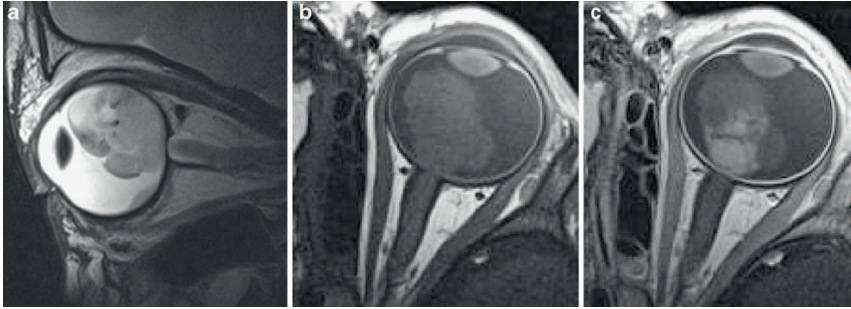


Fig. 8 In unilateral retinoblastoma (or bilateral disease with only one eye strongly affected), high-resolution MRI is done in the (most) affected eye only. Imaging example of a left unilateral lesion. a Sagittal oblique T2-weighted (TR/TE 3,460/110 ms) image. b Transaxial precontrast T1-weighted (TR/TE 360/13 ms) image. c Transaxial postcontrast T1-weighted (TR/TE 360/13 ms) image. Notice the inhomogeneous enhancement pattern, which is common in retinoblastoma

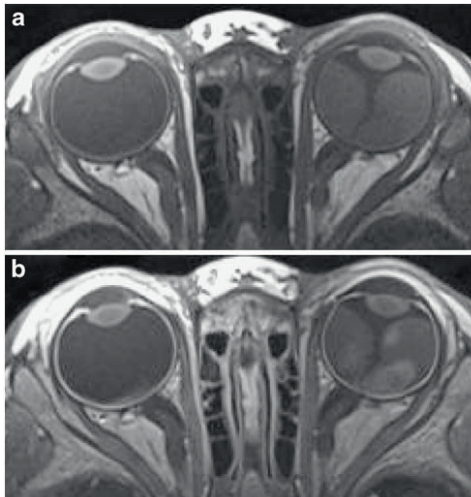


Fig. 9 MRI of bilateral retinoblastoma with extensive disease in both eyes should be performed with two surface coils. The field of view should be slightly increased to cover both eyes in the transaxial plane. Imaging example of bilateral lesions: a Precontrast transaxial T1-weighted (TR/TE, 360/13 ms) image. b Postcontrast transaxial T1-weighted (TR/TE, 360/13 ms) image

Brain

The brain should always be imaged in retinoblastoma patients for analysis of midline structures in order to depict trilateral retinoblastoma (i.e. PNET located mainly in the pineal gland, or more rarely in suprasellar area) or leptomeningeal spread. For a patient presenting with leukocoria suspicious of having retinoblastoma or already diagnosed as retinoblastoma based on clinical findings and US, the baseline evaluation should include an MR imaging of the brain that meets the standardized protocol. Imaging of the brain is performed with (multi-channel) headcoil only and should at least include the following or similar types of sequences:

- Transaxial fast spin-echo T2W sequence (slice thickness, ≤ 4 mm). This sequence provides an overview of the brain anatomy and structural abnormalities (patients with 13q deletion syndrome).

- Transaxial or sagittal contrast-enhanced T1W sequence (2D spin-echo T1W with slice thickness ≤ 3 mm; or 3D gradient-echo with slice thickness ≤ 1 mm). This sequence provides information about enhancement of the pineal gland, presence of a midline PNET, leptomeningeal metastases and extensive optic nerve invasion.
- Coronal and sagittal high-resolution T2W sequence (slice thickness, 1.5 mm). These sequences are optional but should be added to the protocol in case of an atypical pineal gland (partially cystic, irregular, enlarged).

IMAGE ANALYSIS CHECKLIST FOR MR REPORTING (TABLE 2)

Table 2 Retinoblastoma: Checklist for MRI radiology reports

Parameters	
Tumor characteristics	SI relative to the vitreous body; moderately high on T1-W and low on T2-W Laterality Growth Pattern Tumor size and location; in contact with optic nerve Buphthalmia
Tumor extension	Optic nerve and meningeal sheath invasion Ocular wall invasion (choroid and sclera) Extraocular extension
Anterior eye segment	Anterior chamber depth Enhancement Tumor invasion; ciliary body
Brain	Trilateral retinoblastoma; pineal gland and supra- or parasellar region Leptomeningeal metastases Malformations

SI signal intensity

Tumor size and location

Compared to the vitreous body, retinoblastoma has moderately higher signal intensity on T1W and lower on T2W images. Increased size of the globe, globe deformation and reduced anterior chamber depth are signs of increased intraocular pressure and are usually associated with buphthalmia (Fig. 10). These signs should be mentioned since they are associated with a higher risk of globe rupture and secondary orbital seeding during enucleation. Laterality and growth pattern should be mentioned as well as the location of the tumor, with respect to the equator of the eye (anterior, posterior or combined) and with respect to the papilla (the optic nerve disk) and the macula. One should in particular identify tumor close to the optic disk, because this may invade the nerve [22] (Fig. 11).

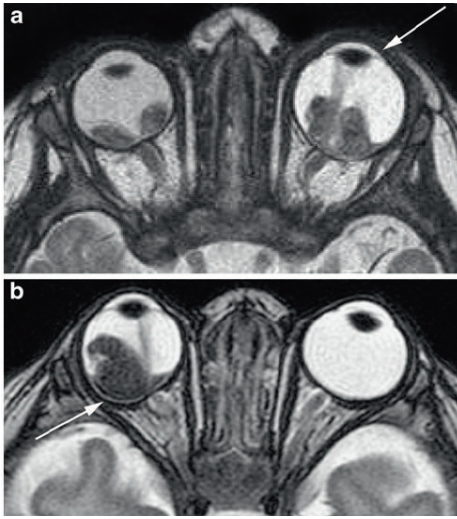


Fig. 10 Retinoblastoma with signs of increased intraocular pressure following subretinal hemorrhage (fluid–fluid levels). a Bilateral retinoblastoma with increased size of the left eye (buphthalmus) and a shallow anterior chamber (arrow) seen on T2-weighted (TR/TE, 4,430/102 ms) image. b Bilateral retinoblastoma with focal bulging of the posterior eye segment (arrow) of the right eye and a shallow anterior chamber seen on T2-weighted (TR/TE, 4,430/102 ms) image

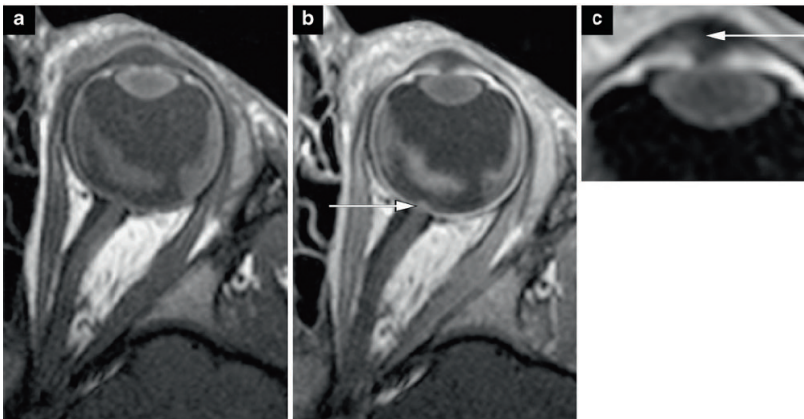


Fig. 11 Pre- (a) and postcontrast (b) transaxial T1-weighted (374/14) MR images show small nodular enhancement at the optic nerve disk (arrow), which represents superficial optic nerve invasion by intraocular tumor seeding (predilection site). c Abnormal contrast enhancement of the anterior eye segment combined with macroscopic tumor seedings (arrow)

Optic nerve and meningeal sheath invasion

In normal-size optic nerves, the direct radiological criterion used to diagnose postlaminar nerve invasion is the presence of abnormal contrast enhancement (enhancement ≥ 2 mm in diameter) in the distal nerve [21] (Fig. 12). Interruption of the normal linear enhancement at the optic nerve disk (choroidoretinal complex) supports a suggestion of optic nerve invasion [22]. Postlaminar optic nerve or optic nerve meningeal sheath invasion should raise suspicion of leptomeningeal metastases. In such situations, additional contrast-enhanced sagittal T1W imaging of the whole spine is recommended.

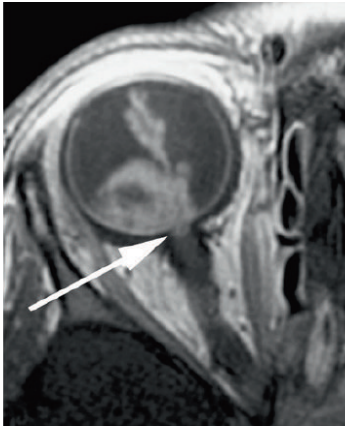


Fig. 12 Postcontrast transaxial T1-weighted (TR/TE, 374/14 ms) MRI. Abnormal enhancement of the distal optic nerve in continuity with tumor is a sign of postlaminar optic nerve invasion

Ocular wall invasion and extraocular extension

Discontinuity of the normal choroidal enhancement is the leading criterion for infiltration [22, 24] (Fig. 13). Massive choroidal invasion presents as focal choroidal thickening (Fig. 13). Increased enhancement and thickening of the entire uveal tract (choroid, ciliary body, iris) is a sign of uveitis, usually secondary to massive (sub) total tumor necrosis [22]. Protrusion of enhancing tissue through the thickened choroid into the (low signal-intensity) sclera or beyond is a sign of scleral invasion or extraocular extension, respectively.

Anterior eye segment

Anterior eye segment enhancement occurs frequently in retinoblastoma and is usually a sign of iris angiogenesis [27, 30]. Tumor invasion into the anterior eye segment (Fig. 11) is an infrequent finding, usually associated with anteriorly located retinoblastoma. Enhancement of the tumor extending into the ciliary body or beyond should raise suspicion of anterior eye segment invasion. Transaxial T2W images of both orbits can be used to depict a decreased anterior chamber depth (Fig. 10).

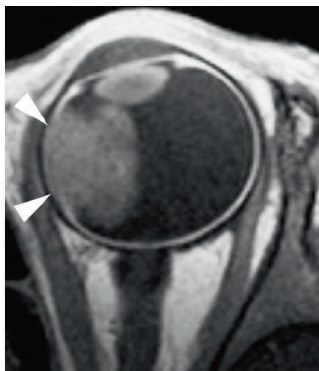


Fig. 13 Postcontrast transaxial T1-weighted (TR/TE, 305/15 ms) MRI. Intraocular enhancing retinoblastoma combined with focal choroidal thickening and a discontinuity of the linear enhancement pattern of the choroid (arrowheads) adjacent to the tumor mass is suspicious for tumor invasion. Histopathological examination of this eye showed massive choroidal invasion

Brain

Careful analysis of midline structures should be performed to depict trilateral retinoblastoma (i.e. PNET located mainly in the pineal gland, or rarely in the suprasellar area) (Fig. 14) or leptomeningeal spread (if patient shows extensive postlaminar optic nerve invasion enhancement). Congenital brain malformations occur mainly in patients with 13q- deletion syndrome [10]. Benign pineal cysts should not be misinterpreted as pineal PNET, even in children with retinoblastoma [10, 66]. Thin-section T2W and contrast-enhanced T1W slices are helpful for differential diagnoses. In doubtful cases, close follow-up with MRI is recommended.

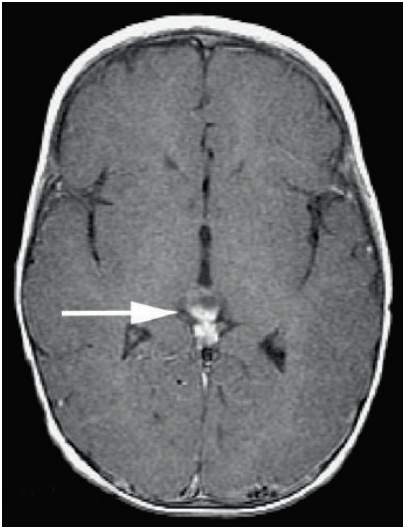


Fig. 14 Pineoblastoma in a patient with hereditary unilateral retinoblastoma. Postcontrast axial T1-weighted (TR/TE, 650/10 ms) MRI shows a cystic enhancing mass of the pineal gland (arrow) suspicious for pineoblastoma (trilateral retinoblastoma)

CONCLUSION

Together with US, high-resolution MR imaging has emerged as the most important imaging modality in the assessment of retinoblastoma—for diagnostic confirmation and for determination of local tumor extent and associated intracranial abnormalities. CT is no longer indicated in children with leukocoria because of (1) ionizing radiation and (2) no added diagnostic value. US combined with MRI using our suggested standardized retinoblastoma MRI protocol provides state-of-the-art pretreatment diagnostic evaluation in children with retinoblastoma.

REFERENCES

1. Moll AC, Kuik DJ, Bouter LM, Den Otter W, Bezemer PD, Koten JW, Imhof SM, Kuyt BP, Tan KE (1997) Incidence and survival of retinoblastoma in The Netherlands: a register based study 1862-1995. *Br J Ophthalmol* 81: 559-562
2. Doz F, Brisse HJ, Stoppa-Lyonnet D, Sastre X, Zucker JM, Desjardins L (2004) Retinoblastoma. In: Pinkerton R, Plowman P, Pieters R (eds) *Paediatric Oncology*. Arnold, London, pp 323-338
3. Shields CL, Shields JA (2010) Retinoblastoma management: advances in enucleation, intravenous chemoreduction, and intra-arterial chemotherapy. *Curr Opin Ophthalmol* 21: 203-212
4. Abramson DH (2005) Retinoblastoma in the 20th century: past success and future challenges the Weisenfeld lecture. *Invest Ophthalmol Vis Sci* 46: 2683-2691
5. Aerts I, Lumbroso-Le Rouic L, Gauthier-Villars M, Brisse H, Doz F, Desjardins L (2006) Retinoblastoma. *Orphanet J Rare Dis* 1:31
6. Dunkel IJ, Khakoo Y, Kernan NA, Gershon T, Gilheeny S, Lyden DC, Wolden SL, Orjuela M, Gardner SL, Abramson DH (2010) Intensive multimodality therapy for patients with stage 4a metastatic retinoblastoma. *Pediatr Blood Cancer* 55: 55-59
7. Dunkel IJ, Chan HS, Jubran R, Chantada GL, Goldman S, Chintagumpala M, Khakoo Y, Abramson DH (2010) High-dose chemotherapy with autologous hematopoietic stem cell rescue for stage 4B retinoblastoma. *Pediatr Blood Cancer* 55: 149-152
8. Baud O, Cormier-Daire V, Lyonnet S, Desjardins L, Turleau C, Doz F (1999) Dysmorphic phenotype and neurological impairment in 22 retinoblastoma patients with constitutional cytogenetic 13q deletion. *Clin Genet* 55: 478-482
9. Ballarati L, Rossi E, Bonati MT, Gimelli S, Maraschio P, Finelli P, Giglio S, Lapi E, Bedeschi MF, Gueneri S, Arrigo G, Patricelli MG, Mattina T, Guzzardi O, Pecile V, Police A, Scarano G, Larizza L, Zuffardi O, Giardino D (2007) 13q Deletion and central nervous system anomalies: further insights from karyotype-phenotype analyses of 14 patients. *J Med Genet* 44: e60
10. Rodjan F, de Graaf P, Moll AC, Imhof SM, Verbeke JI, Sanchez E, Castelijn JA (2010) Brain abnormalities on MR imaging in patients with retinoblastoma. *AJNR Am J Neuroradiol* 31: 1385-1389
11. Kivela T (1999) Trilateral retinoblastoma: a meta-analysis of hereditary retinoblastoma associated with primary ectopic intracranial retinoblastoma. *J Clin Oncol* 17: 1829-1837
12. Dunkel IJ, Jubran RF, Gururangan S, Chantada GL, Goldman S, Khakoo Y, O'Brien JM, Orjuela M, Rodriguez-Galindo C, Souweidane MM, Abramson DH (2010) Trilateral retinoblastoma: potentially curable with intensive chemotherapy. *Pediatr Blood Cancer* 54: 384-387
13. Wright KD, Qaddoumi I, Patay Z, Gajjar A, Wilson MW, Rodriguez-Galindo C (2010) Successful treatment of early detected trilateral retinoblastoma using standard infant brain tumor therapy. *Pediatr Blood Cancer* 55: 570-572
14. Lumbroso-Le Rouic L, Aerts I, Levy-Gabriel C, Dendale R, Sastre X, Esteve M, Asselain B, Bours D, Doz F, Desjardins L (2008) Conservative treatments of intraocular retinoblastoma. *Ophthalmology* 115: 1405-10, 1410
15. Abramson DH, Dunkel IJ, Brodie SE, Marr B, Gobin YP (2010) Superselective ophthalmic artery chemotherapy as primary treatment for retinoblastoma (chemosurgery). *Ophthalmology* 117: 1623-1629
16. Shields CL, Shields JA, Baez K, Cater JR, De Potter P (1994) Optic nerve invasion of retinoblastoma. Metastatic potential and clinical risk factors. *Cancer* 73: 692-698
17. Chantada GL, Dunkel IJ, Antoneli CB, de Davila MT, Arias V, Beaverson K, Fandino AC, Chojniak M, Abramson DH (2007) Risk factors for extraocular relapse following enucleation after failure of chemoreduction in retinoblastoma. *Pediatr Blood Cancer* 49: 256-260
18. Chantada GL, Casco F, Fandino AC, Galli S, Manzitti J, Scopinaro M, Schwartzman E, de Davila MT (2007) Outcome of patients with retinoblastoma and postlaminar optic nerve invasion. *Ophthalmology* 114: 2083-2089
19. Uusitalo MS, Van Quill KR, Scott IU, Matthay KK, Murray TG, O'Brien JM (2001) Evaluation of chemoprophylaxis in patients with unilateral retinoblastoma with high-risk features on histopathologic examination. *Arch Ophthalmol* 119: 41-48

20. Honavar SG, Singh AD, Shields CL, Meadows AT, Demirci H, Cater J, Shields JA (2002) Postenucleation adjuvant therapy in high-risk retinoblastoma. *Arch Ophthalmol* 120: 923-931
21. Brisse HJ, Guesmi M, Aerts I, Sastre-Garau X, Savignoni A, Lumbroso-Le RL, Desjardins L, Doz F, Asselain B, Bours D, Neuenschwander S (2007) Relevance of CT and MRI in retinoblastoma for the diagnosis of postlaminar invasion with normal-size optic nerve: a retrospective study of 150 patients with histological comparison. *Pediatr Radiol* 37: 649-656
22. de Graaf P, Barkhof F, Moll AC, Imhof SM, Knol DL, van der Valk P, Castelijns JA (2005) Retinoblastoma: MR imaging parameters in detection of tumor extent. *Radiology* 235: 197-207
23. Shields CL, Shields JA, Baez KA, Cater J, De Potter PV (1993) Choroidal invasion of retinoblastoma: metastatic potential and clinical risk factors. *Br J Ophthalmol* 77: 544-548
24. Khelifaoui F, Validire P, Aupepin A, Quintana E, Michon J, Pacquement H, Desjardins L, Asselain B, Schlienger P, Vielh P (1996) Histopathologic risk factors in retinoblastoma: a retrospective study of 172 patients treated in a single institution. *Cancer* 77: 1206-1213
25. Chantada GL, Dunkel IJ, de Davila MT, Abramson DH (2004) Retinoblastoma patients with high risk ocular pathological features: who needs adjuvant therapy? *Br J Ophthalmol* 88: 1069-1073
26. Sastre X, Chantada GL, Doz F, Wilson MW, de Davila MT, Rodriguez-Galindo C, Chintagumpala M, Chevez-Barrios P (2009) Proceedings of the consensus meetings from the International Retinoblastoma Staging Working Group on the pathology guidelines for the examination of enucleated eyes and evaluation of prognostic risk factors in retinoblastoma. *Arch Pathol Lab Med* 133: 1199-1202
27. Galluzzi P, Cerase A, Hadjistilianou T, De Francesco S, Toti P, Vallone IM, Filisomi G, Monti L, Bracco S, Gennari P, Ginanneschi C, Venturi C (2003) Retinoblastoma: Abnormal gadolinium enhancement of anterior segment of eyes at MR imaging with clinical and histopathologic correlation. *Radiology* 228: 683-690
28. Pe'er J, Neufeld M, Baras M, Gnessin H, Itin A, Keshet E (1997) Rubeosis iridis in retinoblastoma. Histologic findings and the possible role of vascular endothelial growth factor in its induction. *Ophthalmology* 104: 1251-1258
29. Saket RR, Mafee MF (2009) Anterior-segment retinoblastoma mimicking pseudoinflammatory angle-closure glaucoma: review of the literature and the important role of imaging. *AJNR Am J Neuroradiol* 30: 1607-1609
30. de Graaf P, van der Valk P, Moll AC, Imhof SM, Schouten-van Meeteren AY, Knol DL, Castelijns JA (2010) Contrast-enhancement of the anterior eye segment in patients with retinoblastoma: correlation between clinical, MR imaging, and histopathologic findings. *AJNR Am J Neuroradiol* 31: 237-245
31. Chantada GL, Gutter MR, Fandino AC, Raslawski EC, de Davila MT, Vaiani E, Scopinaro MJ (2008) Treatment results in patients with retinoblastoma and invasion to the cut end of the optic nerve. *Pediatr Blood Cancer* %20.:
32. Marees T, van Leeuwen FE, Schaapveld M, Imhof SM, de Boer MR, Kors WA, Ringens PJ, Moll AC (2010) Risk of third malignancies and death after a second malignancy in retinoblastoma survivors. *Eur J Cancer* 46: 2052-2058
33. Marees T, van Leeuwen FE, de Boer MR, Imhof SM, Ringens PJ, Moll AC (2009) Cancer mortality in long-term survivors of retinoblastoma. *Eur J Cancer* 45: 3245-3253
34. Marees T, Moll AC, Imhof SM, de Boer MR, Ringens PJ, van Leeuwen FE (2008) Risk of second malignancies in survivors of retinoblastoma: more than 40 years of follow-up. *J Natl Cancer Inst* 100: 1771-1779
35. Gombos DS, Hungerford J, Abramson DH, Kingston J, Chantada G, Dunkel IJ, Antoneli CB, Greenwald M, Haik BG, Leal CA, Medina-Sanson A, Scheffer AC, Veerakul G, Wieland R, Bornfeld N, Wilson MW, Yu CB (2007) Secondary acute myelogenous leukemia in patients with retinoblastoma: is chemotherapy a factor? *Ophthalmology* 114: 1378-1383
36. Wong FL, Boice JD, Jr., Abramson DH, Tarone RE, Kleinerman RA, Stovall M, Goldman MB, Seddon JM, Tarbell N, Fraumeni JF, Jr., Li FP (1997) Cancer incidence after retinoblastoma. Radiation dose and sarcoma risk. *JAMA* 278: 1262-1267
37. Brenner D, Elliston C, Hall E, Berdon W (2001) Estimated risks of radiation-induced fatal cancer from pediatric CT. *AJR Am J Roentgenol* 176: 289-296

38. Imhof SM, Mourits MP, Hofman P, Zonneveld FW, Schipper J, Moll AC, Tan KE (1996) Quantification of orbital and mid-facial growth retardation after megavoltage external beam irradiation in children with retinoblastoma. *Ophthalmology* 103: 263-268
39. Vijaykrishnan R, Shields CL, Ramasubramanian A, Emrich J, Rosenwasser R, Shields JA (2010) Irradiation toxic effects during intra-arterial chemotherapy for retinoblastoma: should we be concerned? *Arch Ophthalmol* 128: 1427-1431
40. Moll AC, Hoekstra OS, Imhof SM, Comans EF, Schouten-van Meeteren AY, van der Valk P, Boers M (2004) Fluorine-18 fluorodeoxyglucose positron emission tomography (PET) to detect vital retinoblastoma in the eye: preliminary experience. *Ophthalmic Genet* 25: 31-35
41. Kaste SC, Jenkins JJ, III, Pratt CB, Langston JW, Haik BG (2000) Retinoblastoma: sonographic findings with pathologic correlation in pediatric patients. *AJR Am J Roentgenol* 175: 495-501
42. Galluzzi P, Hadjistilianou T, Cerase A, De Francesco S, Toti P, Venturi C (2009) Is CT still useful in the study protocol of retinoblastoma? *AJNR Am J Neuroradiol* 30: 1760-1765
43. Roth DB, Scott IU, Murray TG, Kaiser PK, Feuer WJ, Hughes JR, Rosa RH, Jr. (2001) Echography of retinoblastoma: histopathologic correlation and serial evaluation after globe-conserving radiotherapy or chemotherapy. *J Pediatr Ophthalmol Strabismus* 38: 136-143
44. Lemke AJ, Kazi I, Mergner U, Foerster PI, Heimann H, Bechrakis N, Schuler A, von Pilsach MI, Foerster M, Felix R, Hosten N (2007) Retinoblastoma - MR appearance using a surface coil in comparison with histopathological results. *Eur Radiol* 17: 49-60
45. Brisse HJ, Lumbroso L, Freneaux PC, Validire P, Doz FP, Quintana EJ, Berges O, Desjardins LC, Neuenschwander SG (2001) Sonographic, CT, and MR imaging findings in diffuse infiltrative retinoblastoma: report of two cases with histologic comparison. *AJNR Am J Neuroradiol* 22: 499-504
46. Finger PT, Khoobehi A, Ponce-Contreras MR, Rocca DD, Garcia JP, Jr. (2002) Three dimensional ultrasound of retinoblastoma: initial experience. *Br J Ophthalmol* 86: 1136-1138
47. Beets-Tan RG, Hendriks MJ, Ramos LM, Tan KE (1994) Retinoblastoma: CT and MRI. *Neuroradiology* 36: 59-62
48. Chung EM, Specht CS, Schroeder JW (2007) From the archives of the AFIP: Pediatric orbit tumors and tumorlike lesions: neuroepithelial lesions of the ocular globe and optic nerve. *Radiographics* 27: 1159-1186
49. James SH, Halliday WC, Branson HM (2010) Best cases from the AFIP: Trilateral retinoblastoma. *Radiographics* 30: 833-837
50. Golding SJ (2010) Radiation exposure in CT: what is the professionally responsible approach? *Radiology* 255: 683-686
51. John-Mikolajewski V, Messmer E, Sauerwein W, Freundlieb O (1987) Orbital computed tomography. Does it help in diagnosing the infiltration of choroid, sclera and/or optic nerve in retinoblastoma? *Ophthalmic Paediatr Genet* 8: 101-104
52. Jacquemin C, Karciglu ZA (1998) Detection of optic nerve involvement in retinoblastoma with enhanced computed tomography. *Eye (Lond)* 12: 179-183
53. Olivecrona H, Agerberg PA, Huaman A (1994) CT diagnosis of retinoblastoma with histopathologic correlations. *Eur Radiol* 4: 307-313
54. Mafee MF, Mafee RE, Malik M, Pierce J (2003) Medical imaging in pediatric ophthalmology. *Pediatr Clin North Am* 50: 259-286
55. Apushkin MA, Apushkin MA, Shapiro MJ, Mafee MF (2005) Retinoblastoma and simulating lesions: role of imaging. *Neuroimaging Clin N Am* 15: 49-67
56. Barkovich AJ (2005) *Pediatric neuroimaging*. Lippincott Williams & Wilkins, Philadelphia
57. Gizewski ER, Wanke I, Jurklics C, Gungor AR, Forsting M (2005) T1 Gd-enhanced compared with CISS sequences in retinoblastoma: superiority of T1 sequences in evaluation of tumour extension. *Neuroradiology* 47: 56-61
58. Schueler AO, Hosten N, Bechrakis NE, Lemke AJ, Foerster P, Felix R, Foerster MH, Bornfeld N (2003) High resolution magnetic resonance imaging of retinoblastoma. *Br J Ophthalmol* 87: 330-335
59. Ainbinder DJ, Haik BG, Frei DF, Gupta KL, Mafee MF (1996) Gadolinium enhancement: improved MRI detection of retinoblastoma extension into the optic nerve. *Neuroradiology* 38: 778-781

60. Barkhof F, Smeets M, van der Valk P, Tan KE, Hoogenraad F, Peeters J, Valk J (1997) MR imaging in retinoblastoma. *Eur Radiol* 7: 726-731
61. Wilson MW, Rodriguez-Galindo C, Billups C, Haik BG, Laningham F, Patay Z (2009) Lack of correlation between the histologic and magnetic resonance imaging results of optic nerve involvement in eyes primarily enucleated for retinoblastoma. *Ophthalmology* 116: 1558-1563
62. Lemke AJ, Hosten N, Bornfeld N, Bechrakis NE, Schuler A, Richter M, Stroszczyński C, Felix R (1999) Uveal melanoma: correlation of histopathologic and radiologic findings by using thin-section MR imaging with a surface coil. *Radiology* 210: 775-783
63. Mafee MF, Rapoport M, Karimi A, Ansari SA, Shah J (2005) Orbital and ocular imaging using 3- and 1.5-T MR imaging systems. *Neuroimaging Clin N Am* 15: 1-21
64. Lemke AJ, ai-Omid M, Hengst SA, Kazi I, Felix R (2006) Eye imaging with a 3.0-T MRI using a surface coil--a study on volunteers and initial patients with uveal melanoma. *Eur Radiol* 16: 1084-1089
65. Brisse HJ (2010) Retinoblastoma imaging. *Ophthalmology* 117: 1051
66. Beck PM, Balmer A, Maeder P, Braganca T, Munier FL (2006) Benign pineal cysts in children with bilateral retinoblastoma: a new variant of trilateral retinoblastoma? *Pediatr Blood Cancer* 46: 755-761

Chapter 3

*Retinoblastoma: value of dynamic contrast-enhanced MR
Imaging and correlation with tumor angiogenesis*

F. Rodjan
P. de Graaf
P. van der Valk
A.C. Moll
J.P.A. Kuijer
D.L. Knol
J.A. Castelijns
P.J.W. Pouwels

ABSTRACT

BACKGROUND AND PURPOSE: Non-invasive evaluation of retinoblastoma treatment response has become more important due to increased use of eye-sparing treatment. We evaluate the relation between dynamic contrast-enhanced magnetic resonance imaging (DCE-MR imaging) and histopathological parameters to determine its value in assessing tumor angiogenesis and provide new radiologic prognostic indicators in retinoblastoma.

METHODS: Fifteen consecutive retinoblastoma patients (mean age 24 months, range 2-70 months) and enucleation of the eye as primary treatment (15 eyes), were scanned at 1.5T using dedicated surface coils. Pre-treatment DCE-MR imaging of the most affected eye was evaluated by two observers using curve-pattern analysis. The first 5min of each curve and the full time series were described by $\kappa 5\text{min}$ and $\kappa 17\text{min}$, respectively. Assessed histopathological and immunologic parameters included known metastatic risk factors (optic nerve invasion, choroid invasion and microvessel density (MVD)), tumor necrosis, and expression of vascular endothelial growth factor (VEGF) and its receptor, Flt-1.

RESULTS: The median value of $\kappa 5\text{min}$ was 1.28 (range 0.87 – 2.07) and correlated positively with MVD ($P = 0.008$). The median value of $\kappa 17\text{min}$ was 1.33 (range 0.35 – 3.08), and correlated negatively with tumor necrosis ($P = 0.002$). Other (immuno)histopathological parameters did not correlate with DCE-MR imaging parameters. Interobserver agreement for $\kappa 5\text{min}$ was 0.53, and for $\kappa 17\text{min}$ a strong agreement of 0.91 was observed.

CONCLUSION: In retinoblastoma, the early phase of the DCE time curve positively correlates with MVD while the presence of late enhancement is correlated with necrosis. Thus, the potential for DCE-MR imaging to non-invasively assess tumor angiogenesis and necrosis in retinoblastoma tumors is promising and warrants further investigation.

INTRODUCTION

In retinoblastoma, increasing eye preservation and tumor control has been achieved due to introduction of conservative treatment strategies. Especially the recent introduction of selective intra-arterial chemotherapy infusion via the ophthalmic artery as an effective treatment method for intraocular retinoblastoma will dramatically decrease the number of enucleations (1-3). In the near future more and more patients will be treated without histopathological confirmation of the diagnosis, leading to uncertainty about risk factors that can predict disease dissemination and prognosis. Histopathology is still the gold standard for detection of tumor spread and therefore prognosis of retinoblastoma (4). Currently, the risk for metastatic disease and the decision about the use of prophylactic therapy is based on the following characteristics; (i) tumor invasion in the optic nerve posterior to the lamina cribrosa, (ii) invasion in the anterior eye segment, and (iii) extensive invasion of the ocular coats (massive choroidal, scleral invasion). These characteristics can well be detected on histopathology, but detection by conventional magnetic resonance (MR) imaging is not optimal so far (5-13). Therefore, it is important to assess prospects of other MR imaging methods that could further optimize the tumor tissue characterization *in vivo*.

Tumor angiogenesis is a key element in the pathophysiology of tumor growth and metastases. It has been shown that tumor microvessel density (MVD) as marker for angiogenesis correlates statistically significant with both local invasive growth and presence of metastases in retinoblastoma (4;14). Thus, tumor angiogenesis in retinoblastoma is considered to be a metastatic risk factor. Currently, tumor angiogenesis can only be assessed *in vitro* on histopathological specimens by assessment of MVD and angiogenic growth factors such as vascular endothelial growth factor (VEGF) and its receptor (Flt-1). In addition to promoting angiogenesis these growth factors cause an increased vascular permeability in neovascular capillary beds.

A noninvasive evaluation of tumor angiogenesis might be obtained with dynamic contrast-enhanced MR (DCE-MR) imaging. Using a fast T1W MR imaging technique before, during and after intravenous bolus administration of a gadolinium contrast agent, the change of signal intensity (SI) over time reflects the delivery of the contrast into the tumor interstitial space. The rates of contrast washin and subsequent washout from the tumor are related to tissue vascularization and perfusion, capillary permeability and composition of the interstitial space (15-20). To our knowledge, the correlation between DCE-MR imaging and retinoblastoma microvasculature has not been described before. However, a noninvasive imaging biomarker for tumor angiogenesis *in vivo* could have potential value in patients treated with eye-preservation treatment strategies.

The purpose of this study was to evaluate the relation between DCE-MR imaging and histopathological parameters to determine its value in assessing tumor angiogenesis and providing new radiologic prognostic indicators in retinoblastoma.

METHODS

Patient population

From May 2006 to September 2009 retinoblastoma patients, diagnosed with extensive fundoscopy and ultrasound under general anaesthesia, were included in this prospective study if they met the following criteria: (a) having undergone pretreatment DCE-MR imaging, (b) enucleation of the eye due to retinoblastoma as primary treatment and (c) availability of diagnostic-quality pathological material. Twenty-one patients with retinoblastoma had DCE-MR imaging before enucleation. Five patients were excluded because of insufficient histopathological material (3 patients) or inadequate DCE-MR images (2 patients) and one patient was treated with chemotherapy prior to enucleation. The final study population consisted of 15 patients (5 girls and 10 boys), with a mean age of 24 months (median 23 months, range 2-70 months). Five patients had bilateral disease of which only the most affected eye was enucleated. Clinical records were reviewed by one reviewer (F. R.) to assess age at diagnosis, days between MR and enucleation, laterality, presence of vitreous/ subretinal tumor seeding (yes/no), extra-ocular tumor recurrence and last known follow-up date. This study was performed in agreement with the recommendations of the local ethics committee, with waiver of informed consent.

MR Imaging

All MR imaging examinations were performed under general-anesthesia on a 1.5-T scanner (Siemens Sonata; Erlangen, Germany) using a dedicated surface coil focused on the (most) affected eye. MR imaging included transversal and sagittal spin-echo T1W images (repetition time/echo time 420/13ms; 3 and 2 acquisitions respectively) and transversal spin-echo T2W images (2470/120ms; one acquisition). All conventional images had an in-plane resolution of 0.58 x 0.58 mm² and a slice thickness of 2 mm. Transverse DCE-MR images were obtained with 3D fast low-angle shot (FLASH), 8.6/4.8ms; flip angle 25°; in-plane resolution of 0.66 x 0.66 mm². One 3D volume consisted of 16 partitions of 3 mm thickness (acquisition time per volume 17s). A total of 20 consecutive volumes were acquired in 5min39s. During DCE-MR imaging an i.v. bolus injection of 0.2 mmol/L Gd-DTPA (Magnevist, Schering, Berlin, Germany) per kg body weight was administered after the first volume. To determine late enhancement, two short DCE series consisting of 3 volumes were acquired at t=13 min and t=17 min after contrast injection. After each DCE-MR imaging series fat-suppressed T1W spin-echo images were obtained (653/11ms; three acquisitions) in transverse, sagittal and coronal orientation. Thus, the three DCE series lasted less than 8 min in total and were acquired interleaved with the conventional sequences.

Image Analysis

a) Conventional MR imaging

Tumor volume measurements were performed by two observers in consensus (F.R. and P.d.G.) on post-contrast transverse T1W MR images with use of a computerized image analysis tool (Centricity Radiology RA 600; GE Medical Systems, Milwaukee, WI.). On every slice in which tumor was present, this structure was manually outlined as a region of interest (ROI). The ROI covered the whole tumor on each slice. Surfaces of the ROIs were calculated and tumor volume was obtained from the surfaces on consecutive slices multiplied by slice thickness and interslice gap. In addition, tumor enhancement was scored as either homogeneous or heterogeneous.

b) ROI placement for dynamic analysis

DCE-MR imaging data were analyzed using the time series of an ROI, which was placed by two observers independently (F.R. and P.d.G.). Both observers were blinded to histological findings. On a workstation (Leonardo, Siemens, Erlangen, Germany), ROIs were manually drawn on a volume at the end of the first DCE series. The ROI was positioned on one slice within the most enhancing part of the tumor. Care was taken to avoid areas with necrosis within the tumor on the basis of focal high SI on T2W images and absence of enhancement on postcontrast images. As some ROIs were small, it was verified that the position of the ROIs remained strictly within the tissue during the dynamic series, and was not influenced by minor motion (despite anaesthesia). For each ROI, SI as a function of time was extracted.

c) Dynamic analysis

Preferably, quantitative analysis of DCE-MR imaging is performed to obtain values of the volume transfer constant K^{trans} and the volume of extravascular extracellular, i.e. interstitial space per unit volume of tissue v_e (21). This, however, requires determination of both an arterial input function and pre-contrast T1 relaxation times, which were not included in the current protocol. Recently, Guo and Reddick (17) have proposed a curve pattern analysis based only on the dynamic measurements, yielding a value κ which showed a close correlation with the rate constant k_{ep} , which is defined as $k_{ep} = K^{trans}/v_e$.

This curve pattern analysis was performed using Matlab (MathWorks, Natick, MA) (P.J.W.P. and J.P.A.K.) both for the first DCE time series (resulting in a κ -value for 5min) and for the full dataset (κ -value for 17min). The κ 17min can therefore be considered as a parameter for late enhancement. The analysis was performed on smoothed curves through the actual time points. The smoothed SI of the first series ($t = 0 - 5$ minutes 39 seconds) was estimated by an exponential fit of the form $S(t) = S(0)\exp(-k(t-\Delta t))$ in which Δt incorporates the time delay of contrast injection. For each of the second and third series (at $t = 13$ min and $t = 17$ min) the SI of the three volumes within these series was simply averaged.

Histopathological analyses and immunohistochemical staining

All included eyes were re-evaluated by one pathologist (P.v.d.V.) with 11-years of experience in ophthalmopathology, who was blinded to patients' clinical records and MR imaging findings. Histopathologic evaluation, using hematoxylin-eosin (HE) staining, included the following: tumor necrosis (semi-quantitatively estimated according to the percentage of necrotic tumor area); involvement of choroid (inflammation; minimal or massive tumor invasion); optic nerve invasion ((pre)laminar or postlaminar); tumordifferentiation (poor-, moderate- and well-differentiated).

From all affected eyes, deparaffinized 4- μ m sections were immunohistochemically stained by using the avidin-biotin-peroxidase complex and direct antibodies against CD-31 (DAKO, Glostrup, Denmark), VEGF (Santa Cruz Biotechnology, Santa Cruz, CA) and VEGF-receptor-1 (Flt-1) (Santa Cruz Biotechnology). In representative parts of the tumor, in 5 high-power-fields (magnification, x20) the mean MVD of tumor was calculated on CD-31 stained specimens. Evaluation of VEGF and Flt-1 staining intensity in the tumor was graded as follows: negative, weak or strong staining. These methods have been described previously by De Graaf et al (9).

Statistical analysis

Interobserver variability for κ 5min and κ 17min was analyzed by calculating the intraclass correlation coefficient (ICC). Subsequent analyses were performed using the average of the two observers. All statistical calculations were performed using SPSS, version 15.0 (SPSS, Chicago III). Spearman rank correlations were calculated to test the strength of the association between DCE-MR imaging parameters and histopathologic parameters. Only two-tailed tests were used. A P-value of less than .05 was considered statistically significant.

RESULTS

Clinical findings

MR imaging was performed at a mean of 6 days (median, 6 days; range 1 – 13 days) before enucleation of the eye. In 6 out of 15 eyes, vitreous and/or subretinal seedings were observed. Mean follow-up time after enucleation was 35 months (range 10 - 54 months). No patients developed histological proven extra-ocular recurrences and all patients were still alive at the time of follow-up.

Conventional and DCE-MR imaging parameters

Results of all patients are summarized in Table 1. Mean tumor volume was 2513 mm³ (range 288-4847 mm³). All 15 tumors showed heterogeneous enhancement, as for example shown in fig 1-3.

Table 1: Dynamic MR imaging and histologic findings in retinoblastoma patients

Patient	Tumor volume (mm ³)	κ 5min	κ 17min	MVD	VEGF-Rb	Flt-1	Optic nerve invasion	Choroid invasion	Necrosis (%)
1	1690	2.07	1.53	29	weak	weak	no	no	5
2	4782	1.74	3.08	21	negative	positive	postlaminar	no	10
3	656	1.01	0.35	21	negative	negative	(pre)laminar	no	90
4	2927	0.93	0.69	10	weak	negative	(pre)laminar	no	50
5	4727	1.26	0.61	14	positive	negative	postlaminar	minimal	70
6	2664	0.93	1.49	11	weak	weak	no	no	20
7	1955	1.44	2.50	37	positive	negative	(pre)laminar	no	0
8	2153	0.87	0.85	11	positive	negative	no	no	5
9	2333	0.97	1.06	11	weak	negative	no	no	30
10	960	0.99	1.53	23	positive	negative	postlaminar	no	10
11	1931	1.84	1.07	17	positive	weak	no	no	10
12	4463	1.05	1.02	12	positive	weak	(pre)laminar	no	50
13	1325	1.20	1.28	15	weak	weak	(pre)laminar	no	15
14	288	1.80	2.30	16	weak	negative	no	no	20
15	4847	1.12	0.62	27	positive	negative	(pre)laminar	no	50

Note: MVD = micro vessel density

DCE-MR imaging parameters determined in all 15 patients by both observers resulted in an intraclass correlation coefficient of 0.53 for κ 5min, and 0.91 for κ 17min. A comparison between the two observers showed that one patient (patient 15) with a large and heterogeneous tumor was the main cause of disagreement. When disregarding this patient, and considering 14 out of 15 patients, intraclass correlation coefficient for κ 5min increased to 0.92, while intraclass correlation coefficient for κ 17min did not change.

A large range was observed both for κ 5min (mean 1.28; median 1.12; range 0.87 – 2.07) and κ 17min (mean 1.33; median 1.06; range 0.35 – 3.08). Examples of the DCE curves of 3 patients as measured by one observer are shown in Fig. 1-3. Fig. 1c (patient 9) shows a slow initial uptake of contrast agent, resulting in a low value for κ 5min of 0.76. Seventeen minutes after contrast injection, SI of tumor continues to increase slowly, resulting in an intermediate value for κ 17min of 1.06. Fig. 2c (patient 2) shows another dynamic behaviour: a fast uptake of contrast agent with maximum SI reached already 3min after contrast injection, resulting in κ 5min = 1.67. At later time points the SI remains similar, resulting in κ 17min = 2.79. Generally, a steep slope and an early arrival at equilibrium lead to a higher κ -value, causing the high value of κ 17min in this case. Instead, if the curve continues to increase during the 2nd and 3rd time series, κ 5min and κ 17min have more similar (and lower) values, as illustrated for patient 5 in Fig. 3. In our study, in none of the tumor ROIs a clear decrease of SI could be observed in the covered time frame of 17 min.

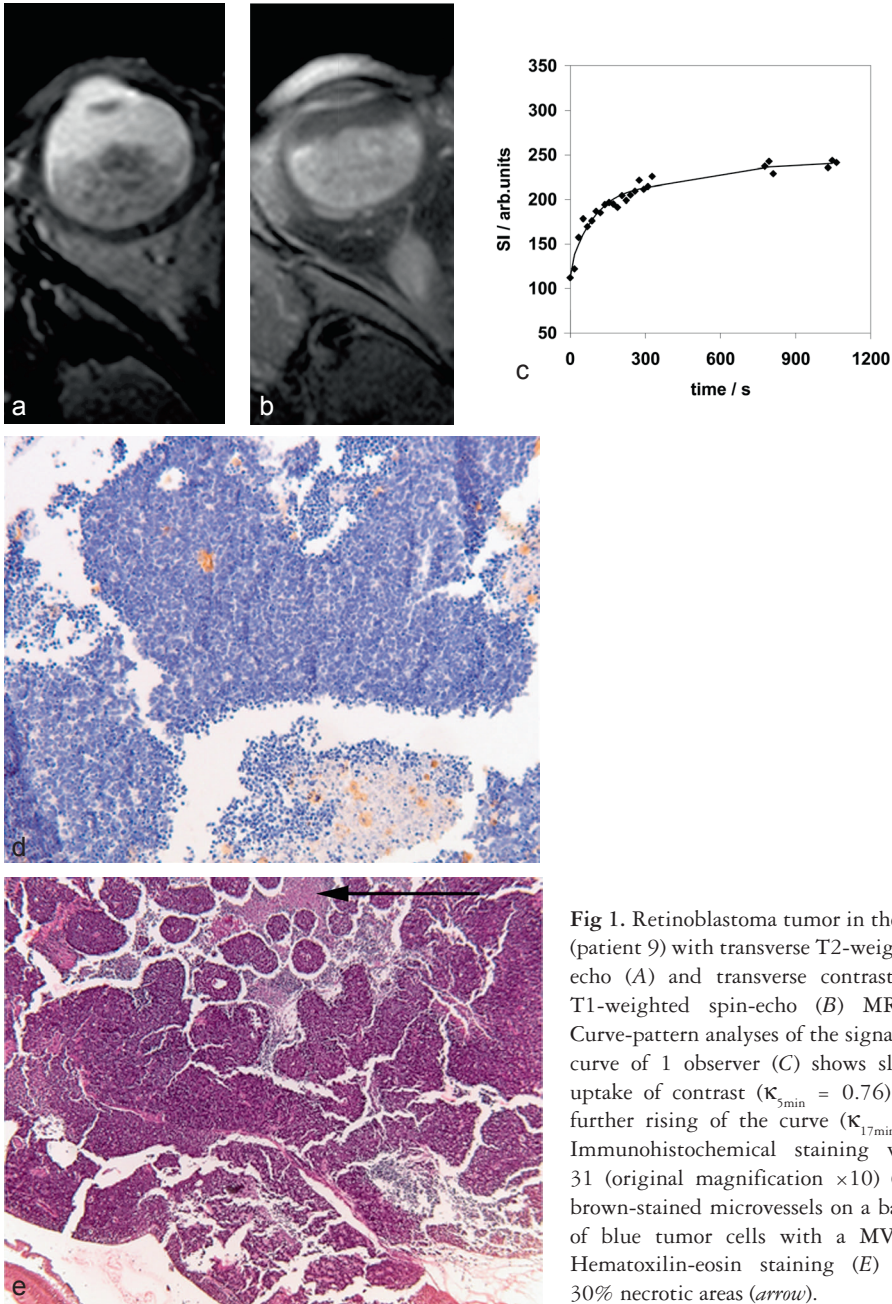


Fig 1. Retinoblastoma tumor in the right eye (patient 9) with transverse T2-weighted spin-echo (A) and transverse contrast-enhanced T1-weighted spin-echo (B) MR images. Curve-pattern analyses of the signal intensity curve of 1 observer (C) shows slow initial uptake of contrast ($\kappa_{5\min} = 0.76$) and slow further rising of the curve ($\kappa_{17\min} = 1.06$). Immunohistochemical staining with CD-31 (original magnification $\times 10$) (D) shows brown-stained microvessels on a background of blue tumor cells with a MVD of 11. Hematoxylin-eosin staining (E) illustrates 30% necrotic areas (arrow).

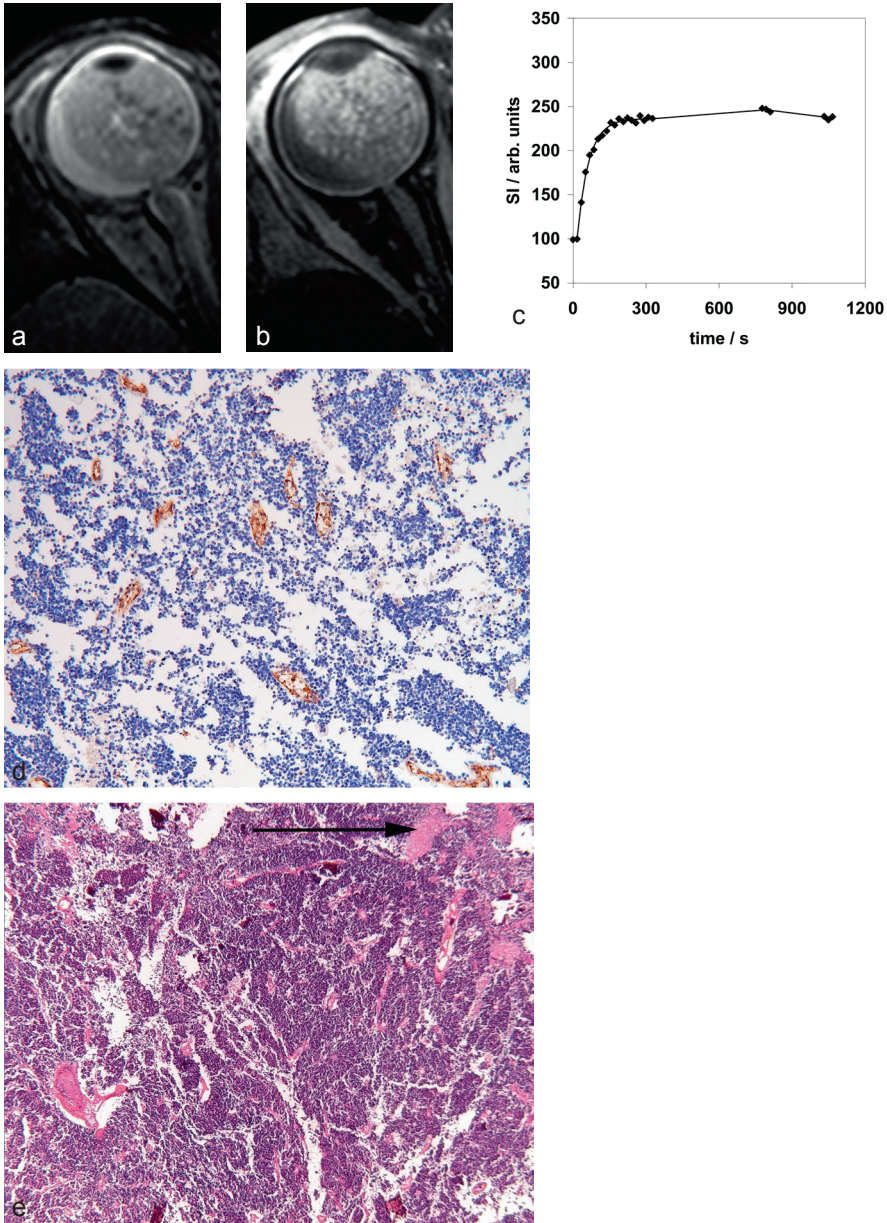


Fig 2. Retinoblastoma tumor in the right eye (patient 2) with transverse T2-weighted spin-echo (A) and transverse contrast-enhanced T1-weighted spin-echo (B) MR images. Curve-pattern analysis of the signal intensity curve of 1 observer (C) shows fast uptake of contrast agent ($\kappa_{5min} = 1.67$) and early arrival at equilibrium ($\kappa_{17min} = 2.79$). Immunohistochemical staining with CD-31 (original magnification $\times 10$) (D) shows a high MVD of 21, and hematoxylin-eosin staining shows only 10% necrosis (arrow) (E).

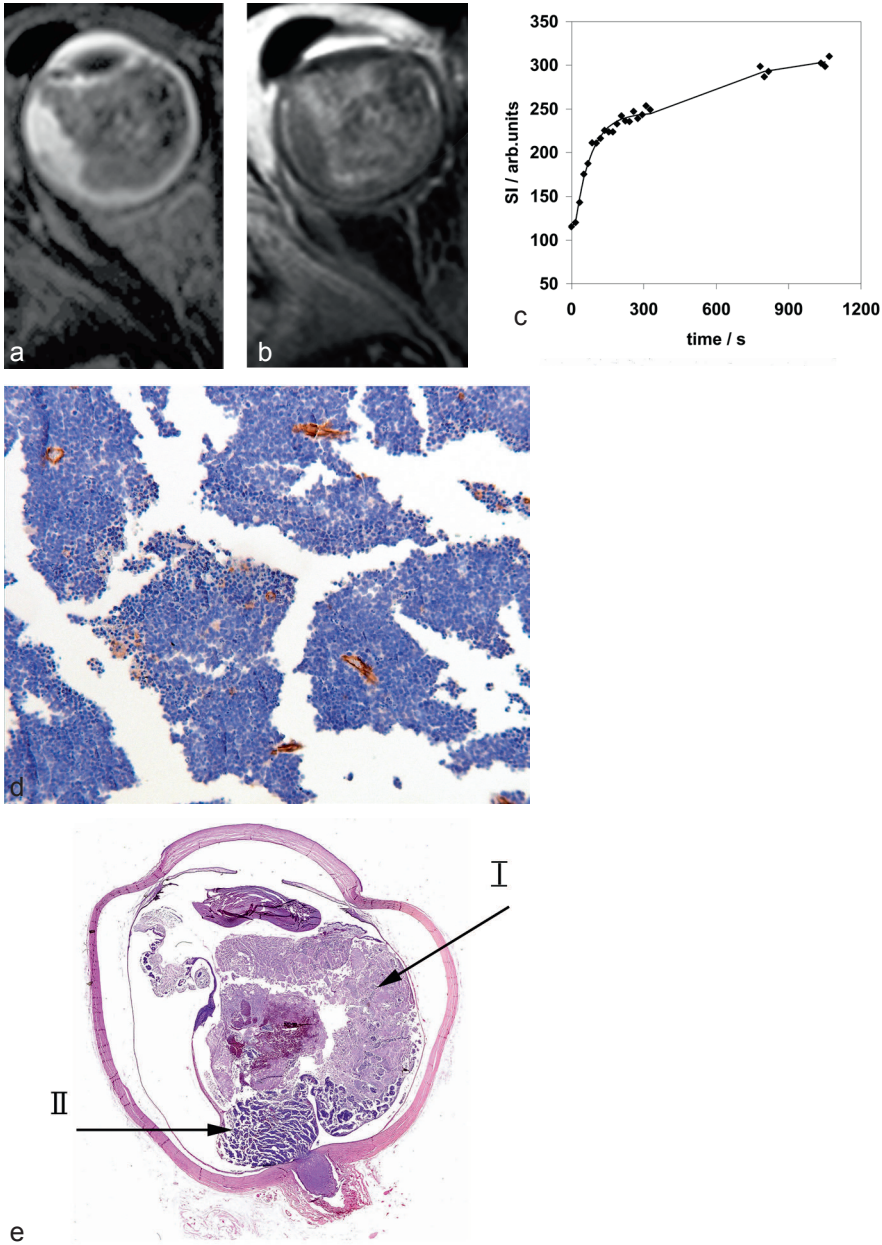


Fig 3. Retinoblastoma tumor in the right eye (patient 5) with transverse T2-weighted spin-echo (A) and transverse contrast-enhanced T1-weighted fat-suppressed spin-echo (B) MR images. Curve-pattern analysis of the signal intensity curve of 1 observer (C) shows a moderate uptake of contrast agent ($\kappa_{5\min} = 1.22$) and a continuing increase leading to $\kappa_{17\min} = 0.84$. Immunohistochemical staining with CD-31 (original magnification $\times 10$) (D) shows an MVD of 14. Hematoxylin eosin staining (E) shows a large area of necrosis (70%) (arrow I) in vital tumor tissue (arrow II).

Histopathologic and Immunohistochemical Findings

The mean amount of tumor necrosis was 29% (median 20%; range 0 – 90%), for example fig. 1-3. Minimal tumor infiltration of the choroid occurred in 1 and inflammation in 2 of the 15 eyes. Massive invasion in choroid is a metastatic risk factor and did not occur in our patients. Post-laminar optic nerve invasion is an important risk factor for extra-ocular recurrence and occurred in 3 eyes. (Pre)laminar optic nerve infiltration occurred in 6 out of 15 eyes. In 6 eyes no optic nerve infiltration was scored. In one patient the optic nerve was cut at surgery at the scleral surface without a stump. The tumor however reached the cut surface and was considered as positive for postlaminar optic nerve invasion. Ten out of 15 tumors were poor-, 4 moderate- and 1 well-differentiated.

The mean value of MVD was 18.4 per 20x field (range, 10 - 37). for example fig. 1-3. VEGF immunoreactivity was positive in 7, weak in 6 and negative in 2 patients. Flt-1 staining was determined as positive in 1 patient, weak in 5 and negative in 9 patients.

Correlation between DCE-MR parameters and Histopathology /Immunohistochemistry

A positive correlation in retinoblastoma was found between κ_{5min} and mean MVD ($P = 0.008$) (Fig.4a) and a negative association between κ_{17min} and the percentage necrosis ($P = 0.002$) (Fig.4b). No statistically significant correlation between κ_{5min} or κ_{17min} was found with other clinical or histopathological data (choroid invasion; resp. $P = 0.66$ and $P = 0.17$, optic nerve invasion; resp. $P = 0.27$ and $P = 0.90$, VEGF; resp. $P = 0.91$ and $P = 0.59$ and Flt-1; resp. $P = 0.14$ and $P = 0.13$). After disregarding patient 15 because of the interobserver disagreement in this patient, results remained similar. In fact, we found an additional positive correlation between κ_{17min} and MVD ($P = 0.03$).

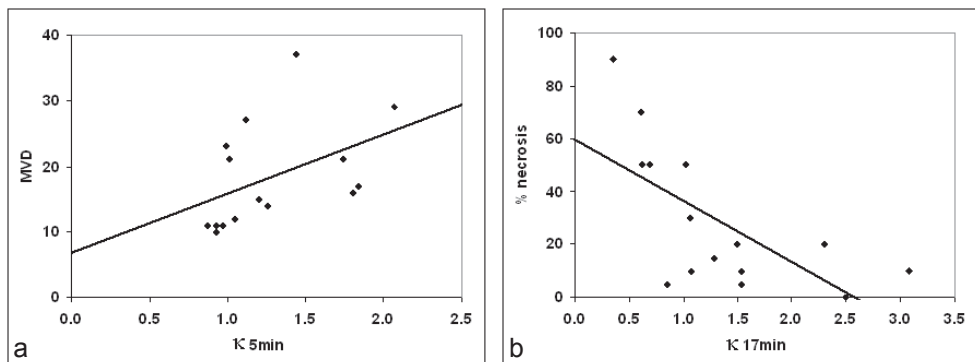


Fig 4. Graphs show the positive correlation (A) between κ_{5min} and mean MVD ($P = .008$) and the negative correlation (B) between κ_{17min} (a measure for late enhancement) and tumor necrosis ($P = .002$).

DISCUSSION

Our study showed that DCE-MR imaging parameters correlated significantly with MVD and tumor necrosis. We observed a statistically significant correlation between mean MVD and $\kappa 5\text{min}$. MVD is an important parameter to assess tumor angiogenesis in vitro, which has been associated with local invasive growth and hematogenous metastases in retinoblastoma (14). Highly vascularized tissue typically shows rapid enhancement after contrast injection. Indeed, tumors with a high MVD were described by a DCE MR imaging curve with a steep slope and therefore a high value of $\kappa 5\text{min}$. The parameter κ obtained with curve pattern analysis has a strong correlation with the rate constant k_{ep} (17). And because k_{ep} has been shown sensitive to treatment in previous literature (22;23) this suggests a similar role for κ .

In addition, we observed a negative correlation between the amount of tumor necrosis and $\kappa 17\text{min}$, a parameter which represents the shape of the curve over a long time frame of 17 minutes. The occurrence of late enhancement is represented by a DCE MR imaging curve that gradually but steadily increases, resulting in a low value of $\kappa 17\text{min}$. In literature, similar curves with late enhancement are associated with tumor necrosis (24;25). Using curve pattern analysis we can semi-quantitatively determine the occurrence of late enhancement, but we cannot differentiate between physiological factors such as vascularization, transfer rates, volume of the interstitial space, or a combination of these factors. Although clearly necrotic areas were not included in the ROIs, DCE MR imaging was sensitive enough to be negatively associated with the degree of necrosis, as also observed in some preclinical tumor models (26). In necrotic tumors, the central portions of the tumor become relatively hypovascular and eventually necrotic as the tumor grows (27). This regional hypoxia induces damage to vessels in the border zones adjacent to central necrosis (28). We assume that at a later stage, contrast may leak from the damaged vessels into the more vital parts of the tumor, causing late enhancement.

Severe hypoxia, present in necrotic tumors, contributes to resistance to radiation therapy and decreases the efficacy of cytotoxic drugs including carboplatin and melphalan (29;30). These are both important chemotherapeutic agents in retinoblastoma treatment for chemoreduction and selective intra-arterial chemotherapy, respectively. Thus, evaluation of $\kappa 17\text{min}$ as a non-invasive marker for tumor necrosis could become a useful parameter in the choice of treatment or to monitor treatment response (31;32). Other treatment strategies, such as vascular targeting with antiangiogenic (anti-VEGF drugs) and angiostatic agents, are emerging as a possible treatment option for retinoblastoma (33-36). VEGF is correlated with tumor MVD in different tumors (37-39). Although we observed a correlation between $\kappa 5\text{min}$ and MVD, we did not find an association between DCE-MR imaging parameters and VEGF, possibly due to small sample size.

Although not directly related to physiological parameters, curve pattern analysis could prove a stable measure for DCE-MR imaging analysis. The method has only recently been suggested, and has not yet been generally used. Application in retinoblastoma and the correlation with

MVD and necrosis suggest the applicability of this curve pattern analysis method, which does not require arterial input function or baseline T1 relaxation time measurements.

Some limitations of our study should be addressed. The spatial alignment of MR imaging and histopathology is not perfect. Because of the poverty of clear landmarks it is difficult to get the same cross-section between MR imaging and histopathologic specimens. However, tumor angiogenesis influences all vital tumor tissue and not only the part in which the ROI was placed, as can be concluded from the convincing correlation between $\kappa_{17\text{min}}$ and mean MVD. In our study, the intraclass correlation coefficient of 0.53 for $\kappa_{5\text{min}}$ indicated only modest agreement. This low intraclass correlation coefficient was due to only one patient with a large and heterogeneous tumor, while for the other 14 patients the interobserver agreement of both κ -values was excellent. Especially in large heterogeneous tumors a localized comparison between histopathology and DCE-MR imaging will be useful. For instance, it may be expected that a voxel-wise evaluation of DCE-MR imaging data of the whole tumor will separately identify highly vascularized regions and regions near necrotic areas based on high $\kappa_{5\text{min}}$ in and low $\kappa_{17\text{min}}$, respectively. In this respect, a higher field strength of 3T, possibly in combination with a multi-channel head coil, would be advantageous for voxel-wise evaluations, because of the higher signal-to-noise ratio. Another study limitation is the 17 minutes time frame of DCE-MR imaging after contrast injection. In this time frame we did not observe a decrease of SI which would be interpreted as washout of contrast agent. Although in other tumor types this curve pattern is common, and characteristic for a malignant tumor (40;41), it was not observed in these 15 cases of retinoblastoma. Finally, because of the small size of our patient cohort our findings have to be considered preliminary and therefore the discriminatory value of DCE MR imaging in predicting aggressive in a single patient is not possible yet. Our results are the first in DCE MR imaging in retinoblastoma patients and need validation in a much larger group of patients, preferentially in a multicentric study.

In conclusion, in retinoblastoma the early phase of the DCE time curve positively correlates with MVD, while the presence of late enhancement is correlated with necrosis. Thus, the potential for DCE-MR imaging to non-invasively assess angiogenesis and necrosis in retinoblastoma tumors is promising and warrants further investigation.

REFERENCES

1. Abramson DH, Dunkel IJ, Brodie SE, Marr B, Gobin YP. Superselective ophthalmic artery chemotherapy as primary treatment for retinoblastoma (chemosurgery). *Ophthalmology* 2010;117:1623-9.
2. Gobin YP, Dunkel IJ, Marr BP, Brodie SE, Abramson DH. Intra-arterial Chemotherapy for the Management of Retinoblastoma: Four-Year Experience. *Arch.Ophthalmol.* 2011;129:732-7.
3. Suzuki S, Yamane T, Mohri M, Kaneko A. Selective ophthalmic arterial injection therapy for intraocular retinoblastoma: the long-term prognosis. *Ophthalmology* 2011;118:2081-7.
4. Marback EF, Arias VE, Paranhos A, Jr., Soares FA, Murphree AL, Erwenne CM. Tumour angiogenesis as a prognostic factor for disease dissemination in retinoblastoma. *Br.J.Ophthalmol.* 2003;87:1224-8.
5. Uusitalo MS, Van Quill KR, Scott IU, Matthay KK, Murray TG, O'Brien JM. Evaluation of chemoprophylaxis in patients with unilateral retinoblastoma with high-risk features on histopathologic examination. *Arch.Ophthalmol.* 2001;119:41-8.
6. Schueler AO, Hosten N, Bechrakis NE, Lemke AJ, Foerster P, Felix R et al. High resolution magnetic resonance imaging of retinoblastoma. *Br.J.Ophthalmol.* 2003;87:330-5.
7. Lemke AJ, Kazi I, Mergner U, Foerster PI, Heimann H, Bechrakis N et al. Retinoblastoma - MR appearance using a surface coil in comparison with histopathological results. *Eur.Radiol.* 2007;17:49-60.
8. Honavar SG, Singh AD, Shields CL, Meadows AT, Demirci H, Cater J et al. Postenucleation adjuvant therapy in high-risk retinoblastoma. *Arch.Ophthalmol.* 2002;120:923-31.
9. de Graaf P, van d, V, Moll AC, Imhof SM, Schouten-van Meeteren AY, Knol DL et al. Contrast-enhancement of the anterior eye segment in patients with retinoblastoma: correlation between clinical, MR imaging, and histopathologic findings. *AJNR Am.J.Neuroradiol.* 2010;31:237-45.
10. de Graaf P, Goricke S, Rodjan F, Galluzzi P, Maeder P, Castelijns JA et al. Guidelines for imaging retinoblastoma: imaging principles and MRI standardization. *Pediatr.Radiol.* 2012 Jan;42(1):2-14.
11. Chantada GL, Dunkel IJ, Antoneli CB, de Davila MT, Arias V, Beaverson K et al. Risk factors for extraocular relapse following enucleation after failure of chemoreduction in retinoblastoma. *Pediatr. Blood Cancer* 2007;49:256-60.
12. Chantada GL, Casco F, Fandino AC, Galli S, Manzitti J, Scopinaro M et al. Outcome of patients with retinoblastoma and postlaminar optic nerve invasion. *Ophthalmology* 2007;114:2083-9.
13. Brisse HJ, Guesmi M, Aerts I, Sastre-Garau X, Savignoni A, Lumbroso-Le RL et al. Relevance of CT and MRI in retinoblastoma for the diagnosis of postlaminar invasion with normal-size optic nerve: a retrospective study of 150 patients with histological comparison. *Pediatr.Radiol.* 2007;37:649-56.
14. Rossler J, Dietrich T, Pavlakovic H, Schweigerer L, Havers W, Schuler A et al. Higher vessel densities in retinoblastoma with local invasive growth and metastasis. *Am.J.Pathol.* 2004;164:391-4.
15. Brasch RC. New directions in the development of MR imaging contrast media. *Radiology* 1992;183:1-11.
16. de Lussanet QG, Langereis S, Beets-Tan RG, van Genderen MH, Griffioen AW, van Engelshoven JM et al. Dynamic contrast-enhanced MR imaging kinetic parameters and molecular weight of dendritic contrast agents in tumor angiogenesis in mice. *Radiology* 2005;235:65-72.
17. Guo JY, Reddick WE. DCE-MRI pixel-by-pixel quantitative curve pattern analysis and its application to osteosarcoma. *J.Magn Reson.Imaging* 2009;30:177-84.
18. Hamm B, Wolf KJ. Contrast material for computed tomography and magnetic resonance imaging of the gastrointestinal tract. *Curr.Opin.Radiol.* 1991;3:474-82.
19. Ikeda O, Nishimura R, Miyayama H, Yasunaga T, Ozaki Y, Tuji A et al. Evaluation of tumor angiogenesis using dynamic enhanced magnetic resonance imaging: comparison of plasma vascular endothelial growth factor, hemodynamic, and pharmacokinetic parameters. *Acta Radiol.* 2004;45:446-52.
20. Verstraete KL, De DY, Roels H, Dierick A, Uyttendaele D, Kunnen M. Benign and malignant musculoskeletal lesions: dynamic contrast-enhanced MR imaging--parametric "first-pass" images depict tissue vascularization and perfusion. *Radiology* 1994;192:835-43.

21. Tofts PS, Brix G, Buckley DL, Evelhoch JL, Henderson E, Knopp MV et al. Estimating kinetic parameters from dynamic contrast-enhanced T(1)-weighted MRI of a diffusable tracer: standardized quantities and symbols. *J.Magn Reson.Imaging* 1999;10:223-32.
22. Cho JH, Cho G, Song Y, Lee C, Park BW, Lee CK et al. Feasibility of FAIR imaging for evaluating tumor perfusion. *J.Magn Reson.Imaging* 2010;32:738-44.
23. Padhani AR, Husband JE. Dynamic contrast-enhanced MRI studies in oncology with an emphasis on quantification, validation and human studies. *Clin.Radiol.* 2001;56:607-20.
24. Cho H, Ackerstaff E, Carlin S, Lupu ME, Wang Y, Rizwan A et al. Noninvasive multimodality imaging of the tumor microenvironment: registered dynamic magnetic resonance imaging and positron emission tomography studies of a preclinical tumor model of tumor hypoxia. *Neoplasia.* 2009;11:247-59, 2p.
25. Dadiani M, Margalit R, Sela N, Degani H. High-resolution magnetic resonance imaging of disparities in the transcappillary transfer rates in orthotopically inoculated invasive breast tumors. *Cancer Res.* 2004;64:3155-61.
26. Egeland TA, Gaustad JV, Galappathi K, Rofstad EK. Magnetic resonance imaging of tumor necrosis. *Acta Oncol.* 2011;50:427-34.
27. Miles KA. Tumour angiogenesis and its relation to contrast enhancement on computed tomography: a review. *Eur.J.Radiol.* 1999;30:198-205.
28. Saeed M, Lund G, Wendland MF, Bremerich J, Weinmann H, Higgins CB. Magnetic resonance characterization of the peri-infarction zone of reperfused myocardial infarction with necrosis-specific and extracellular nonspecific contrast media. *Circulation* 2001;103:871-6.
29. Beasley NJ, Wykoff CC, Watson PH, Leek R, Turley H, Gatter K et al. Carbonic anhydrase IX, an endogenous hypoxia marker, expression in head and neck squamous cell carcinoma and its relationship to hypoxia, necrosis, and microvessel density. *Cancer Res.* 2001;61:5262-7.
30. Vaupel P, Harrison L. Tumor hypoxia: causative factors, compensatory mechanisms, and cellular response. *Oncologist.* 2004;9 Suppl 5:4-9.
31. Jockovich ME, Suarez F, Alegret A, Pina Y, Hayden B, Cebulla C et al. Mechanism of retinoblastoma tumor cell death after focal chemotherapy, radiation, and vascular targeting therapy in a mouse model. *Invest Ophthalmol.Vis.Sci.* 2007;48:5371-6.
32. Mineo TC, Mineo D, Onorati I, Cufari ME, Ambrogio V. New Predictors of Response to Neoadjuvant Chemotherapy and Survival for Invasive Thymoma: a Retrospective Analysis. *Ann.Surg.Oncol.* 2010.
33. Jockovich ME, Bajenaru ML, Pina Y, Suarez F, Feuer W, Fini ME et al. Retinoblastoma tumor vessel maturation impacts efficacy of vessel targeting in the LH(BETA)T(AG) mouse model. *Invest Ophthalmol.Vis.Sci.* 2007;48:2476-82.
34. Knopp MV, Weiss E, Sinn HP, Mattern J, Junkermann H, Radeleff J et al. Pathophysiologic basis of contrast enhancement in breast tumors. *J.Magn Reson.Imaging* 1999;10:260-6.
35. George ML, Dzik-Jurasz AS, Padhani AR, Brown G, Tait DM, Eccles SA et al. Non-invasive methods of assessing angiogenesis and their value in predicting response to treatment in colorectal cancer. *Br.J.Surg.* 2001;88:1628-36.
36. Lee SY, Kim DK, Cho JH, Koh JY, Yoon YH. Inhibitory effect of bevacizumab on the angiogenesis and growth of retinoblastoma. *Arch.Ophthalmol.* 2008;126:953-8.
37. Mattern J, Koomagi R, Volm M. Association of vascular endothelial growth factor expression with intratumoral microvessel density and tumour cell proliferation in human epidermoid lung carcinoma. *Br.J.Cancer* 1996;73:931-4.
38. Stitt AW, Simpson DA, Boockch C, Gardiner TA, Murphy GM, Archer DB. Expression of vascular endothelial growth factor (VEGF) and its receptors is regulated in eyes with intra-ocular tumours. *J.Pathol.* 1998;186:306-12.
39. Viglietto G, Romano A, Maglione D, Rambaldi M, Paoletti I, Lago CT et al. Neovascularization in human germ cell tumors correlates with a marked increase in the expression of the vascular endothelial growth factor but not the placenta-derived growth factor. *Oncogene* 1996;13:577-87.
40. Buadu LD, Murakami J, Murayama S, Hashiguchi N, Sakai S, Masuda K et al. Breast lesions: correlation of contrast medium enhancement patterns on MR images with histopathologic findings and tumor angiogenesis. *Radiology* 1996;200:639-49.

41. Pennasilico GM, Arcuri PP, Laschena F, Potenza C, Ruatti P, Bono R et al. Magnetic resonance imaging in the diagnosis of melanoma: in vivo preliminary studies with dynamic contrast-enhanced subtraction. *Melanoma Res.* 2002;12:365-71.

Chapter 4

*Detection of calcifications in retinoblastoma using
gradient-echo MR imaging sequences:
comparative study between in-vivo MR imaging
and ex-vivo high resolution CT*

Firazia Rodjan

Pim de Graaf

Paul van der Valk

Theodora Hadjistilianou

Alfonso Cerase

Paolo Toti MD

Marcus C. de Jong

Annette C. Moll

Jonas A. Castelijns

Paolo Galluzzi MD

on behalf of the European Retinoblastoma Imaging Collaboration (ERIC)

ABSTRACT

Background: Intratumoral calcifications are very important in the diagnosis of retinoblastoma. Although CT is considered to be superior in detecting calcification, the radiation hazard in especially hereditary retinoblastoma patients should be avoided. The purpose of our study is to validate the value of T2*WI for detection of calcifications in retinoblastoma with ex-vivo CT as gold standard.

Materials and methods: Twenty-two consecutive patients with retinoblastoma (mean age, 21 months, range 1-71 months) with enucleation as primary treatment were imaged with a 1.5 T using a dedicated surface coil. Signal intensity void (SIV) indicating calcification on T2*WI were compared with ex-vivo high resolution CT (HRCT) and correlation was scored by two independent observers as poor, moderate or good correlation. Other parameters included shape and location of SIVs. In five tumors susceptibility-weighted images (SWI) were evaluated.

Results: All calcifications visible on HRCT could be matched with SIVs on T2*WI and correlation was scored as good in 17 (77%) and moderate in 5 (23%) eyes. In total, 93% (25/27) of the SIVs inside the tumor correlated with calcifications compared to none (0/8) of the SIVs outside the tumor. Areas of nodular shaped SIVs correlated with calcifications in 92% (24/26) and linear shaped SIVs correlated with hemorrhage in 67% (6/9) of the cases. The correlation between SIVs on SWI was better in 4 out of 5 tumors compared to T2*WI.

Conclusion: SIVs on in-vivo T2*WI correlates good with calcifications on ex-vivo HRCT in retinoblastoma. Gradient-echo sequences may be helpful in the differential diagnosis of retinoblastoma. Therefore the combination of fundoscopy, ultrasound and high-resolution MRI with gradient-echo sequences should become the standard diagnostic approach to diagnose retinoblastoma.

BACKGROUND

Retinoblastoma is generally treated on basis of fundoscopic, ultrasound and imaging findings without prior histopathologic confirmation of diagnosis. Prevalence of calcifications is approximately 85%¹, and is considered to be the key-finding in differentiating retinoblastoma from simulating lesions (Coats disease, persistent hyperplastic primary vitreous (PHPV) or toxocara endophthalmitis) in young children². Only rare cases such as medulloepithelioma and retinocytoma, may also contain calcifications causing difficulty in clinical and radiological differentiation³.

Ultrasound is the most commonly used imaging technique for evaluation of intraocular tumors. Combination of fundoscopy and ultrasound allows for the identification of calcifications in 91%-95% of patients⁴. However, sensitivity for depiction of small calcifications decreases in the presence of massive retinal detachment, vitreous hemorrhage and subretinal fluid, sometimes hampering confirmation of diagnosis. In these complicated eyes, CT is likely the method of choice for studying intraocular calcifications with reported sensitivities of 81%–96%⁵. However, its diagnostic performance in staging retinoblastoma disease extent is limited and the theoretical increased risk of radiation induced cataract and fatal cancers in children who underwent CT should be considered⁶. Especially, since hereditary patients are at an even higher risk to develop radiation induced tumors compared to normal children.

MRI is the non-invasive technique of choice for evaluation of retinoblastoma. The combination of ultrasound and MRI are considered to be the first-line diagnostic tools in the evaluation of children with suspected retinoblastoma, surpassing CT⁷. However, MRI does not allow facile identification of tumoral calcifications on routinely used clinical sequences. The lack of spatial resolution with standard clinical sequences provides an additional challenge for visualization of small punctate tumoral calcifications. Scarce data on high-resolution ocular MRI using surface coils show that various amounts of calcifications can be detected with reasonable diagnostic accuracy⁸.

Gradient-echo T2*-weighted imaging (T2*WI) sequences are sensitive to susceptibility differences among tissues that cause magnetic field inhomogeneity leading to signal loss and is used to depict blood products, deoxygenated venous blood in dilated vessels (venous congestion) and calcifications^{9,10}. Previous work by Galluzzi et al showed that T2*WI can be a feasible technique to detect intraocular calcifications¹¹. Calcified areas in retinoblastoma emerged as hypointense foci of signal intensity voids (SIVs) within the soft tissue mass. Most of the SIVs on T2*WI correlated to spots of intratumoral of calcifications on CT. However, it was not investigated if the shape and spatial arrangement of the intra-ocular SIVs on MR can all be matched with calcifications on CT. Especially, since additional SIVs can appear on high-resolution T2*WI, without a corresponding hyperintensity on CT.

The purpose of our study is to assess the ability of gradient echo T2*WI in visualization and morphologic evaluation of retinoblastoma calcifications and to compare T2*WI with ex-vivo CT scans of the enucleated eyes as gold standard.

MATERIALS AND METHODS

Patient population

This study included patients from two European retinoblastoma reference centers and was performed in agreement with recommendations of both local ethics committees, with waiver of informed consent. From October 2009 to September 2011, retinoblastoma patients diagnosed with fundoscopy and ultrasound under general anesthesia, were included if: (a) adequate pretreatment T2*WI was available, (b) enucleation of the eye was the primary treatment for retinoblastoma and (c) high-resolution CT (HRCT) images of the enucleated eye were present. In patients with bilateral retinoblastoma, only the most affected eye was enucleated and included. Three patients were excluded because of inadequate T2*WI. Final study population included 22 patients. Patient records were reviewed for age at retinoblastoma diagnosis.

MR imaging

Pre-treatment MRI examinations were performed under general-anesthesia on 1.5T systems (Siemens Avanto or Sonata; Erlangen, Germany) using a dedicated surface coil (loop- or temporo-mandibular coils featuring a diameter of 4 and 7 cm, respectively) focused on the (most) affected eye. Imaging was performed according to published guidelines⁷. In all patients, MR images included transverse and sagittal spin-echo T1W imaging (repetition time/echo time 300-420/13-15ms; slice thickness 2mm), transverse spin-echo T2WI (1200-2470/120-166ms; 2mm) and transverse 2D T2*WI (300-650/15-25ms; 2mm). Additionally, 5 patients underwent susceptibility-weighted imaging (SWI) (TR/TE 46/38ms, matrix 192×162, voxel size 0.4×0.6×1 mm³, no gap, 35 slices, averages = 2, flip angle 15°, acquisition time 7.34 min. SWI datasets included phase images and minimum intensity projection (minIP) images.

Ex-vivo HRCT

HRCT was performed immediately after enucleation of the eye using either a BrightSpeed (GE Healthcare, Milwaukee, Wis.) or Sensation-64 (Siemens, Erlangen, Germany) system. Eyes were carefully positioned in a small cardboard tray supported with gauze and in the same orientation as the transverse plane of the MR images. Axial images were acquired with a section thickness of 0.6mm, collimation of 0.5mm, pitch of 0.8, 120kV, 250 mAs, field of view 16cm and a 512×512 matrix. From the raw data, individual data sets were reformatted into images of 0.6mm slice thickness in all 22 eyes. Raw data remained available for additional multi-planar reconstructions, which were made afterwards by one observer (FR) to provide accurate information of the obtained

data in the axial plane. Finally, two data sets of CT images were reconstructed and were available for all patients; one with slice thickness of 2mm (the same orientation and slice-thickness as T2*WI) and one with very thin slices (0.6mm).

Image analysis

Retrospectively, two independent observers (P.G. and P.d.G., with 15 and 11-years of experience in ocular MRI, respectively), reviewed all T2*WI and HRCT images. Afterwards, differences in scoring were resolved in consensus. Both observers were blinded to results of clinical and histopathological findings. Ex-vivo HRCT was considered to be the gold standard for detecting calcifications. Presence or absence of calcifications on HRCT was assessed. Calcifications were defined as hyperdense foci within the tumor on HRCT images. MR images were independently reviewed by the same observers. After analyzing the MR images, detection of calcifications was confirmed in correlation with HRCT images by using anatomical landmarks so as to adjust for section thicknesses, angulation, and obliquity. Criteria used to define calcifications on MR were as follows: calcifications had to have the same morphologic pattern as on the HRCT (same shape and same spatial arrangement), and were considered to be localized foci of marked hypointense SIV on T2*WI. Correspondence between intraocular hyperdense areas on CT and intraocular SIV observed on MRI were scored as good, moderate or poor. Good correspondence was scored if all calcifications on HRCT perfectly matched with SIV on T2*WI, whether or not with the presence of evident artifacts or hemorrhage on MRI. Moderate correspondence was scored if there was an evident correlation between MRI and HRCT in some parts of the tumor, but additional SIVs on MRI were present without an evident explanation on basis of other MR sequences or hyperdense structures on CT. If no correlation could be observed at all, the correspondence was scored as poor. Location of SIVs in the tumor was categorized as central, peripheral or a combination of both. Shape of SIVs was categorized as nodular or linear. SIVs on T2*WI secondary to intravitreal or subretinal hemorrhage were considered if fluid-fluid levels (in correspondence with T2WI) or a smooth hypointense outlining of tumor or retina was present in the affected eye. Eyes with moderate or poor correlation based on (additional) SIVs without corresponding calcification on HRCT, or other explanation on conventional MR sequences were selected for additional correlation with histopathology. In 5 tumors SIVs in SWI images were evaluated and compared with the T2*WI and were scored as worse, equal or better correlation with calcifications on HRCT. Furthermore, feasibility of using phase images for detection of calcifications in retinoblastoma was studied. Calcium undergoes a positive phase shift (paramagnetic susceptibility) and is displayed as a high SI area on the phase image, whereas a negative phase shift (diamagnetic susceptibility) occurs for veins, iron, and hemorrhage, making them appear uniformly dark.

Histopathologic examination

Eyes were fixed in saline-buffered formalin, sampled, embedded in paraffin and sectioned in the same orientation as the axial plane of the MR images (thickness 4 μm) and stained with hematoxylin-eosin. Histopathological slices were only evaluated in tumors with additional SIVs on T2*WI without evident cause on other MR sequences or CT by two pathologists (P.v.d.V and P.T.).

RESULTS

All 22-patients (22-eyes) in this study had histopathological proven retinoblastoma (mean age 21-months; range, 1-73months). Mean time-interval between diagnosis and MRI was 5-days (range 0-8days). Mean time-interval between MRI and CT was 5-days (range 0-8days). Patient characteristics are summarized in table 1.

Table 1: Patient findings and correlation of CT with MRI in calcium detection

Patient (lat)	Age	Int. MR-En	Corr. T2*WI-CT	SWI	Corr. T2*WI-SWI
1 (U)	1	1	moderate	no	NA
2 (U)	4	8	moderate	no	NA
3 (U)	46	6	moderate	no	NA
4 (U)	3	0	moderate	no	NA
5 (U)	26	6	moderate	no	NA
6 (U)	73	1	well	no	NA
7 (B)	8	4	well	no	NA
8 (U)	11	5	well	no	NA
9 (U)	8	1	well	no	NA
10 (U)	16	1	well	no	NA
11 (U)	3	8	well	no	NA
12 (B)	12	8	well	no	NA
13 (B)	35	8	well	no	NA
14 (U)	29	1	well	nn	NA
15 (B)	29	8	well	no	NA
16 (B)	13	6	well	no	NA
17 (U)	45	8	well	no	NA
18 (U)	5	8	well	yes	equal
19 (U)	9	7	well	yes	better
20 (U)	38	1	well	yes	better
21 (U)	5	8	well	yes	better
22 (U)	37	5	well	yes	better

lat= tumor laterality, int. MR-En= interval MRI and enucleation, Corr = correlation, T2*WI= T2*weighted imaging, SWI= susceptibility weighted imaging
 median age 12,5
 mean age 20,73

Areas of calcification were present on HRCT in the tumors of all 22-eyes. Furthermore, all eyes showed foci of SIVs on T2*WI. A total of 35 areas of SIVs were depicted; 27 areas of SIVs inside the tumor and 8 areas outside the tumor. Shape was classified as nodular (n=26) and linear (n=9). Nodular SIVs were predominantly located within the tumor (25 out of 26 SIVs; 96 %) and 19 (76%) in the tumor center, whereas linear shaped SIVs were predominantly located outside the tumor (7 out of 9 SIVs; 78%). Of the two linear SIVs, one was located at the periphery of the tumor while the other was located centrally within the tumor.

Correlation between calcifications on CT and areas SIVs on T2*WI was scored as good in 17 (77%) and moderate in 5 (23%) eyes. Poor correlations were not observed. Of 27 areas of SIVs located inside the tumor, 25 areas (93%) correlated with calcifications, 1 with intratumoral hemorrhage and 1 with dilated venous vessel (venous congestion). Of the 8 areas of SIVs located outside the tumor, 6 (75%) correlated with hemorrhage (5 subretinal and 1 intratumoral) and 2 with susceptibility artifacts secondary to air-tissue interface. Areas of nodular shaped SIVs correlated to calcifications in 92% (24/26) and linear shaped SIVs correlated to hemorrhage in 67% (6/9).

The 17 good-corresponding eyes showed evident matching (same shape and same spatial arrangement) between hyperdense structures on CT and areas of SIVs on T2*WI (Fig.1). Additional SIVs in good-corresponding tumors were mostly located outside the tumor with a linear aspect corresponding with artifacts or hemorrhage (Fig. 2). In 3 good-corresponding tumors additional SIVs were observed on T2*WI, and did not have any corresponding hyperdensity on HRCT. However, on histopathology, these SIVs did correlate with spots of calcifications (Fig. 3). 1

In 5 moderately-corresponding eyes, the hypointense areas on MRI could only be correlated in part with hyperdense areas on CT. Additional SIVs were all located outside the tumor and correlated with hemorrhage and venous congestion.

Discrepancies between observers occurred in two good-corresponding cases. In one case a linear hypointense structure which indicated hemorrhage caused confusion. In the other case more SIVs were observed on MRI compared to the poor resolution of CT. The spots of calcification on CT however matched well with T2*WI.

In 5 patients SWI datasets were available and all eyes were good-corresponding. In 4 eyes the correlation between SIVs on SWI images and the calcifications on HRCT was better compared to the T2*WI images (Fig. 4) and in 1 eye the correlation showed no difference between the two gradient-echo techniques. In two patients the quality of the phase images was diminished due to image distortions. Phase images showed hyperintense SI of calcification in the other 3 eyes, which was confirmed on the HRCT. None of these eyes showed intraocular or intratumoral hemorrhage clinically or on histopathology.

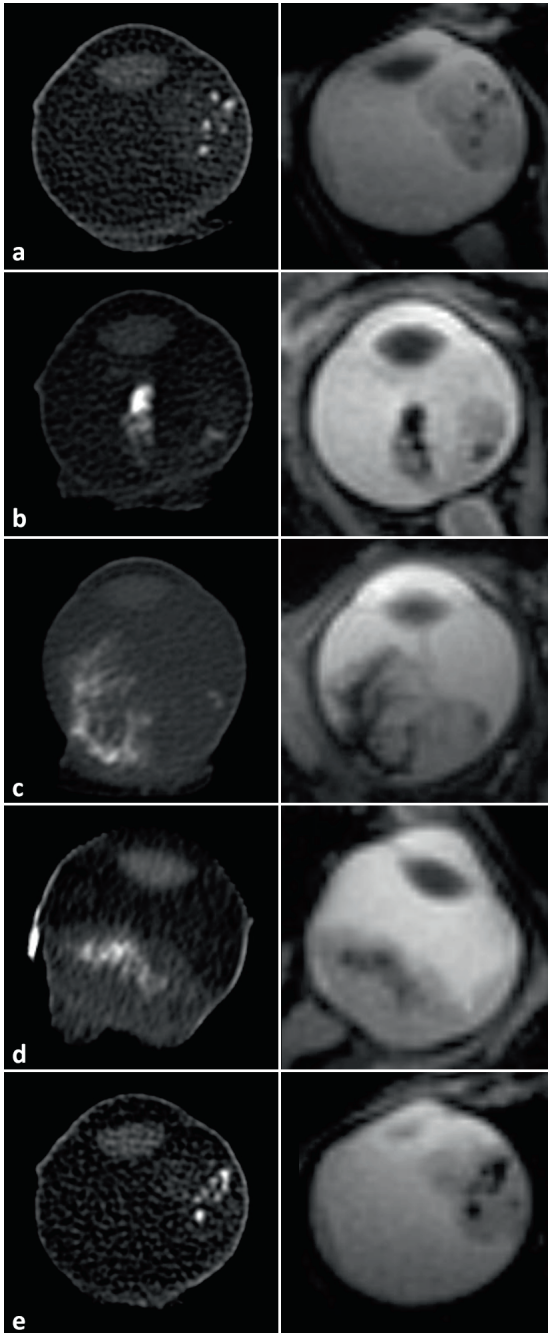


Fig. 1: Excellent-matching hyperdense calcifications on ex-vivo high-resolution CT (left column) with signal intensity void spots on gradient-echo T2*-weighted MR images (right column) in patient 12 [a], 16 [b], 18 [c], 19[d], 14 [e].

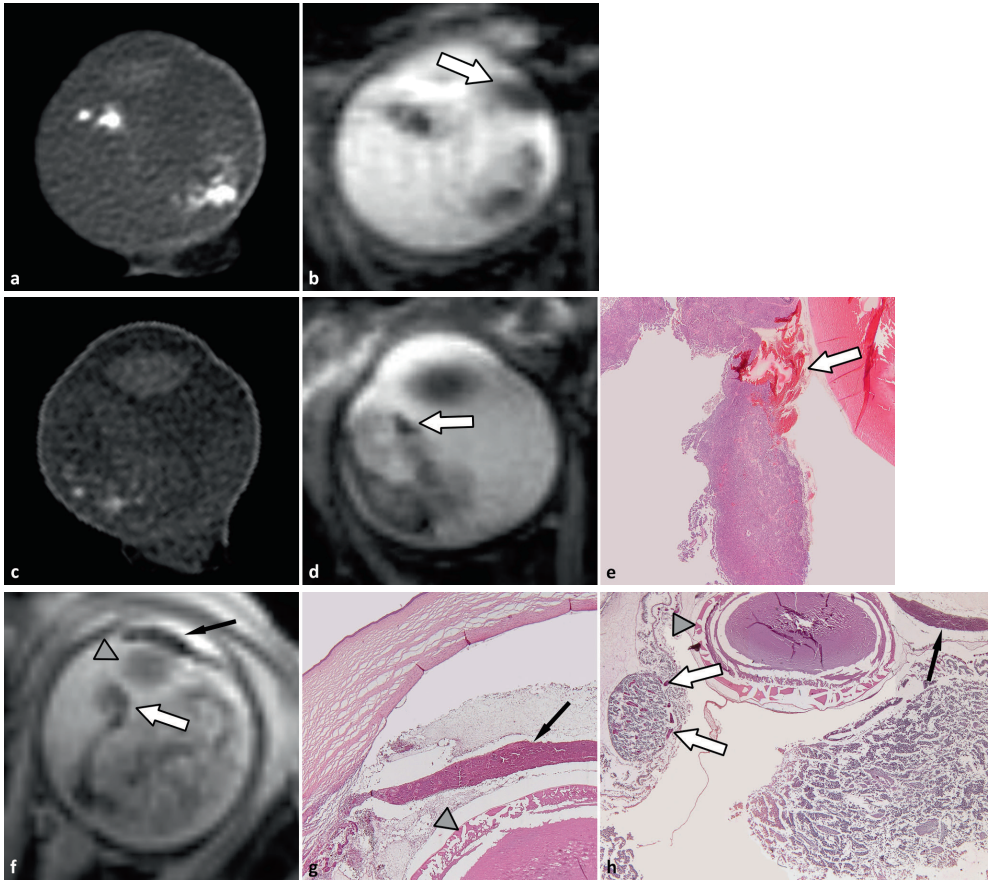


Fig. 2: Examples of additional signal intensity voids on T2*-weighted MR images without correspondence with ex-vivo high resolution CT.

Patient 13 shows a hypo-intense nodular structure (a) in the anterior part of the eye (arrow) on T2*-weighted imaging without corresponding hyperdensity on ex-vivo high-resolution CT (b). Histopathology demonstrated a hemorrhage (arrow) precisely matching this additional SIV (c). Adjacent to this hemorrhage multiple linear-arranged spots matched with hyperdense spots on CT.

In patient 11 (d) a linear band of SIV on T2*WI is shown outside the tumor along the detached retina (white arrow) as well as in the iris (black arrow). The grey arrowhead is pointing to the lens which is dislocated. Histology (e, f) showed necrotic tumor with dilated vessels (venous congestion) (white arrow) and hemorrhagic necrosis of the iris also combined with venous congestion (black arrow). The anterior chamber is infiltrated by neoplastic cells and cellular debris.

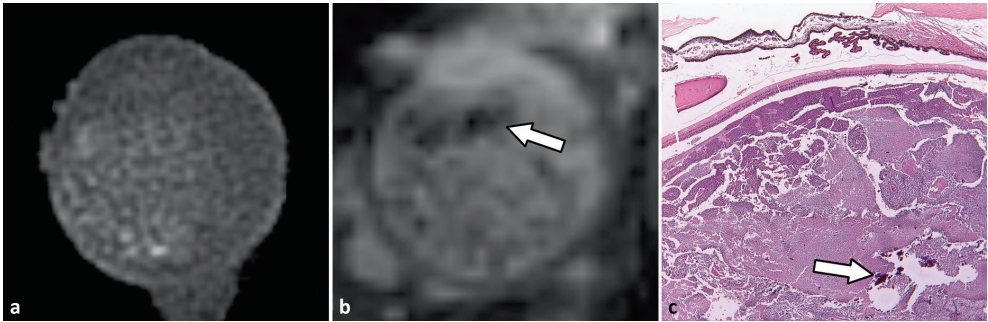


Fig. 3: Extra signal intensity void spots in the anterior part of the eye on gradient echo T2*-weighted images (arrow) (a) were observed in patient 21 with excellent correspondence with HRCT (b). However, a band of additional signal intensity void spots were present in the anterior part of the tumor on gradient-echo T2*-weighted MR image (arrow) without correspondence on ex-vivo high-resolution CT. Histopathologic correlation (c) showed multiple foci of calcifications in the anterior part of the tumor (arrow).

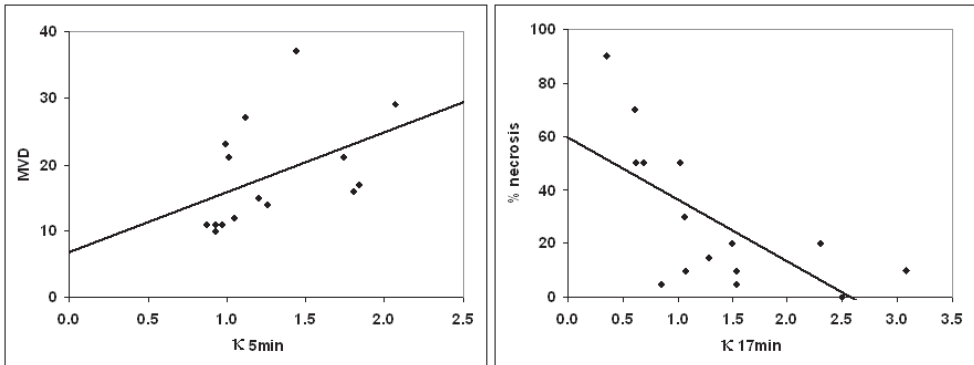


Fig. 4: Value of phase imaging in identifying calcification in retinoblastoma (patient 22). Signal intensity void spots can be seen on T2*-weighted (a) and SWI minIP image (b). Phase image (c) shows high signal intensity centrally identifying calcification, confirmed on the ex-vivo high resolution CT image (d).

DISCUSSION

T2*WI allows for accurate identification of calcified areas in retinoblastoma. In our study, all calcifications seen on ex-vivo HRCT could be matched with SIVs on T2*WI and this technique even depicted small SIVs better than HRCT. SIVs located in the tumor center are more likely to be calcification whereas peripheral SIVs and other intraocular SIVs can also indicate hemorrhage, slow flowing blood in venous congestion or artifact.

Detection of calcifications is critical for the differential diagnosis of retinoblastoma. After funduscopy, the first-line diagnostic tool is always ocular ultrasound. In experienced hands, ophthalmologists demonstrate calcifications in the majority of patients. When calcifications are not detected, cross-sectional imaging studies can be used as a problem solving technique^{12;13}. MRI is the technique of choice for evaluation of intraocular pathology, especially in children presenting with leukocoria.

The guidelines for imaging retinoblastoma by de Graaf et al serves as a checklist for minimal requirements for pretreatment diagnostic evaluation of retinoblastoma or mimicking lesions⁷. They concluded that together with ultrasound, high resolution MRI is the most important imaging modality for retinoblastoma diagnosis and evaluation of associated intracranial abnormalities. CT was highly discouraged in retinoblastoma children because of ionizing radiation and no added diagnostic value.

Historically MRI is considered to be an inferior technique for detection of calcifications compared to CT. However, accuracy to successfully depict small foci of calcifications by T2*WI was already reported in other studies^{14,15}. Galluzzi et al showed that T2*WI is a feasible technique to detect calcifications in retinoblastoma (8). In their study all SIVs matched with calcifications. SIVs on T2*WI could however also represent other pathology than calcifications. In our study we further characterize SIVs based on calcifications, hemorrhage or artefact by discussing different accompanying patterns.

We were able to confirm the capability of this sequence for calcification detection. In some tumors T2*WI was even more sensitive in depicting small intraocular calcifications in-vivo compared to HRCT ex-vivo. It must be stressed that the HRCT protocol in this study is considered to be more sensitive for detection of small punctate calcification compared to commonly used clinical protocols for pediatric orbital CT.

Additional hypointense areas however on MRI can cause confusion. Intratumoral hemorrhage is the most important cause of false-positive SIVs¹⁶. Hemorrhage is more likely to appear in large necrotic tumors and can cause extensive intraocular complications such as massive subretinal or intravitreal haemorrhage with subsequent increase in intraocular pressure. Smooth and linear SIVs in retinoblastoma on T2*WI are indicative for intratumoral haemorrhage and are predominantly located in the tumor periphery, whereas calcifications more frequently present as hypointense SIVs in the tumor center. Massive subretinal or intravitreal haemorrhage can easily be diagnosed on conventional T2WI with fluid-fluid (sedimentation) levels. We considered smooth and linear SIVs on T2*WI indicative for intraocular hemorrhage. They are predominantly on the surface of the tumors or aligning with the (usually) detached retina. Close correlation with findings during funduscopy and ultrasound might further help in interpretation of SIVs on tumor surface.

Advanced disease with massive tumor necrosis can also present with secondary neovascular glaucoma, uveitis and/or aseptic orbital cellulitis. These conditions are associated with venous congestion, i.e. extremely dilated intraocular venous structures. Susceptibility effects in venous blood is caused by the presence of deoxyhemoglobin and becomes more pronounced in venous congestion with increased intravascular space and slow flowing venous blood (Fig 4)¹⁷. Susceptibility artifacts due to air beneath the eyelid or within the paranasal sinuses can also cause SIVs on T2*WI. These artifacts can be distinguished from calcifications by the linear aspect and location. Susceptibility artifacts caused by air are usually located in or near the anterior eye segment.

SWI was available for review in a small subset of patients, which allowed us to explore for the first time the potential value of this sequence in retinoblastoma. This technique showed to be more sensitive than T2*WI in detecting (micro)calcifications and differentiating them from intratumoral (micro)hemorrhage, necrosis and artifacts in oligodendroglioma, vestibular schwannoma and diffuse infiltrating pontine gliom^{10;18;19}. In contrast to T2*WI, SWI is based on a long echo time, high-resolution, flow-compensated three-dimensional gradient-echo imaging technique with filtered phase information in each voxel. The combination of magnitude- and phase-data creates an enhanced contrast magnitude image that is particularly sensitive to hemorrhage, calcium, iron storage and slow flowing venous blood, therefore allowing a significant improvement in sensitivity and specificity compared to T2*WI^{18;20}. Preliminary results in our study showed that correlations between SWI and HRCT in retinoblastoma are equal to or even better compared to T2*WI. Therefore, further studies with more patients are required to determine diagnostic accuracy of SWI in detection of microcalcifications in retinoblastoma.

Our study has some limitations. First, we did not perform histopathologic correlation to confirm presence of calcifications in all eyes, but only of SIVs for which a corresponding hyperdensity on HRCT was lacking. However, accuracy of CT in depicting calcifications in soft-tissues is well accepted, and this technique has been used as a reference in several studies in the past^{5;11;21}. Second, the lesions studied were all retinoblastomas, without a number of simulating lesions for comparison. It is thus impossible to determine whether the (theoretical) absence of SIVs on T2*WI or SWI in simulating diseases can be a reliable parameter to narrow down the differential diagnosis. Third, all included patients required enucleation, which resulted in selection bias, since small tumors are usually treated with conservative (eye-sparing) treatment options. The amount of calcifications might be higher in larger tumors, which makes detection of calcification by CT and MRI easier. A potential reduction in sensitivity might become apparent for both techniques by adding smaller tumors. We recommend further research on this topic, in which retinoblastoma as well as simulating lesions are studied with T2*WI or SWI to evaluate presence of SIVs in these diseases. Ideally, these studies should include close correlation with histopathology to explore possible false-positive findings in simulating lesions. The small sample size of SWI studies in retinoblastoma is another limitation in our study. However, these initial positive findings are the first described in literature and warrants further research, especially since SWI including information provided by the phase-images harbors the potential to be a sensitive as well as a specific technique to detect or exclude calcifications in retinoblastoma.

CONCLUSION

Our study shows a good correlation between SIVs as detected on in-vivo T2*WI or SWI sequences and calcifications on ex-vivo HRCT in retinoblastoma. Gradient-echo sequences may be helpful in suggesting the diagnosis of retinoblastoma. In retinoblastoma patients it is important to

always avoid radiation hazards, especially from CT. The combination of fundoscopy, ultrasound and high-resolution MRI with gradient-echo sequences should become the standard diagnostic approach to diagnose retinoblastoma and removes potentially harmful ionizing radiation from the study protocol.

REFERENCES

1. Levy J, Frenkel S, Baras M, et al. Calcification in retinoblastoma: histopathologic findings and statistical analysis of 302 cases. *Br J Ophthalmol* 2011;95:1145-50
2. Chung EM, Specht CS, Schroeder JW. From the archives of the AFIP: Pediatric orbit tumors and tumorlike lesions: neuroepithelial lesions of the ocular globe and optic nerve. *Radiographics* 2007;27:1159-86
3. Saunders T, Margo CE. Intraocular medulloepithelioma. *Arch Pathol Lab Med* 2012;136:212-16
4. Roth DB, Scott IU, Murray TG, et al. Echography of retinoblastoma: histopathologic correlation and serial evaluation after globe-conserving radiotherapy or chemotherapy. *J Pediatr Ophthalmol Strabismus* 2001;38:136-43
5. Beets-Tan RG, Hendriks MJ, Ramos LM, et al. Retinoblastoma: CT and MRI. *Neuroradiology* 1994;36:59-62
6. Brenner D, Elliston C, Hall E, et al. Estimated risks of radiation-induced fatal cancer from pediatric CT. *AJR Am J Roentgenol* 2001;176:289-96
7. de Graaf P, Goricke S, Rodjan F, et al. Guidelines for imaging retinoblastoma: imaging principles and MRI standardization. *Pediatr Radiol* 2011;42:2-14
8. Lemke AJ, Kazi I, Mergner U, et al. Retinoblastoma - MR appearance using a surface coil in comparison with histopathological results. *Eur Radiol* 2007;17:49-60
9. Chavhan GB, Babyn PS, Thomas B, et al. Principles, techniques, and applications of T2*-based MR imaging and its special applications. *Radiographics* 2009;29:1433-49
10. Zulfqar M, Dumrongpisutikul N, Intrapromkul J, et al. Detection of intratumoral calcification in oligodendrogliomas by susceptibility-weighted MR imaging. *AJNR Am J Neuroradiol* 2012;33:858-64
11. Galluzzi P, Hadjistilianou T, Cerase A, et al. Is CT still useful in the study protocol of retinoblastoma? *AJNR Am J Neuroradiol* 2009;30:1760-65
12. de Graaf P, van der Valk P, Moll AC, et al. Retinal dysplasia mimicking intraocular tumor: MR imaging findings with histopathologic correlation. *AJNR Am J Neuroradiol* 2007;28:1731-33
13. Mafee MF, Goldberg MF, Cohen SB, et al. Magnetic resonance imaging versus computed tomography of leukocoric eyes and use of in vitro proton magnetic resonance spectroscopy of retinoblastoma. *Ophthalmology* 1989;96:965-75
14. Fatemi-Ardekani A, Boylan C, Noseworthy MD. Identification of breast calcification using magnetic resonance imaging. *Med Phys* 2009;36:5429-36
15. Tsushima Y, Endo K. Hypointensities in the brain on T2*-weighted gradient-echo magnetic resonance imaging. *Curr Probl Diagn Radiol* 2006;35:140-50
16. Atlas SW, Grossman RI, Hackney DB, et al. Calcified intracranial lesions: detection with gradient-echo-acquisition rapid MR imaging. *AJR Am J Roentgenol* 1988;150:1383-89
17. Kvistad KA, Rydland J, Vainio J, et al. Breast lesions: evaluation with dynamic contrast-enhanced T1-weighted MR imaging and with T2*-weighted first-pass perfusion MR imaging. *Radiology* 2000;216:545-53
18. Lobel U, Sedlacik J, Sabin ND, et al. Three-dimensional susceptibility-weighted imaging and two-dimensional T2*-weighted gradient-echo imaging of intratumoral hemorrhages in pediatric diffuse intrinsic pontine glioma. *Neuroradiology* 2010;52:1167-77
19. Thamburaj K, Radhakrishnan VV, Thomas B, et al. Intratumoral microhemorrhages on T2*-weighted gradient-echo imaging helps differentiate vestibular schwannoma from meningioma. *AJNR Am J Neuroradiol* 2008;29:552-57
20. Gasparotti R, Pinelli L, Liserre R. New MR sequences in daily practice: susceptibility weighted imaging. A pictorial essay. *Insights Imaging* 2011;2:335-47
21. Brisse HJ, Guesmi M, Aerts I, et al. Relevance of CT and MRI in retinoblastoma for the diagnosis of postlaminar invasion with normal-size optic nerve: a retrospective study of 150 patients with histological comparison. *Pediatr Radiol* 2007;37:649-56

Chapter 5

*Brain Abnormalities on MR Imaging in
Patients with Retinoblastoma*

Firazia Rodjan
Pim de Graaf
Annette C. Moll
Saskia M. Imhof
Jonathan I.M.L. Verbeke
Esther Sanchez
Jonas A. Castelijns

AJNR Am J Neuroradiol 2010; 31:1385-1389

ABSTRACT

Background and purpose. Although pineoblastoma is the main brain abnormality associated with hereditary retinoblastoma, recent studies suggest an association with pineal cysts. This association is important because some pineoblastomas mimic pineal cysts. If there is a relationship, then radiologists should be aware of it because diagnostic confusion is possible. Mental retardation and congenital brain anomalies are also reported in patients with retinoblastoma, mostly in combination with 13q deletion syndrome. In this retrospective study, the presence of brain abnormalities on MR images in a large group of consecutive patients with retinoblastoma is evaluated.

Materials and Methods. Brain MR images of 168 patients with retinoblastoma from 1989 to 2009 were evaluated by 2 radiologists for tumors, structural anomalies, myelination, and coincidental findings. Clinical records were reviewed for laterality, heredity, and the presence of the 13q deletion syndrome.

Results. The hereditary group (patients with bilateral and unilateral proved RB1-germline mutation) included 90 (54%) of 168 patients. Seven patients had 13q deletion syndrome. Normal findings on brain MR images were seen in 150 (89%) patients. Five pineoblastomas were detected, all in patients with hereditary retinoblastoma (5.5% in the hereditary subgroup). Nine pineal cysts were detected (2.2% in the hereditary subgroup). Corpus callosum agenesis was found in 1 patient and a Dandy-Walker variant in 1 patient, both in combination with 13q deletion syndrome.

Conclusions. Pineoblastoma is associated with hereditary retinoblastoma, and structural brain abnormalities are restricted to patients with the 13q deletion syndrome. The incidence of pineal cysts in patients with retinoblastomas is similar to that in healthy children and is not associated with hereditary retinoblastoma.

INTRODUCTION

Retinoblastoma is the most common intraocular tumor in early childhood, occurring in 1/17,000 live births (1). Retinoblastoma cells contain a mutation or deletion of the retinoblastoma gene (RB1 gene), a tumor-suppressor gene, located on chromosome 13q14 (2,3). Approximately 40% of patients with retinoblastoma have hereditary disease (mostly bilateral tumors), while the remainder (60%) have unilateral nonhereditary disease. A minority is due to a cytogenetically detectable interstitial deletion of variable size with a minimal overlapping region in band 13q14 (4). It is reported that midline intracranial neuroblastic tumors of either the suprasellar or the pineal region (pineoblastoma) are present in approximately 5%–15% of patients with hereditary retinoblastoma (5).

Besides midline malignant tumors, benign intracranial abnormalities are also reported in the retinoblastoma population, in particular the presence of pineal cysts. In the literature, an association between hereditary retinoblastoma and pineal cysts is suggested. Popovic et al (6) reported an incidence of pineal lesions (cysts and pineoblastoma) of 6.4% in their retinoblastoma population. All pineal lesions were present in the bilaterally affected hereditary patients. In this subgroup, they found an equal incidence of 5.3% for both pineal cysts and pineoblastoma. The combination of retinoblastoma, suprasellar tumor, and pineal cysts is also reported, which, according to Popovic et al,(7) further adds to a possible relationship between hereditary retinoblastoma and pineal lesions. Karatza et al.(8) reported 11 patients with retinoblastoma with pineal cysts simulating pineoblastoma. They recommended that clinicians should be aware of the presence of this benign lesion when performing routine neuroimaging, especially in patients with bilateral disease.

However, pineal cysts are quite common in the general population. In postmortem cases, pineal cysts are encountered in 25%–40% of people of all ages (9,10). In recent literature, an incidence of 0.4%–2.2% on MR images in the general pediatric population between 0 and 5 years of age has been reported (11). It is already known that pineoblastoma is associated with retinoblastoma. If the same is true for pineal cysts, then radiologists should be aware of the association. Distinct imaging criteria in distinguishing pineoblastomas from pineal cysts should be evaluated to avoid diagnostic and therapeutic confusion.

Retinoblastoma may occur in the presence of 13q deletion syndrome. The risk of retinoblastoma development in patients with this syndrome is approximately 80% (3,4) Besides retinoblastoma, this syndrome has a spectrum of clinical features, including moderate-to-severe developmental delay. Baud et al (4) reported a variable degree of mental retardation in patients with retinoblastoma with associated 13q cytogenic abnormalities. Only in case reports, describing patients with 13q deletion syndrome or in combination with retinoblastoma, are congenital brain abnormalities or brain disorders indicative of cognitive symptoms reported (4,7,12–24). Ballarati et al.(25) reported central nervous system anomalies such as Dandy-Walker malformation,

cerebellar hypoplasia, cortical dysplasia, and agenesis of the corpus callosum in patients with 13q deletion. Although one can assume that these symptoms are due to 13q deletion syndrome, it is interesting to evaluate whether (structural) brain abnormalities are involved in patients with retinoblastoma. To our knowledge, no large correlative study has been performed on the presence of retinoblastoma and brain abnormalities on MR imaging.

The purpose of this retrospective study was to evaluate the presence of brain abnormalities on MR images in a large group of consecutive patients with retinoblastoma.

MATERIALS AND METHODS

Patients

Patients eligible for this retrospective study were those at our institution with retinoblastoma who had undergone MR imaging of the brain that enabled adequate image interpretation between 1989 and 2009. To avoid alteration in the brain due to aging, we only evaluated patients younger than 5 years of age. The diagnosis of retinoblastoma was confirmed in all patients with extensive funduscopy, sonography, and MR imaging. In case of enucleation, the diagnosis was confirmed by histopathology. In this period, we identified 245 patients with retinoblastoma, and all patients had undergone MR imaging. However, in 77 patients, brain imaging studies were absent or incomplete and, therefore, excluded. The total number of included patients was 168. The need for informed consent was waived because of the retrospective nature of the study.

Clinical records were reviewed by 1 reviewer for the patient's sex, age at first MR imaging, laterality, heredity, and the presence of 13q deletion syndrome. In patients with brain abnormalities, the evaluation of pre- or posttreatment MR imaging had to exclude treatment-induced brain abnormalities.

Patients with bilateral disease or a positive family history of retinoblastoma or a defect in the RB1 gene found in chromosomal/deoxyribonucleic acid analysis were classified as having hereditary disease. All other patients were classified as having nonhereditary disease (1).

MR Imaging

MR imaging was performed at 1T (Magnetom Impact Expert; Siemens, Erlangen, Germany) and 1.5T (Magnetom Vision and Sonata, Siemens). Within the past 20 years, MR imaging protocols for retinoblastoma have changed. In the beginning, whole-brain MR imaging sequences were more common in retinoblastoma MR imaging protocols in combination with a standard-quadrature head coil. Due to technologic developments and improved coil design, attention shifted to small-FOV imaging of the orbits by using surface coils. MR imaging protocols did not differ between unilaterally and bilaterally affected patients. Postcontrast axial T1W MR images covering the whole brain were available in all included patients. In only 48 of 168 patients were axial T2W MR images of the brain available.

Image Analysis

MR imaging examinations were individually reviewed by 2 radiologists with, respectively, 4 and 9 years of experience in pediatric neuroradiology. Disagreement was resolved by consensus. The parameters evaluated on MR imaging were selected on the basis of literature study (4,7,12–24) and were divided into the following categories: benign or malignant tumor (tumor of the pineal gland, pineal cyst, or other); structural anomalies (corpus callosum agenesis, holoprosencephaly, encephalocele, Dandy-Walker malformation or a variant, hypoplasia of the basic pontis, microcephaly and polymicrogyria, or other); and degree of myelination, ventriculomegaly, or coincidental findings. Special attention was paid to myelination to clarify possible cognitive symptoms. The diagnosis of a pineal tumor was made if the pineal gland was enlarged, solid, and isointense to gray matter on T1W images with homogeneous and intense contrast enhancement.⁶ A pineal cyst was diagnosed if the pineal gland was enlarged and had a central region hypointense with respect to white matter on T1W images and isointense with respect to CSF on T2W images and a thin wall of 2 mm with discrete rim enhancement after gadolinium injection.⁶ The diameters of pineal cysts and pineoblastomas were measured.

RESULTS

Clinical Findings

The mean age at first MR imaging of the 168 patients was 17 months (range, 0–59 months). Bilateral retinoblastoma was present in 78 patients (46%) and unilateral disease in 90 patients (54%). Seventy-nine patients with retinoblastoma were female (47%) (41 bilateral, 38 unilateral) and 89 (53%) were male (36 bilateral, 53 unilateral). The hereditary group consisted of 90 patients and the nonhereditary group of 78 patients. Seven hereditary patients (8%) were diagnosed with 13q deletion syndrome.

MR Imaging Findings

Brain MR imaging showed no abnormalities in 150 (89%) patients. Brain abnormalities were found in 18 patients (11%), with the pineal gland as the most commonly affected site (14 patients, 78%) (Table). Pineoblastoma was found in 5 patients at a mean age of 20 months (range, 1–39 months), all with hereditary retinoblastoma (3.0% overall incidence, and 5.5% in the hereditary group). The mean interval between diagnosis of ocular and intracranial tumor was 16.4 months. In 1 patient (10 months of age), the pineoblastoma was detected with the diagnosis of retinoblastoma (synchronous tumors). In the other 4 patients, the pineoblastoma was discovered at a later stage; 6, 15, 25, and 37 months after the diagnosis of retinoblastoma (metachronous tumors). In patients 6, 8, and 9, the tumor presented as a solid mass isointense with respect to gray matter on precontrast T1W images and showed a homogeneous intense contrast enhancement in the pineal region (diameters respectively, 55, 16, and 49 mm) (Table).

Table 1: MR imaging findings in retinoblastoma patients

Patient (age/sex)	Heredity	Pre-t. MRI	MRI findings (side)	Size (mm)
1 (1/ M)	Y	Yes	DV (temporal and atrium)	
2 (13/ M)	Y	Yes	Dandywalker variant with DV	
3 (4/ F)	Y	Yes	CCA (corpus/splenum), vermishypoplasia, DV	
4 (10/ M)	Y	Yes	trigonocephalia, DV	
5 (10/ M)	Y	Yes	pineoblastoma	15
6 (39/ F)	Y	Yes	pineoblastoma	55
7 (5/ F)	Y	Yes	pineoblastoma	59
8 (1/ M)	Y	Yes	pineoblastoma	16
9 (37/ F)	Y	Yes	pineoblastoma	49
10 (34/ M)	N	Yes	pineal cyst	7
11 (16/ F)	N	Yes	pineal cyst	6
12 (31/ M)	N	Yes	pineal cyst	6
13 (15/ F)	Y	Yes	pineal cyst	5
14 (0/ F)	N	Yes	pineal cyst	4
15 (23/ F)	N	Yes	pineal cyst	3
16 (9/ F)	Y	Yes	pineal cyst	3
17 (10/ M)	N	Yes	pineal cyst	4
18 (18/ M)	N	Yes	pineal cyst	3

Note: age in months. Pre-t MRI= pre-treatment MRI, DV=dilatated ventricles, CCA= corpus callosum agenesis

In patients 5 and 7, the tumor consisted of a heterogeneous mass with intense contrast enhancement and areas with low signal intensity on T1W images and high signal intensity on T2W images, suspicious for central necrosis. In patient 5, the configuration of the lesion mimicked a pineal cyst (Fig 1). On axial images however, the diagnosis of pineoblastoma was more evident because there was an asymmetric nodular thickening of the enhancing wall. The thickness of the enhancing wall varied from 3 to 7 mm. Histopathology revealed a pineoblastoma with central necrosis.

The total incidence of pineal cysts in our study was 5.4% (9 patients), with an incidence of 9.0% in the nonhereditary group (7 patients; mean age, 20 months; range, 10–34 months) and 2.2% in the hereditary group (2 patients; mean age, 9 months; range, 9–10 months) (Fig 2). The mean size of the cysts in the nonhereditary group was 4.8 mm (range, 3–7 mm) and 4 mm in the hereditary group (range, 3–5 mm). In 2 patients, follow-up MR imaging was available and showed no change in the pineal cysts.

Besides pineoblastoma and pineal cysts, a diversity of brain abnormalities was found. Corpus callosum agenesis occurred in 1 patient with hereditary retinoblastoma (Fig 3), and in another patient, a hereditary Dandy-Walker variant occurred. Both were known to have a 13q deletion syndrome. In the other 5 patients (71%) with 13q deletion syndrome, no brain abnormalities were present. One patient with hereditary retinoblastoma showed DV.

Evaluation of white matter abnormalities was only possible in 48 patients because of incomplete series of T2W images of the brain in 120 patients. In this subgroup, no white matter abnormalities were observed and all patients with retinoblastoma showed normal myelination.

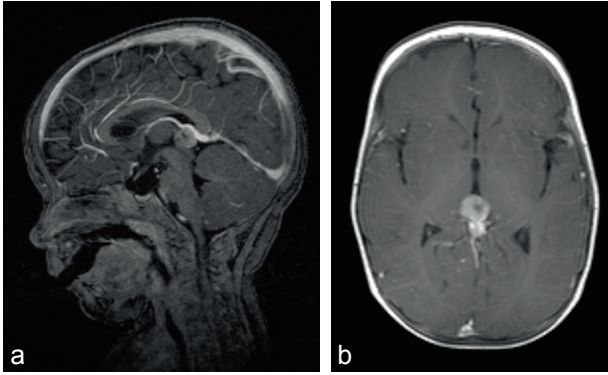


Fig 1. Patient 5, a 10-month-old with hereditary retinoblastoma and pineoblastoma. *A*, Sagittal T1-weighted postgadolinium MR image shows a cystic mass in the pineal gland. *B*, Axial T1-weighted image shows an asymmetric nodular thickening of the tumor wall. The thickness of the enhancing wall varies from 3 to 7 mm, suspicious for pineoblastoma.

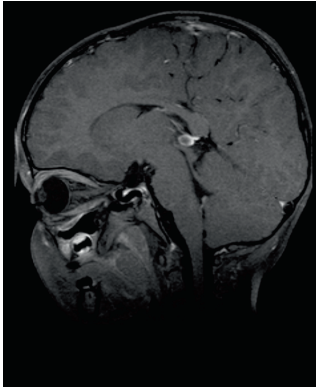


Fig 2. Patient 10. Contrast-enhanced T1-weighted MR image of a 34-month-old patient with nonhereditary retinoblastoma with a pineal cyst, with a diameter of 7 mm.

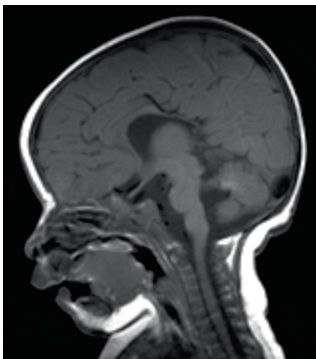


Fig 3. Patient 3. Sagittal T1-weighted image of a 4-month-old with 13q deletion syndrome and bilateral retinoblastoma shows agenesis of the splenium of the corpus callosum.

DISCUSSION

In this study, we present an overview of brain abnormalities in a large group of patients with retinoblastoma. Pineoblastoma is the most well-known brain pathology associated with retinoblastoma, a combination known as trilateral retinoblastoma, occurring in 1.5%–5% of all patients and in 5%–15% in the hereditary subgroup (5,22). Besides the pineal region, tumors may also occur in the suprasellar or parasellar region. Our study showed similar results, with an incidence of 3.0% in the whole study group and 5.5% concerning only the hereditary group.

Three of 5 pineoblastomas showed a typical imaging pattern: a solid homogeneous lobulated enlarged pineal gland, isointense with gray matter on T1W images with intense homogeneous contrast-enhancement. In the other 2 pineoblastomas, low signal intensity on T1W images and high signal intensity on T2W images with heterogeneous enhancement areas were present. One pineoblastoma even mimicked a pineal cyst due to a large central area of histopathologically proved necrosis. The thickness of this cyst wall (7 mm), however, did not correspond with the criteria of pineal cyst (thickness, 2 mm). This finding can cause confusion in the diagnosis of pineoblastoma, and it could have been erroneously diagnosed as a pineal cyst, with severe clinical consequences (8). This has been reported only once before. Sugiyama et al.(26) reported a case of a pineoblastoma with a large central cyst, histopathologically due to central necrosis. In our patient, the pineoblastoma was discovered in an early stage synchronously with the intraocular tumor on baseline MR imaging without clinical symptoms due to pineoblastoma.

Central necrosis can be present in large and small pineoblastomas, and especially small pineoblastomas with central necrosis can mimic a pineal cyst. In our experience, the thickness and appearance of the cyst wall before and after contrast administration on MR imaging are indeed important to differentiate a pineal cyst and pineoblastoma. Pineal cysts show a thin wall (<2 mm) with discrete enhancement, whereas pineoblastomas with central necrosis show a nodular thickened wall with homogeneous wall enhancement.

In our screening for brain abnormalities in 168 patients with retinoblastoma, pineal cysts were detected in 5.4% of the patients. Sener (10) performed a review of MR imaging in 500 children and 500 adults and found no pineal cysts in children younger than 12 years of age. The sensitivity of this study, however, could have been limited by using 0.5T MR imaging in evaluation. Sawamura et al.(27) found 79 cysts in 6023 patients but none in children younger than 10 years of age. However, only MR images in 73 children of 10 years of age and younger were evaluated.

The study of Al-Holou et al.(11) was the only one in which the incidence of pineal cysts on MR imaging was examined in healthy children younger than 5 years of age. They reported an incidence of 2.0%, almost similar to that in our hereditary group. In this study, the pineal cyst population was compared with an age- and sex-matched control population. Popovic et al.(6,7) also reported almost the same incidence as in our overall study group (5.3%). They found cysts

in patients with bilateral hereditary retinoblastoma, but no pineal cysts in the patients with nonhereditary retinoblastoma. These previously mentioned studies included only pineal cysts of >5 mm. In our study of patients with retinoblastoma younger than 5 years of age, 5 of the 9 cysts were <5 mm (4 of the 5 pineal cysts in the nonhereditary group).

A follow-up study in a matched control group would be necessary to examine the high incidence of pineal cysts in the patients with nonhereditary compared with hereditary retinoblastoma with the same criteria used in our study. In previous studies, only Karatza et al.(8) reported the occurrence of pineal cysts in patients with nonhereditary retinoblastoma. They reviewed 1400 medical records of patients with retinoblastoma and found 3 pineal cysts (0.2%) in patients with unilateral and 8 pineal cysts (0.6%) in patients with bilateral retinoblastoma. These low incidences are probably due to screening for pineal cysts in medical records instead of re-evaluation of MR images. In our experience, these cysts are not always described in medical records as a finding. However, for assessing the association between retinoblastoma and pineal cysts, the incidence of pineal cysts in the hereditary group is interesting. Given the incidence of 2.2% in the hereditary group, which is similar to the incidence in the healthy population (11) there is no association between hereditary retinoblastoma and pineal cysts. Although it is important to be aware of pineoblastomas mimicking a pineal cyst, there is no evidence that pineal cysts occur more often in patients with retinoblastoma compared with the healthy pediatric population.

In our study group, larger structural brain abnormalities occurred only in combination with a 13q deletion syndrome. One patient with 13q deletion syndrome had a corpus callosum agenesis and another patient showed a Dandy-Walker variant with DV. This brain abnormality is also described in previous case reports. Alanay et al.(28) reported a patient with a thin corpus callosum and a Dandy-Walker malformation.

CONCLUSION

In conclusion, pineoblastoma is associated with hereditary retinoblastoma, and structural brain abnormalities are restricted to the patients with 13q deletion syndrome. The incidence of pineal cysts in retinoblastoma is similar to that in healthy children and is not associated with hereditary retinoblastoma.

REFERENCES

1. Moll AC, Kuik DJ, Bouter LM, et al. Incidence and survival of retinoblastoma in The Netherlands: a register based study 1862–1995. *Br J Ophthalmol* 1997; 81:559–562
2. Friend SH, Bernards R, Rogelj S, et al. A human DNA segment with properties of the gene that predisposes to retinoblastoma and osteosarcoma. *Nature* 1986; 323:643–646
3. Ganesh A, Kenue RK, Mitra S. Retinoblastoma and the 13q deletion syndrome. *J Pediatr Ophthalmol Strabismus* 2001; 38:247–250
4. Baud O, Cormier-Daire V, Lyonnet S, et al. Dysmorphic phenotype and neurological impairment in 22 retinoblastoma patients with constitutional cytogenetic 13q deletion. *Clin Genet* 1999; 55:478–482
5. Kivela T. Trilateral retinoblastoma: a meta-analysis of hereditary retinoblastoma associated with primary ectopic intracranial retinoblastoma. *J Clin Oncol* 1999; 17:1829–1837
6. Popovic MB, Balmer A, Maeder P, et al. Benign pineal cysts in children with bilateral retinoblastoma: a new variant of trilateral retinoblastoma? *Pediatr Blood Cancer* 2006; 46:755–761
7. Popovic MB, Diezi M, Kuchler H, et al. Trilateral retinoblastoma with suprasellar tumor and associated pineal cyst. *J Pediatr Hematol Oncol* 2007; 29:53–56
8. Karatza EC, Shields CL, Flanders AE, et al. Pineal cyst simulating pinealoblastoma in 11 children with retinoblastoma. *Arch Ophthalmol* 2006; 124:595–597
9. Fleege MA, Miller GM, Fletcher GP, et al. Benign glial cysts of the pineal gland: unusual imaging characteristics with histologic correlation. *AJNR Am J Neuroradiol* 1994; 15:161–166
10. Sener RN. The pineal gland: a comparative MR imaging study in children and adults with respect to normal anatomical variations and pineal cysts. *Pediatr Radiol* 1995; 25:245–248
11. Al-Holou WN, Garton HJ, Muraszko KM, et al. Prevalence of pineal cysts in children and young adults: clinical article. *J Neurosurg Pediatr* 2009; 4:230–236
12. Araujo JE, Filho HA, Pires CR, et al. Prenatal diagnosis of the 13q-syndrome through three-dimensional ultrasonography: a case report. *Arch Gynecol Obstet* 2006; 274:243–245
13. Chung JL, Choi JR, Park MS, et al. A case of del(13)(q22) with multiple major congenital anomalies, imperforate anus and penoscrotal transposition. *Yonsei Med J* 2001; 42:558–562
14. Desai VN, Shields CL, Shields JA, et al. Retinoblastoma associated with holoprosencephaly. *Am J Ophthalmol* 1990; 109:355–356
15. Duncan JL, Scott IU, Murray TG, et al. Routine neuroimaging in retinoblastoma for the detection of intracranial tumors. *Arch Ophthalmol* 2001; 119:450–452
16. Ibarra MS, O'Brien JM. Is screening for primitive neuroectodermal tumors in patients with unilateral retinoblastoma necessary? *J AAPOS* 2000; 4:54–56
17. Kasyan AG, Benirschke K. Genetic haploinsufficiency as a phenotypic determinant of a deletion 13q syndrome. *Pediatr Dev Pathol* 2005; 8:658–665
18. Kennerknecht I, Barbi G, Greher J. Diagnosis of retinoblastoma in a presymptomatic stage after detection of interstitial chromosomal deletion 13q. *Ophthalmic Genet* 1994; 15:19–24
19. Koestenberger M, Kroisel PM, Lackner H, et al. Simultaneous occurrence of retinoblastoma and neurofibromatosis I in a young child. *Med Pediatr Oncol* 2003; 40:124–125
20. Kogan JM, Egelhoff JC, Saal HM. Interstitial deletion of 13q associated with polymicrogyria. *Am J Med Genet A* 2008; 146:910–916
21. Melis D, Pia Sperandeo M, Perone L, et al. Mosaic 13q13.2-ter deletion restricted to tissues of ectodermal and mesodermal origins. *Clin Dysmorphol* 2006; 15:13–18
22. Provenzale JM, Gururangan S, Klintworth G. Trilateral retinoblastoma: clinical and radiologic progression. *AJR Am J Roentgenol* 2004; 183:505–511
23. Skrypnik C, Bartsch O. Retinoblastoma, pinealoma, and mild overgrowth in a boy with a deletion of RB1 and neighbor genes on chromosome 13q14. *Am J Med Genet* 2004; 124:397–401
24. Skulski M, Egelhoff JC, Kollias SS, et al. Trilateral retinoblastoma with suprasellar involvement. *Neuroradiology* 1997; 39:41–43
25. Ballarati L, Rossi E, Bonati MT, et al. 13q deletion and central nervous system anomalies: further insights from karyotype-phenotype analyses of 14 patients. *J Med Genet* 2007; 44: e60

26. Sugiyama K, Arita K, Okamura T, et al. Detection of a pineoblastoma with large central cyst in a young child. *Childs Nerv Syst* 2002; 18:157–160
27. Sawamura Y, Ikeda J, Ozawa M, et al. Magnetic resonance images reveal a high incidence of asymptomatic pineal cysts in young women. *Neurosurgery* 1995; 37:11–15
28. Alanay Y, Aktas D, Utine E, et al. Is Dandy-Walker malformation associated with “distal 13q deletion syndrome”? Findings in a fetus supporting previous observations. *Am J Med Genet* 2005; 136:265–268

Chapter 6

*Trilateral retinoblastoma: neuroimaging characteristics
and value of routine brain screening on admission*

Firazia Rodjan
Pim de Graaf
Herve J. Brisse
Jonathan I.L.M. Verbeke
Esther Sanchez
Paolo Galluzzi
Sophia Göricke
Philippe Maeder
Isabelle Aerts
Remi Dendale
Laurence Desjardins
Sonia de Franscesco
Norbert Bornfeld
Wolfgang Sauerwein
Maja Beck Popovic Dirk L. Knol
Annette C. Moll
Jonas A. Castelijns

ABSTRACT

BACKGROUND: Trilateral retinoblastoma (TRb) is a rare disease associating intraocular retinoblastoma with intracranial primitive neuroectodermal tumor. Treatment is difficult and prognosis is poor. This multicenter study evaluates clinical findings and MR imaging characteristics of associated intracranial tumors in Rb-patients.

METHODS: Clinical data of 17 patients (16 TRb- and 1 quadrilateral Rb-patients) included time-intervals between Rb- and TRb-diagnosis and presence of baseline brain-imaging (BBI). Two reviewers reviewed all images individually and one reviewer per center evaluated their images. Consensus was reached during a joint scoring session. Studies were reviewed for tumor location, size and imaging characteristics (signal intensity (SI) on T1W- and T2W images, enhancement pattern and cystic appearance).

RESULTS: Of 18 intracranial tumors, 78% were located in the pineal gland and 22% suprasellar. All tumors showed well-defined borders with mostly heterogenous enhancement (72%) and isointense SI on T1W (78%) and T2W images (72%) compared to grey matter. The majority of pineal TRBs showed a cystic component (57%). TRb detected synchronously with the intraocular tumors on BBI (n=7) were significantly smaller ($P = 0.02$), and mainly asymptomatic than TRb detected later on (n=10). Overall 5-year-survival of TRb patients detected on BBI was 67% (95%-confidence interval 29%-100%) compared to 11% (95%-confidence interval 0%-32%) for the group with delayed diagnosis.

CONCLUSIONS: TRb mainly develops in the pineal gland and frequently presents with a cystic appearance that could be misinterpreted as benign pineal cysts. Routine BBI in all newly diagnosed Rb-patients can detect TRb in a subclinical stage.

INTRODUCTION

Trilateral retinoblastoma (TRb) is a disease associating unilateral or bilateral retinoblastoma (Rb) with an intracranial midline primitive neuroectodermal tumor (PNET) which usually arises in the pineal gland (PG) (77%) (1). In hereditary Rb patients, the neural ectoderm destined to form both retinal and pineal tissue is prone to develop multifocal neoplasms. This results in histologically similar but separately located tumors (2). The risk of developing TRb in Rb patients, is less than 0.5% for sporadic unilateral disease (3), 5-13% in sporadic bilateral disease and 5-15% in familial bilateral Rb (1). Patients with TRb frequently present with signs of intracranial hypertension (3-7). Few long-term survivors are reported and especially in symptomatic patients prognosis is poor (1;3;8-10).

Previous studies on TRb detection, neuroimaging screening and prognosis all focused on time intervals between detection of Rb and TRb (metachronous tumor development) (1;10-13). Reported median time between Rb and TRb diagnosis is 21 months (1;3;9;10). However, Kivela et al reported that with inclusion of brain MR screening during first MRI examination for Rb (i.e., baseline brain imaging; BBI) approximately 50% of TRb cases can potentially be found (1). These are considered synchronous tumors, detected on baseline MRI. Approximately another 25% of TRbs can be found during the first year after Rb detection. However, recent literature states that TRb is rarely present at diagnosis of Rb (14). We hypothesize that the exact prevalence of synchronous occurrence of TRb and Rb in literature is underestimated. In most studies, it remains unclear whether BBI was performed at Rb diagnosis, at some time-point during follow-up or only in a later stage for detection of symptomatic TRb; and if imaging was performed with CT or MR. This complicates the evaluation of “true” synchronous TRb in literature.

Only few radiological articles on TRb have been reported, and these were mainly individual case reports. To our knowledge, only two studies described radiologic findings on MRI in trilateral retinoblastoma, both within small groups of patients (10;15). Because of these modest study populations, it is relevant to identify specific MRI characteristics of TRb in a larger group of patients.

The primary purpose of this multicenter study was to evaluate clinical findings and MRI characteristics of associated intracranial tumors in Rb patients. The secondary purpose was to assess clinical, radiological and prognostic differences between TRb depicted on BBI and those depicted later on.

MATERIALS AND METHODS

Patient population

This retrospective study was performed in agreement with the recommendations of the local ethics committees within a European multicenter partnership (ERIC) with five participating Rb-centers. Review of clinical records between 1991 and 2010, revealed 17 Rb-patients with MRI and intracranial tumors. TRb was diagnosed on basis of histopathological confirmation (surgery or presence of tumor cells in cerebrospinal fluid [CSF]) or clinical disease progression during follow-up MRI. TRb was defined as a mass lesion in the PG or suprasellar region in Rb patients. Tumor in both PG and suprasellar regions in combination with bilateral Rb was classified as a quadrilateral Rb (QRb).

Record Review

Clinical records were reviewed for tumor laterality, family history for Rb, age of Rb-diagnosis, time-interval from Rb- to TRb-diagnosis and TRb-diagnosis to death or last follow-up date. Symptoms at first presentation of TRb and treatment received for Rb and TRb were recorded. Laboratory records were analyzed for tumor cells in CSF acquired by lumbar puncture (LP) performed either at diagnosis or during follow-up. Particular attention was paid to the presence of BBI, which is necessary to evaluate the simultaneous occurrence of TRb at Rb-diagnosis. TRbs were categorized in synchronous or metachronous tumors to the intraocular tumor. Patients with bilateral retinoblastoma, a positive family history of retinoblastoma or mutations in the RB1 gene found in chromosomal/DNA analysis were classified as hereditary. Disease progression was defined as either tumor recurrence, intracranial or intraspinal leptomeningeal spread or distant metastases.

Image Review

Patients underwent various imaging protocols for the assessment of TRb. MRI sequences varied in different institutions. Brain MRI protocols at least included either sagittal or transverse unenhanced T1W images or T2W images in 14 patients. Post-contrast T1W images of TRb were available in 16 patients.

Two observers (J.C. and P.d.G.) with respectively 22 and 10 years experience individually reviewed all MRI examinations and one radiologist from each participating center (H.J.B., P.G., P.M. and S.G.) evaluated their images. Agreement was reached during a joint scoring session. MR images were evaluated for mass lesions in the PG and suprasellar regions and for leptomeningeal tumor dissemination. Regarding the TRb, maximal axial diameter (MAD) at diagnosis, tumor border, presence of tumor necrosis, tumor aspect (solid; solid with cystic component; or complete cystic), SI on T1W and T2W images compared to grey matter, aspect of contrast enhancement, presence of vessel encasement, hydrocephalus and leptomeningeal metastases were scored.

Statistics

Statistical calculations were performed using SPSS, version 15.0 (SPSS, Chicago III). BBI and MAD were analyzed by using the Mann-Whitney test. Difference in mean MAD between pineoblastomas and suprasellar tumors was analyzed using an independent t-test. Associations between other clinical dichotomous parameters and BBI were assessed using Fisher exact tests. A 95%-confidence interval for 5-year survival was calculated based upon the Kaplan-Meier survival function. A *P*-value of less than 0.05 was considered statistically significant.

RESULTS

Clinical findings

Clinical data of part of this study were previously reported (Table 1) (1). Ten patients had familial Rb (59%) and 11 patients also a positive RB1-gene mutation (65%). Sixteen patients (94%) were classified as hereditary Rb. Mean age of Rb-diagnosis was 9 months (median age 5 months) and of TRb 26 months (median age, 23 months). Mean time-interval between detection of Rb and TRb was 18 months (median, 14 months). In none of the patients, TRb was found before Rb.

Nine patients had signs of intracranial hypertension, whereas the other 8 patients were asymptomatic at detection. LP at baseline were performed in 7 patients (positive for tumor cells in 5 patients) and during follow-up in 11 patients (positive in 5 additional patients). Histopathologic specimen was available in 4 TRbs and were classified as PNETs. Rb was treated with external beam radiotherapy (EBRT) (mean age 10 months, median 5 months) in 3 out of 10 metachronous patients. These patients developed TRb after a mean interval of 19 months (range 5-37 months). Rb was treated with chemotherapy in 2 out of 10 metachronous TRb patients (mean interval 35 months; range 30-40 months). Treatment for TRb was initiated in 13 patients. Two patients received palliative treatment because of tumor spread, one patient was not treated because of parental refusal, and one patient was lost of follow-up.

Table 1: Clinical patient characteristics

Patient (Rb-lat)	Confirmation TRb	Age Rb	Age TRb	Int. RB- TRb	Year Rb-date	BBI	Death	Int TRb- death	Int TRb- FU	Treatment RB (OD; OS)	Treatment TRb
1 (B)	histopathology	3	52	49	1986	no	yes	57	57	PT	ChT, EBRT
2 (B)	CSF	2	39	37	1990	no	yes	21	21	EBRT	ChT, EBRT
3 (B)	histopathology	5	10	5	1991	no	yes	7	7	En; EBRT	palliation
4 (B)	DP on MR	23	38	15	1992	no	yes	0	0	EBRT	palliation
5 (B)	CSF	2	26	24	1992	no	yes	13	13	CrT; En.	ChT
6 (B)	DP on MR	12	12	0	1997	yes	yes	14	14	CrT; En.	no
7 (U)	CSF	3	57	54	1997	no	no		93	no; En.	ChT
8 (B)	histopathology	2	42	40	1998	no	yes†	11	11	ChT	ChT, EBRT, surgery
9 (B)	DP on MR	3	3	0	2000	yes	no		74	ChT/CrT; En.	ChT
10 (B)	CSF	17	17	0	2001	yes	yes	7	7	ChT	ChT
11 (B)	CSF	3	15	12	2001	no	NA*		3	CrT; En.	ChT
12 (B)	CSF	7	23	16	2002	no	yes	16	16	En; En	ChT
13 (B)	CSF	1	31	30	2002	no	yes	15	15	ChT; CrT	ChT, surgery
14 (B)	CSF	10	10	0	2003	yes	no		50	ChT	ChT
15 (B)	CSF	12	12	0	2005	yes	no		63	ChT; CrT;	ChT
16 (U)	histopathology	10	10	0	2006	yes	no		56	ChT	ChT, surgery
17 (U)	no	38	38	0	2008	yes	NA	NA	NA	no; En.	NA

Note: Rb-lat = laterality Rb, B = bilateral Rb, U = unilateral Rb, Int. Rb - TRb = interval between Rb and TRb in months
 Int TRb-death = interval TRb and death in months, CSF = cerebrospinal fluid, DP = disease progression
 BBI = Baseline Brain Imaging, PT = plaque therapy, ChT = chemotherapy, EBRT = external beam radiation therapy, CrT = cryotherapy
 † due to intoxicity after chemotherapy, * lost to follow-up after 3 mo with progressive disease, NA = not available

MRI characteristics of TRb

MRI characteristics are summarized in Table 2. In our group of 17 patients, 18 intracranial tumors were detected.

Of the 14 pineoblastomas, 6 (42%) showed a completely solid aspect (fig 1a), 4 (29%) solid with cystic component (fig. 2) and 4 (29%) were completely cystic with an irregularly thickened rim (fig. 3). Pineoblastomas mimicking pineal cysts, showed an irregular (patient 6, fig 3a) or thickened (patient 16, fig. 3c) cyst wall, sometimes with tiny nodules. Follow-up imaging in patient 6 showed progression of the pineal lesion into a solid tumor with diffuse leptomeningeal metastases 14 months after refusal of treatment (Fig 3b). Patient 16 showed an obvious solid tumor part on the axial MR images (fig. 3d). Secondary hydrocephalus occurred in 8 patients (57%) with pineoblastoma (fig 1 b, 2b) and leptomeningeal metastases in 3 patients (21%) (fig. 1d, 2b). One suprasellar tumor showed a homogenous solid aspect with a cystic component (fig 2a).

Overall, the mean MAD was 30mm (range 9 – 59mm).

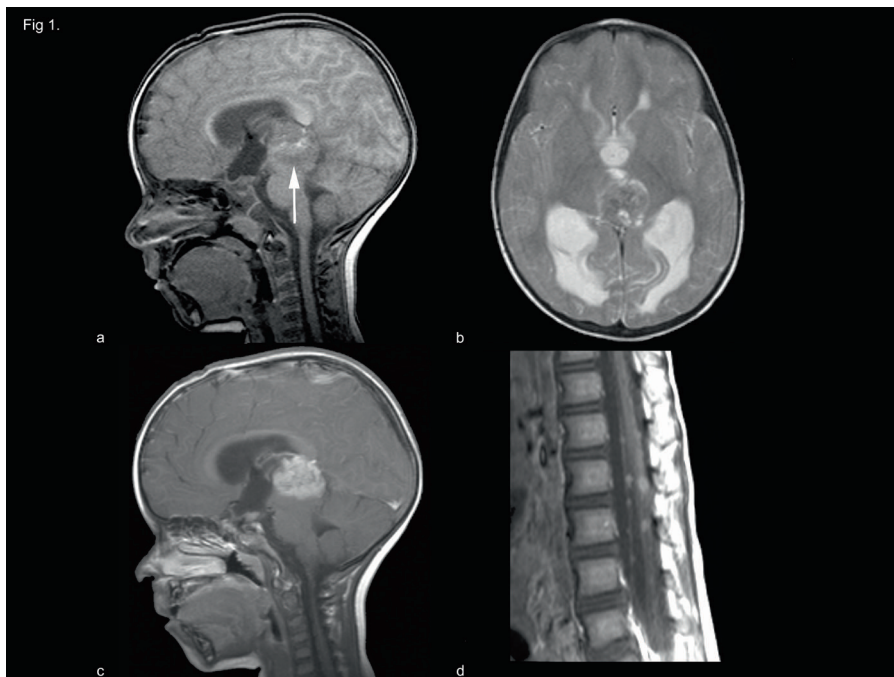


Fig. 1 Solid pineoblastoma with hydrocephalus and extensive leptomeningeal metastases. Sagittal T1-weighted (a), axial T2-weighted (b), contrast-enhanced sagittal T1-weighted images of the brain (c) and spine (d) of patient 13. Pineoblastoma showed mostly isointense SI on both T1-weighted (a) and T2-weighted (b)MR images with respect to gray matter and homogenous contrastenhancement (c). The large tumor mass (33 mm) showed mostly isointense SI on both T1-weighted (a) and T2-weighted (b)MR images with respect to gray matter and homogenous contrastenhancement (c). The large tumor mass (33 mm) showed compression on the brainstem (mesencephalon) and cerebral aqueduct (a, c) with secondary hydrocephalus (b). Multiple nodular leptomeningeal tumor seedings are present in the spinal canal (d)

Table 2: Imaging characteristics

Patient	Intracranial tumorlocation	MAD	Tumorborder	AL	Necrosis	SIT1	SIT2	Enhancement	LM	Hydrocephalus	VE
1	PG	25	well-defined	solid	no	NA	NA	homogeneous	no	yes	yes
2	PG	55	well-defined	PC	yes	isointense	hypointense	heterogeneous	no	yes	yes
3	PG	59	well-defined	PC	yes	isointense	isointense	heterogeneous	no	yes	yes
4	PG	49	well-defined	PC	yes	hypointense	isointense	heterogeneous	yes	yes	yes
5	PG	18	well-defined	solid	no	isointense	hypointense	heterogeneous	yes	yes	no
6	PG	9	well-defined	cystic	yes	isointense	isointense	heterogeneous	no	no	no
7	PG	51	well-defined	PC	yes	isointense	isointense	heterogeneous	ntb	yes	no
8	PG	22	well-defined	solid	yes	isointense	isointense	heterogeneous	no	yes	no
9	PG	13	well-defined	cystic	no	NA	NA	heterogeneous	no	no	no
10	SS	15	well-defined	solid	no	isointense	isointense	homogeneous	no	no	no
11	PG	13	well-defined	solid	yes	isointense	isointense	NA	ntb	no	no
12	PG	11	well-defined	solid	yes	NA	isointense	heterogeneous	no	no	yes
12	SS	44	well-defined	solid	no	NA	isointense	homogeneous	no	no	yes
13	PG	33	well-defined	solid	yes	isointense	isointense	heterogeneous	yes	yes	no
14	SS	23	well-defined	solid	no	isointense	isointense	homogeneous	no	no	no
15	SS	34	well-defined	PC	yes	isointense	isointense	heterogeneous	yes	no	no
16	PG	21	well-defined	cystic	yes	isointense	isointense	heterogeneous	no	no	no
17	PG	11	well-defined	cystic	yes	isointense	NA	heterogeneous	no	no	no

Note: PG = pineal gland, SS = supra sellar, MAD = maximal axial diameter, AL = aspect lesion

PC= partly cystic, NA = not available, SI T1-W = signal intensity on T1-weighted images compared to grey matter

SI T2-W = signal intensity on T2-weighted images compared to grey matter, LM= leptomeningeal metastases, VE = vessel encasement

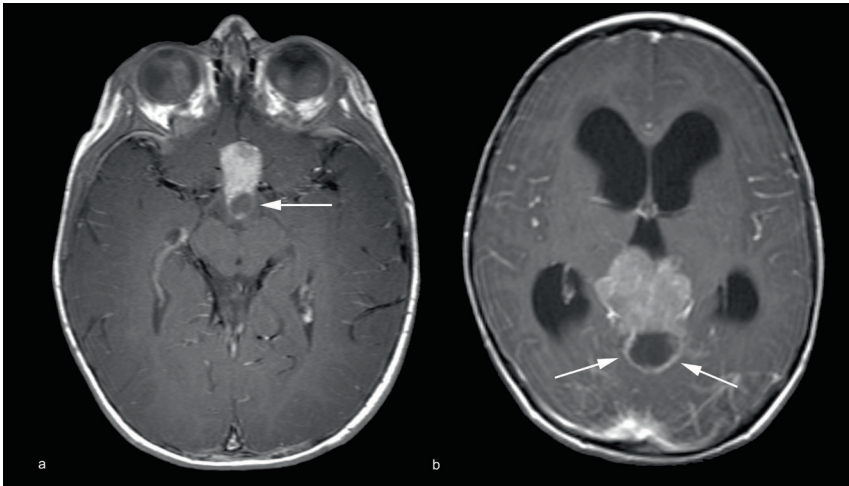


Fig. 2 Suprasellar and pineal gland trilateral retinoblastoma. Contrast-enhanced axial T1-weighted images showing solid tumor masses with cystic components in both the suprasellar region (patient 15) (a) and pineal gland (patient 7) (b). The pineal gland mass causes a secondary hydrocephalus because of brainstem compression (b)

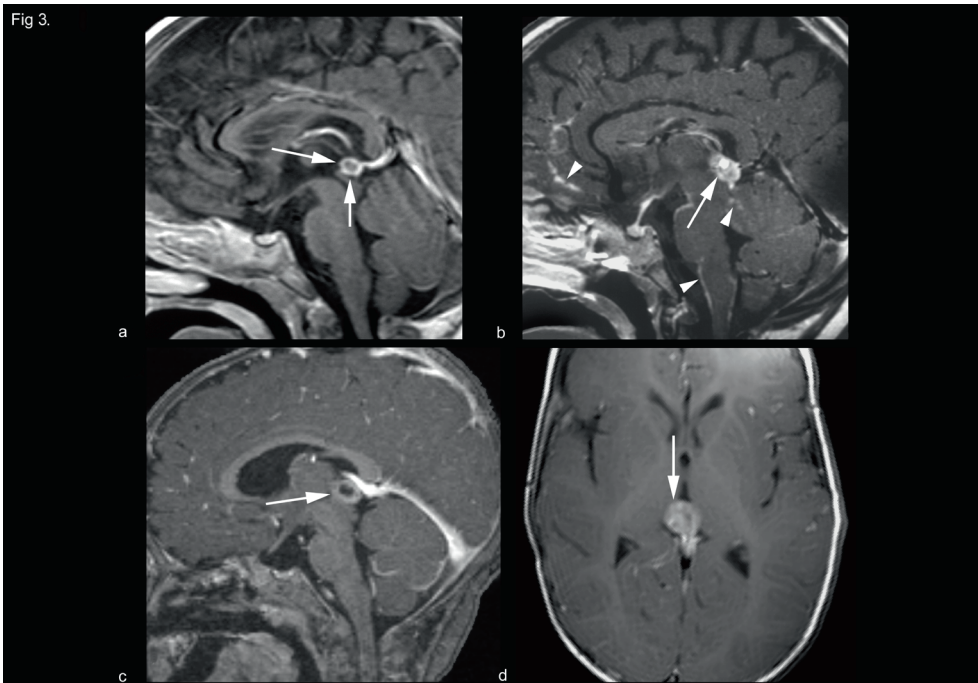


Fig. 3 Pineoblastoma presenting as suspicious cyst. Contrast-enhanced sagittal (a–c) and axial (d) T1-weighted images of the brain in patient 6 (a, b) and patient 16 (c, d). The pineal gland in a shows an irregular cyst wall with tiny nodules, which progressed into a solid tumor with diffuse (nodular) leptomeningeal metastases 14 months later after treatment refusal (b). The pineal gland in patient 16 mimics a pineal cyst on the sagittal image (c), but shows a solid part of the lesion on the axial image (d), suspicious for pineoblastoma

Clinical and radiological patterns according to time of diagnosis

BBI was available in 7 cases and in all Rb and TRb were diagnosed simultaneously (mean age 15 months, median 12 months; range 3- 38 months). These 7 patients did not have any signs of intracranial hypertension at first presentation.

In the remaining 10 patients without BBI, mean interval between Rb and TRb diagnosis was 27 months (median 24 months; range 5 – 54 months). Symptoms of intracranial hypertension occurred in 8 patients. A significant difference was observed in tumorsize ($P= 0.02$) and hydrocephalus ($P= 0.002$) in favour of patients with BBI. In 1 patient with TRb no symptoms occurred, and in 1 QRb patient symptoms could not be retrieved from the clinical records. Furthermore, other differences were observed in the patients with BBI compared to patients without BBI. Tumor size was significantly smaller in patients with BBI (mean MAD 18mm [range 9-34mm]) compared to patients without BBI (mean MAD 35mm [range 11-59mm]) ($P = 0.02$). Hydrocephalus ($P = 0.002$) occurred more often in patients without BBI and thus in larger tumors. Lumbar puncture in patients with BBI was positive in 29% of the cases and 70% in patients without BBI ($P = 0.15$).

In addition, more synchronous tumors were detected after the year 2000 as illustrated in Table 1, because BBI was more routinely included in current imaging protocols.

Survival

One out of 17 patients was lost to follow-up and excluded from survival analysis. One out of these 16 patients was treated with chemotherapy and lost to follow-up after 3 months with progressive disease and one died from intoxicity after intensive chemotherapy.

Five out of 16 patients (33%) are still alive (mean survival, 67 months; median 63 months, range, 50 – 93 months). Four of these 5 patients (80%), presented with synchronous TRb detected on BBI and were free of disease (mean survival, 61 months; range 50- 74 months). The other survivor was diagnosed with a pineoblastoma of 51 mm (54 months after RB-diagnosis without BBI). This patient had local tumor recurrences but is still in second complete remission, 93 months after complete resection of the pineoblastoma and intensive chemotherapy.

The remaining 10 patients died after a mean interval of 24 months. Eight presented with metachronous TRb and without BBI. Cause of death in these 10 patients included local spread of the initial TRb (3 patients), leptomeningeal metastases (4 patients), tumor recurrence (2 patients) and side effects of intensive chemotherapy (1 patient).

Difference in survival of PNET early detected with BBI compared to those with delayed diagnosis was not significant ($P = 0.064$). The overall 5-year-survival of PNET detected on BBI was 67% (95% confidence interval 29%-100%) compared to 11% (95% confidence interval 0%-32%) for the group without BBI.

DISCUSSION

Most important imaging finding of this retrospective analysis is that the majority of the pineoblastomas in our study were partially or totally cystic. Other main findings are that TRBs detected synchronously with the Rb on BBI were significantly smaller, more frequently asymptomatic and could have a better prognosis compared to TRBs found after diagnosis of Rb (metachronous TRBs).

In literature, the simultaneous occurrence of Rb and intracranial tumor is rare (14;16). Kivela et al. reported that intracranial tumors were detected before Rb-diagnosis in 3% of the cases, 14% simultaneously with Rb and 83% after Rb-diagnosis. However, the incidence of synchronous TRB is probably underestimated, as historically little documentation about the presence of BBI at Rb-diagnosis is available. Most TRBs described are diagnosed after first presentation with symptoms and signs of intracranial hypertension. Diagnosis and treatment for retinoblastoma is usually completed by then (3-7). In our study, in all patients with synchronous tumors detected on BBI, significantly smaller TRBs were detected compared to metachronous TRB. Furthermore, 70% of patients with metachronous tumors presented with symptoms due to intracranial hypertension and 80% died due to their intracranial tumor. This indicates that the majority of metachronous tumors could have been detected in an earlier stage if BBI would have been performed. Remarkably, the majority of synchronous tumors were detected in TRB-patients after the year 2000, as cerebral imaging was performed more frequently in our centers. We found a lower median time-interval of 14 months in our group compared to a median time-interval of 21 months mentioned in literature (1;13). In these studies however, the majority of the TRBs (83% and 62% respectively) were detected after diagnosis and treatment for Rb, while in our study a higher rate of synchronous tumors (41%) were present.

Pineoblastomas and suprasellar tumors presented as typically well-defined lesions with relatively isointense SI on T1W and T2W images compared to grey matter. Contrast enhancement in these tumors was mostly heterogenous due to cystic components or tumor necrosis. Similar SIs on T1W images were reported in 4 and 8 patients respectively on MRI (10;15), but diverse enhancement patterns and SIs on T2W images were described (13;15;17;18). Hydrocephalus was a typical complication of large pineoblastomas. Therefore, we stress the need for BBI to detect smaller TRBs.

The majority of the pineoblastomas in our study were partially or totally cystic. Pineal cysts have been reported in Rb patients but not associated with hereditary Rb (19). The presence of suspicious pineal cystic tumors however, are a point of discussion (19-24). Because of life-threatening side effects that may be related with curative aggressive treatment in TRB patients (25), it is important that cysts are not misinterpreted as tumor. Pineal cysts are diagnosed if a) an enlarged PG is present, b) with a hypointense central region with respect to white matter on T1W images and isointense with respect to CSF on T2W images and c) a thin wall of 2 mm or

less with discrete rim enhancement after gadolinium injection (20). Although these criteria are formulated, pineal lesions in retinoblastoma are causing radiological dilemmas, especially if the cyst wall is irregularly thickened (> 2 mm) or shows a fine nodular aspect of the wall (19;20). In our study, only 6 out of 14 pineoblastomas were completely solid, whereas 29% (4 tumors) had both a cystic and solid component and 4 tumors mimicked a pineal cyst. Hence, the need for imaging characteristics of early stage (cystic) pineoblastoma and follow-up scheme in suspicious cystic lesions of the PG is necessary to these from benign pineal cysts. Identification of such criteria is only possible in a large group of suspicious cystic PGs in Rb patients. Because these tumors are rare, a multicentric prospective study is necessary to define evident criteria for detection of early stage (cystic) pineoblastoma. Meanwhile, we recommend that pineal cystic lesions depicted on BBI should be classified into three groups: (1)“probably benign pineal cyst”, (2)“obvious cystic pineoblastoma”, or (3)“suspicious pineal cyst”. The first group contains patients with a cystic PG with discrete rim enhancement and a thin smooth wall; we recommend repeating MRI once after 6 months and if stable; no further follow-up. The latest group requires close MR follow-up after 3 months. As currently MRI of every new Rb patient is performed routinely in most centers, screening could easily be obtained by performing at least one brain MR sequence (26). This screening could be achieved by a post-contrast 3D T1W sequence with 1 mm slice thickness, and if a cystic portion is detected in the PG, an additional 2 mm T2W sequence can further characterize the lesion.

In our series, a trend was observed for a better survival of patients who had PNET early detected with BBI. However, due to the small sample size, this difference did not reach significance. Several studies advise brain imaging screening in Rb-patients in order to detect TRb in an early stage (1;9;27). Although improvement of prognosis in TRb patients is important, caution with screening programs should be considered. First, prognosis of TRb patients detected by screening compared to patients with symptomatic disease should be evaluated. Duncan et al were the first to evaluate screening for TRb with CT at baseline and additional brain MRI every 6 months in 83 hereditary Rb patients (12). No improved outcome was observed despite early diagnosis. Kivela et al (1), discovered that screening identified TRb in an earlier stage, but without better survival. This indicates that longer survival was due to lead-time bias. A disadvantage of early detection without better outcome is severe treatment-related morbidity and distress in these children leading to lower quality of life. In recent literature however, high-dose chemotherapy has successfully been introduced for TRb, gradually leading to an increase in survival time (14;28). Especially TRb detected in an early stage could benefit from these new treatment strategies, since reported survivors are almost inevitably the synchronous or early metachronous patients. These early metachronous patients (TRb diagnosed a few months after Rb-diagnosis) should be classified as “missed synchronous” rather than “early metachronous”. Therefore we stress the need for routine brain MRI in every single newly diagnosed retinoblastoma patient on admission, which is a potentially simple and (cost-)effective screening method for early TRb detection. The

value of extending brain MRI screening after BBI is under discussion and therefore sporadically applied in European retinoblastoma referral centers.

The rare incidence of TRb in all participating Rb-centers in Europe is in agreement with the observed declining incidence of TRb over the last decades (29-31) and is still a matter of debate. An increasing use of neoadjuvant chemotherapy for intraocular retinoblastoma (chemoreduction) preventing development of TRb has been suggested by Shields et al. who registered fewer TRb since the introduction of chemoreduction as primary treatment for Rb (31). However, cases of TRb are reported even after an intensive scheme of chemoreduction therapy in advance (32). In our study, two out of 10 metachronous TRb patients received chemotherapy and still developed TRb. The decreasing incidence of TRb could be due to the declining use of EBRT in patients with hereditary retinoblastoma (33). In three patients, intraocular Rb was treated with EBRT and these patients developed metachronous pineoblastomas.

A limitation of this study is the absence of BBI in all included metachronous TRbs. Therefore, the true incidence of metachronous TRb is likely to be still overestimated. Also, the small size of our patient cohort was a study limitation for statistical analysis.

In conclusion, TRb mainly develops in the PG and frequently presents with a cystic appearance that may be misleading. We recommend a three-group classification of pineal cystic lesions depicted in Rb patients. Routine BBI in all newly diagnosed Rb is strongly recommended as it may detect TRb in a subclinical and potentially curable stage.

REFERENCES

1. Kivela T. Trilateral retinoblastoma: a meta-analysis of hereditary retinoblastoma associated with primary ectopic intracranial retinoblastoma. *J Clin Oncol* 1999;17:1829-1837
2. Bader JL, Miller RW, Meadows AT, Zimmerman LE, Champion LA, Voute PA. Trilateral retinoblastoma. *Lancet* 1980;2:582-583
3. De Potter P, Shields CL, Shields JA. Clinical variations of trilateral retinoblastoma: a report of 13 cases. *J Pediatr Ophthalmol Strabismus* 1994;31:26-31
4. Michaud J, Jacob JL, Demers J, Dumas J. Trilateral retinoblastoma: bilateral retinoblastoma with pinealoblastoma. *Can J Ophthalmol* 1984;19:36-39
5. Whittle IR, McClellan K, Martin FJ, Johnston IH. Concurrent pineoblastoma and unilateral retinoblastoma: a forme fruste of trilateral retinoblastoma? *Neurosurgery* 1985;17:500-505
6. Bejjani GK, Donahue DJ, Selby D, Cogen PH, Packer R. Association of a suprasellar mass and intraocular retinoblastoma: a variant of pineal trilateral retinoblastoma? *Pediatr Neurosurg* 1996;25:269-275
7. Holladay DA, Holladay A, Montebello JF, Redmond KP. Clinical presentation, treatment, and outcome of trilateral retinoblastoma. *Cancer* 1991;67:710-715
8. Jubran RF, Erdreich-Epstein A, Butturini A, Murphree AL, Villablanca JG. Approaches to treatment for extraocular retinoblastoma: Children's Hospital Los Angeles experience. *J Pediatr Hematol Oncol* 2004;26:31-34
9. Paulino AC. Trilateral retinoblastoma: is the location of the intracranial tumor important? *Cancer* 1999;86:135-141
10. Provenzale JM, Gururangan S, Klintworth G. Trilateral retinoblastoma: clinical and radiologic progression. *AJR Am J Roentgenol* 2004;183:505-511
11. Blach LE, McCormick B, Abramson DH, Ellsworth RM. Trilateral retinoblastoma--incidence and outcome: a decade of experience. *Int J Radiat Oncol Biol Phys* 1994;29:729-733
12. Duncan JL, Scott IU, Murray TG, Gombos DS, van Quill K, O'Brien JM. Routine neuroimaging in retinoblastoma for the detection of intracranial tumors. *Arch Ophthalmol* 2001;119:450-452
13. Provenzale JM, Weber AL, Klintworth GK, McLendon RE. Radiologic-pathologic correlation. Bilateral retinoblastoma with coexistent pinealoblastoma (trilateral retinoblastoma). *AJNR Am J Neuroradiol* 1995;16:157-165
14. Wright KD, Qaddoumi I, Patay Z, Gajjar A, Wilson MW, Rodriguez-Galindo C. Successful treatment of early detected trilateral retinoblastoma using standard infant brain tumor therapy. *Pediatr Blood Cancer* 2010;55:570-572
15. Bagley LJ, Hurst RW, Zimmerman RA, Shields JA, Shields CL, de Potter P. Imaging in the trilateral retinoblastoma syndrome. *Neuroradiology* 1996;38:166-170
16. Antoneli CB, Ribeiro KC, Sakamoto LH, Chojniak MM, Novaes PE, Arias VE. Trilateral retinoblastoma. *Pediatr Blood Cancer* 2007;48:306-310
17. Cho EY, Suh YL, Shin HJ. Trilateral retinoblastoma: a case report. *J Korean Med Sci* 2002;17:137-140
18. Jurkiewicz E, Pakula-Kosciesza I, Rutynowska O, Nowak K. Trilateral retinoblastoma: an institutional experience and review of the literature. *Childs Nerv Syst* 2010;26:129-132
19. Rodjan F, de Graaf P, Moll AC, et al. Brain abnormalities on MR imaging in patients with retinoblastoma. *AJNR Am J Neuroradiol* 2010;31:1385-1389
20. Beck PM, Balmer A, Maeder P, Braganca T, Munier FL. Benign pineal cysts in children with bilateral retinoblastoma: a new variant of trilateral retinoblastoma? *Pediatr Blood Cancer* 2006;46:755-761
21. Karatzas EC, Shields CL, Flanders AE, Gonzalez ME, Shields JA. Pineal cyst simulating pinealoblastoma in 11 children with retinoblastoma. *Arch Ophthalmol* 2006;124:595-597
22. Engel U, Gottschalk S, Niehaus L, et al. Cystic lesions of the pineal region--MRI and pathology. *Neuroradiology* 2000;42:399-402
23. Golzarian J, Baleriaux D, Bank WO, Matos C, Flament-Durand J. Pineal cyst: normal or pathological? *Neuroradiology* 1993;35:251-253

24. Mandra M, Marcol W, Bierzynska-Macyszyn G, Kluczevska E. Pineal cysts in childhood. *Childs Nerv Syst* 2003;19:750-755
25. Dunkel IJ, Jubran RF, Gururangan S, et al. Trilateral retinoblastoma: potentially curable with intensive chemotherapy. *Pediatr Blood Cancer* 2010;54:384-387
26. de Graaf P, Goricke S, Rodjan F, et al. Guidelines for imaging retinoblastoma: imaging principles and MRI standardization. *Pediatr Radiol* 2012;42:2-14
27. O'Brien JM. Retinoblastoma: clinical presentation and the role of neuroimaging. *AJNR Am J Neuroradiol* 2001;22:426-428
28. De Ioris MA, Fidani P, Munier FL, et al. Successful treatment of trilateral retinoblastoma with conventional and high-dose chemotherapy plus radiotherapy: a case report. *J Pediatr Hematol Oncol* 2010;32:e343-e345
29. Moll AC, Imhof SM, Bouter LM, et al. Second primary tumors in patients with hereditary retinoblastoma: a register-based follow-up study, 1945-1994. *Int J Cancer* 1996;67:515-519
30. Moll AC, Imhof SM, Schouten-van Meeteren AY, Boers M, van LE, Hofman P. Chemoreduction for retinoblastoma. *Arch Ophthalmol* 2003;121:1513
31. Shields CL, Meadows AT, Shields JA, Carvalho C, Smith AF. Chemoreduction for retinoblastoma may prevent intracranial neuroblastic malignancy (trilateral retinoblastoma). *Arch Ophthalmol* 2001;119:1269-1272
32. Turaka K, Shields CL, Meadows AT, Leahey A. Second malignant neoplasms following chemoreduction with carboplatin, etoposide, and vincristine in 245 patients with intraocular retinoblastoma. *Pediatr Blood Cancer* 2011;
33. Moll AC, Imhof SM, Schouten-van Meeteren AY, Boers M. Screening for pineoblastoma in patients with retinoblastoma. *Arch Ophthalmol* 2002;120:1774

Chapter 7

*Second cranio-facial malignancies in hereditary
retinoblastoma survivors previously treated with
radiation therapy: clinic and radiologic characteristics
and survival outcomes*

Firazia Rodjan

Pim de Graaf

Hervé J. Brisse

Jonathan I.L.M. Verbeke

Esther Sanchez

Paolo Galluzzi

Sophia Göricke

Philippe Maeder

Isabelle Aerts

Remi Dendale

Laurence Desjardins

Sonia de Francesco

Norbert Bornfeld

Wolfgang Sauerwein

Maja Beck Popovic

Dirk L. Knol

Annette C. Moll

Jonas A. Castelijns

ABSTRACT

INTRODUCTION: Hereditary retinoblastoma survivors have an increased risk for cranio-facial second primary tumours (SPT), especially after treatment with external beam radiotherapy (EBRT). This multicentre study evaluates the clinical and imaging characteristics and outcomes of cranio-facial SPTs in irradiated retinoblastoma survivors.

PATIENTS AND METHODS: Clinical and radiological data of 42 retinoblastoma patients with 44 second and third malignancies were reviewed. Radiological data included anatomic location and CT and MR characteristics. Cox regression and likelihood ratio chi-square test were used to evaluate differences in patients' survival rates.

RESULTS: Cranio-facial SPTs were diagnosed at a median age of 13 years. Histological types included osteosarcomas (43%), rhabdomyosarcomas (20%) (57% embryonal, 43% alveolar) and a variety of other types of SPT (37%). Predilection sites were: temporal fossa (39%), ethmoid sinus (23%), orbit (18%), maxillary sinus (16%) and intracranial dura mater (4%). Most of the osteosarcomas (78%) and rhabdomyosarcomas (80%) occurred in patients treated with EBRT in the first year-of-life. Treatment of SPTs with a microscopically complete surgical resection led to a significantly better 5-year overall survival (OS) ($P = 0.017$) and event-free survival (EFS) ($P = 0.012$) compared to patients treated without surgery or incomplete resection (OS: 83% versus 52%; EFS: 80% versus 47%).

CONCLUSIONS: Osteosarcomas and rhabdomyosarcomas are the most common cranio-facial SPTs in irradiated hereditary retinoblastoma survivors, which develop in specific locations and occur predominantly in patients irradiated in their first year-of-life. Microscopically complete surgical resection of SPTs is a major prognostic factor, suggesting the potential benefit of early detection by imaging.

INTRODUCTION

Hereditary Rb survivors are at greater risk of developing second primary tumors (SPTs) (1) because of *RB1*-gene germline mutation. In developed countries, SPTs are the leading cause of death in patients with hereditary Rb (2-6).

The incidence of SPTs in hereditary Rb is 8.4% at 18-years and 36% at 50-years after diagnosis (3,4,6-9). External beam radiotherapy (EBRT) increases the risk for subsequent malignant neoplasms, as up to 70% of SPTs in Rb patients develop inside or at boundaries of the irradiation field (3,4,6,10-14). The age of Rb-diagnosis and subsequent age of irradiation is an additional risk factor: patients irradiated during the first year of their-life develop two to eight times more SPTs than patients irradiated after one year (15-17). The combination of EBRT and chemotherapy in hereditary Rb patients also slightly increases the risk for SPT development compared to EBRT alone (4). Most common histological types of SPT in irradiation fields are osteosarcoma, rhabdomyosarcoma, leiomyosarcoma, other soft tissue sarcomas, meningioma (12,13,18,19) and rarely carcinomas (8,9).

Prognosis of cranio-facial SPTs in Rb survivors is poor despite aggressive treatment. One major prognostic factor of these tumors is the feasibility of complete resection of the SPT (20) and therefore early diagnosis is crucial.

Computed tomography (CT)- and magnetic resonance (MR) imaging features of Rb are well documented. To our knowledge however, except for case reports (18,19), there is only one study (16) describing the spectrum of imaging characteristics of cranio-facial SPTs in Rb survivors.

This multicenter study evaluates the clinical and imaging characteristics and outcomes of cranio-facial SPTs in irradiated hereditary retinoblastoma survivors.

PATIENTS AND METHODS

Study population

This retrospective study originated from an international partnership of five Rb-reference centers (ERIC), from Amsterdam, Essen, Lausanne, Paris and Siena in agreement with the recommendations of each local ethics committee or institutional review board. Patient records from 1989 and 2010 were reviewed and SPTs were included by both ophthalmologists and oncologists from the Rb-reference centers. The following inclusion criteria were set: (1) a cranio-facial second or third malignancies in a retinoblastoma (confirmed by ocular funduscopy, imaging or histopathology) patient, (2) EBRT for retinoblastoma, (3) availability of adequate CT or MRI of the SPT. Patients with either metastatic tumor, retinoblastoma recurrence or trilateral retinoblastoma were not included in the present study. Forty-four second and third malignancies in 42 patients were included in this retrospective study. In the majority of patients the EBRT planning designs could not be retrieved from the medical records and were not digitally available, therefore a clear definition of the radiation fields and boundaries is lacking.

Clinical data and primary retinoblastoma treatment

Clinical records were evaluated for patients' age (at time of Rb-diagnosis, EBRT treatment and SPT-diagnosis), presence of *RBI*-mutation, treatment of Rb and radiation dose. Patients with bilateral Rb, a positive family history of Rb or a *RBI*-gene mutation were classified as "hereditary". Symptoms associated with SPT at first presentation, histopathological type of SPT and treatment for SPT were also recorded. Delay of SPT diagnosis was calculated as the time elapsed from onset of symptoms to confirmation of SPT diagnosis (imaging or biopsy). Surgical treatment was categorized as complete or incomplete microscopic resection. The definition of microscopic complete resection was based on both pathological and surgical information. Microscopic complete resection was defined as if (macroscopically) the whole tumor was resected, with free resection margins at histopathology without macroscopic residual tumor on follow-up imaging. Time-intervals were calculated from EBRT to SPT-diagnosis, and SPT-diagnosis to death or last follow-up date. Clinical data of part of this patient-cohort were previously reported (4,6).

Imaging data and analysis

Only pre-treatment images of SPTs were assessed to avoid treatment effects. Thirty-three MR scans were available for review including unenhanced T1W images in all patients and post-contrast T1-weighted images and T2W images. In addition, 22 CT scans were available for review including 18 contrast-enhanced CT-examinations. In 11 out of 44 tumors both MR and CT was available.

Images were scored for location of SPT and involvement of bones and muscles in the cranio-facial area. Tumor location was afterwards categorized in predilection sites, which were based on the presumed origin of the SPTs; an anatomical compartment or structure which contained the majority of the tumor mass. Additional parameters included regarding tumor spread into neighboring anatomical compartments and structures (e.g. spread into the paranasal sinuses, orbit, intracranial, cavernous sinus and pterygopalatine fossa), perineural spread, invasion through the skullbase and vessel encasement or invasion.

MRI and CT characteristics for SPTs included tumor border (ill- or well-defined), enhancement (homo- or heterogeneous) and necrosis (yes/no). SPTs on MRI were also evaluated for signal intensity (SI) as compared to normal muscles on T1W and T2W images (hypo-, iso- and hyperintense) and on CT (hypo-, iso- and hyperdense) for calcifications and density of the tumor.

Statistics

All data were statistically analyzed using SPSS, version 15.0 (SPSS, Chicago III). Meningiomas were excluded from the survival analysis. For eventfree survival analysis (EFS), an event was considered as if a relapse of the SPT (local recurrence or metastases) or cranio-facial third primary tumor occurred. Cox regression was used to evaluate differences in EFS and overall survival (OS)

in patients treated with or without complete microscopic tumor resection by the likelihood ratio chi-square test. The 95% confidence intervals at 5-year survival were calculated for the EFS and OS. The association between complete microscopic tumor resection and complete disease remission was analyzed by the likelihood ratio chi-square test. Differences between histopathological subtypes and age at SPT diagnosis were analyzed using analysis of variance.

RESULTS

Clinical characteristics

Patient and treatment characteristics are described in Table 1. All patients had hereditary retinoblastoma. EBRT was performed at a mean age of 11 months, and before 1-year of age in 69% of patients. Data regarding EBRT dose were available in all but 2 patients. A mean dose of 45 Gy (range 40–50Gy) was delivered in 15 to 25 fractions of 2 or 3 Gy. Fourteen patients (33%) also received chemotherapy. Chemotherapy regimen included cyclophosphamide in 10, vincristin in 11, actinomycin in 4, carboplatin in 2, etoposide in 2 and cisplatin in 2 patients. In one patient chemotherapy data could not be retrieved.

Table 1: Patient characteristics of retinoblastoma patients with SPT

Characteristic	No. patients (n= 42)
Hereditary retinoblastoma	42
Median age Rb-diagnosis in M (mean, range)	8 (10, 0 - 36)
Median age EBRT in M (mean, range)	10 (11, 1-37)
Median age SPT in Y (mean, range)	13 (15, 3 - 38)
Sex	
male	19
female	23
Positive RB1-gene mutation	35
Treatment Rb	
Enucleation eye	28
EBRT	42
unilateral	28
bilateral	14
Chemotherapy	14
EBRT in 1 st year of life	29

Rb= retinoblastoma, M= months, Y= years EBRT= external beam radiation therapy

SPTs were diagnosed at a median age of 13 years (range, 3–38 years). TPT (2 patients) occurred at a median age of 15 years. Mean time-interval from EBRT to development of SPT was 15 years with a range of 3 to 37 years. In our study population, EBRT performed within the first year-of -life led to SPTs after a mean interval of 14 years compared to 17 years when performed after the first year-of-life.

Delay of diagnosis between onset of symptoms to confirmation of SPT was 56 days (mean 256 days, range 6-707 days). The most frequent presenting symptom was local swelling (60%). Other symptoms included: local pain (14%), headache (19%), sinus symptoms (epistaxis [7%] and persisting rhinorrhoea [5%]), not-fitting eye-prosthesis (10%), symptoms of intracranial hypertension (5%) and ptosis (5%).

Treatment of SPTs

Forty patients underwent treatment for SPT which included chemotherapy in 35 patients (88%), surgery in 25 patients (64%) (out of which only 7 patients showed a microscopic complete tumor resection), EBRT in 4 patients (10%) and brachytherapy in 3 patients (8%). Two patients received only palliative care because of extensive tumor spread.

Clinical and radiological characteristics according to histopathological subtypes

The 44 craniofacial SPTs and TPTs were categorized in the following five groups: osteosarcomas (17 SPTs and 2 TPTs), rhabdomyosarcomas (9 SPTs), other sarcomas, carcinomas and miscellaneous tumors (16 SPTs) (Table 2). Imaging characteristics for osteosarcomas and rhabdomyosarcomas are summarized in Table 3.

Table 2: Histopathology and age at diagnosis of 44 second and third primary tumors

Histopathological subgroups	Number	Median age in years (mean, range)
Osteosarcoma	19	13 (14, 5 - 20)
Rhabdomyosarcoma	9	11 (11, 5 - 22)
Other sarcomas	8	22 (23, 15 - 36)
Leiomyosarcoma	2	
Undifferentiated sarcoma	5	
Liposarcoma	1	
Carcinomas	5	16 (19, 7 - 38)
Sebaceous gland carcinoma	1	
Undifferentiated spindle cell carcinoma	3	
Sinonasal neuroendocrine carcinoma	1	
Miscellaneous	3	11 (14, 3 - 28)
Meningeoma	2	
Esthesioneuroblastoma	1	

More osteosarcomas and rhabdomyosarcomas were found in Rb survivors treated with EBRT within the first year-of-life compared to EBRT after the first year-of-life although this difference was not significant ($P = 0.07$). The median age of occurrence of SPT was significantly younger for the two major histological types ($P = 0.008$ for osteosarcomas and $P = 0.003$ for rhabdomyosarcomas) than for the others. In the subgroup of 14 patients treated with a combination of EBRT and chemotherapy, no significant correlations were found regarding histopathology, age

at presentation or predilection sites of SPTs compared to patients treated for Rb with EBRT alone.

Tumor origin was subdivided into five predilection sites; temporal fossa (39%), ethmoid sinus (23%), orbit (18%), superior maxillary (16%) and intracranial dura mater (4%).

Table 3: CT and MR imaging characteristics of osteosarcoma and rhabdomyosarcoma in %

		Osteosarcoma	Rhabdomyosarcoma
		MR (n= 14); CT (n= 12)	MR (n= 8); CT (n= 2)
Mean TV in cm³(range)		107 (0.4-411)	91 (12-330)
Border			
	well-defined	88 (23)	100 (10)
	ill-defined	12 (3)	0
Necrosis			
	yes	65 (17)	50 (5)
	no	27 (7)	50 (5)
	NA	8 (2)	0
EP			
	homogeneous	4 (1)	15 (2)
	heterogeneous	86 (22)	75 (7)
	NA	12 (3)	10 (1)
SI T1-W (MR)			
	hypointense	21 (3)	0
	isointense	71 (10)	100 (8)
	hyperintense	7 (1)	0
SI T2-W (MR)			
	hypointense	21 (3)	0
	isointense	7 (1)	25 (2)
	hyperintense	64 (9)	75 (6)
	NA	7 (1)	0
Density (CT)			
	hypodense	17 (2)	50 (1)
	isodense	17 (2)	50 (1)
	hyperdense	25 (3)	0
	NA	42 (5)	0
Calcifications (CT)			
	yes	50 (6)	50 (1)
	no	33 (4)	50 (1)
	NA	17 (2)	0

TV= tumorvolume, EP= enhancement pattern, SI T1-W= signal intensity on T1-weighted images
SI T2-W= signal intensity on T2-weighted images, (absolute values in brackets)

Osteosarcoma

Osteosarcoma was the most frequent histologic subtype (43%, 19/44), including 2 TPTs. Fourteen osteosarcoma (78%) developed in patients treated with EBRT within the first year-of-life. Median age for osteosarcoma diagnosis was 13 years (range, 5 – 20 years). The orbit (36%) (Fig 2) and temporal fossa (36%) were the predilection sites in this group, Fig 1. In patients with osteosarcomas with EBRT after the 1st year-of-life, the temporal fossa (50%) was mostly affected. All osteosarcomas in the maxillary sinus and 83% in the orbit were also present in this group. Nine out of 18 patients (50%) with osteosarcoma died (mean interval, 65 months) and 10 patients are currently in complete remission (mean follow-up of 87 months).

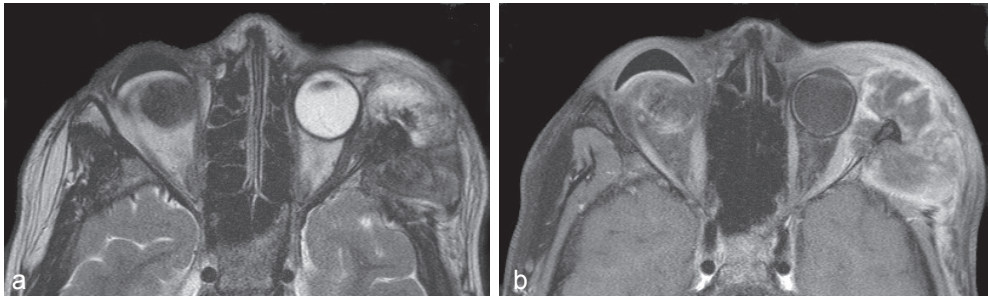


Fig. 1. Typical location of osteosarcoma originating from the lateral orbital wall (greater wing of the sphenoid) and temporal bone with extension into the temporal fossa in a 12 years-old girl with bilateral retinoblastoma. The tumour was treated with chemotherapy only after parental refusal for surgery. This girl died 3 years after diagnosis due to local disease progression.

Rhabdomyosarcoma

Rhabdomyosarcoma was the second most common SPT (20%, 9/44) including 4 embryonal and 3 alveolar subtypes (data not available for 2 patients). Median age of rhabdomyosarcoma was 11 years (range 5 – 22 years). Eight out of 9 rhabdomyosarcomas were detected in patients irradiated in the first year-of-life, with the ethmoid (50%) (Fig. 2a, b) and temporal fossa (38%) as predominantly affected sites. Only 1 tumor developed in a patient irradiated after the first year; tumor occurred in the temporal fossa. In total, 4 out of 9 rhabdomyosarcoma patients died after a mean follow-up of 77 months (range 5-154). Three patients died due to disease progression and 1 patient died 154 months after SPT diagnosis from a TPT (osteosarcoma) occurring 6 years after rhabdomyosarcoma. Five patients are still in complete remission (mean follow-up, 68 months).

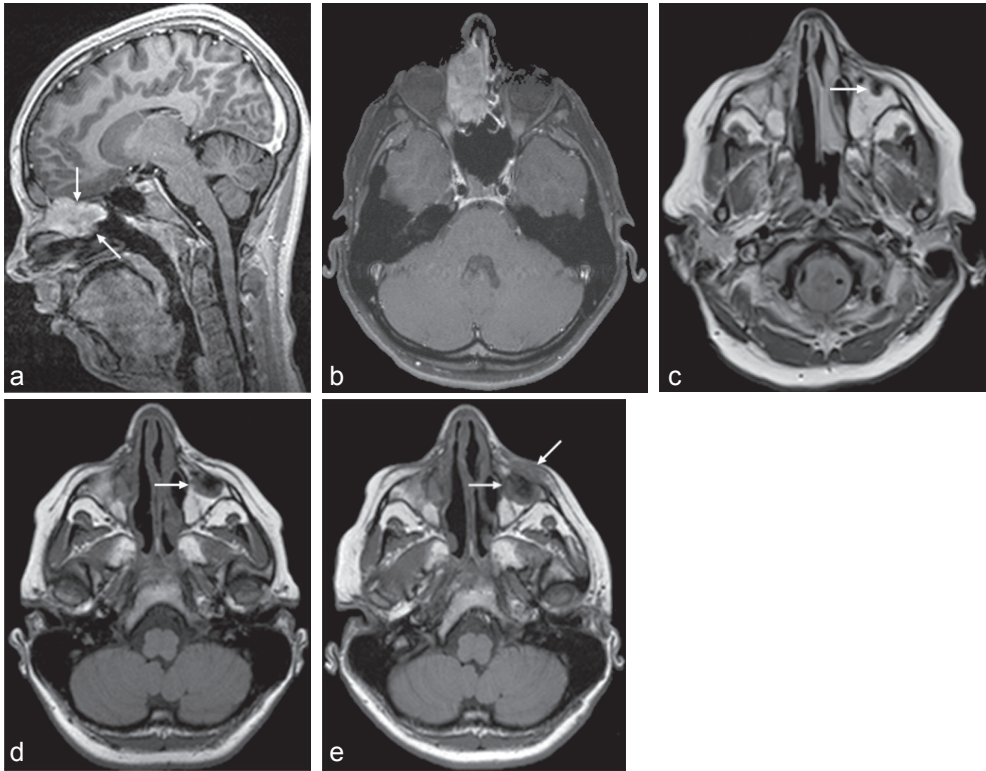


Fig. 2. A 13-year-old girl presenting with a second and third primary tumour after bilateral EBRT at 2 months of age. An embryonal rhabdomyosarcoma of the right ethmoid sinus (a and b) occurred at 13 years of age, which was treated with chemotherapy, surgery and brachytherapy. During follow-up for this second primary tumour, the patient complained about a painful swelling under the left eye and magnetic resonance imaging (MRI) demonstrated an osteosarcoma originating from the orbital floor with soft-tissue invasion (small arrow) (e). Retrospectively, this tumour could be observed 6 months and 2 months earlier without soft-tissue invasion (c and d). This third primary tumour was treated with chemotherapy, extensive surgery and brachytherapy. Both tumours were completely resected and this girl is still in second complete remission.

Other second primary tumors

A variety of other types of SPTs after irradiation were divided in; other sarcomas, carcinomas and miscellaneous tumors (Table 2). In 8 patients with EBRT in the 1st year-of-life, 5 (63%) were other sarcomas, 2 (25%) carcinomas and 1 (12%) miscellaneous tumors. The temporal fossa (40%) and ethmoid sinus (40%) were the predilection sites for patients irradiated within their 1st year-of-life.

Survival

At the study time point, 20 patients were still alive (mean interval, 82 months; median, 73 months; range, 17–168 months) since SPT-diagnosis. Among these 20 patients, 19 were in complete remission (including 3 patients in second complete remission). One patient was disease free and lost to follow-up 1 month after complete microscopic tumor resection. Twenty-two patients died from disease progression (mean interval, 51 months; median, 32 months; range, 6 days–244 months) from diagnosis.

A significant better 5-year OS ($P = 0.017$) (Fig 3a) and EFS ($P = 0.012$) (Fig 3b) was observed in patients with complete microscopic tumor resection and 5-year OS and EFS were respectively 83% (95% CI 54%–100%) and 80% (95% CI 45%–100%). Complete microscopic tumor resection also showed a statistically significant correlation with complete disease remission ($P = 0.036$) (Fig. 4). In patients with incomplete resection, the 5-year OS and EFS were 52% (95% CI 34%–70%) and 47% (95% CI 29%–64%) respectively. Tumor location ($P = 0.38$), histopathological subtype ($P = 0.33$) and age of EBRT (< 1 year; > 1 year) ($P = 0.53$) were not associated with a significant difference in survival.

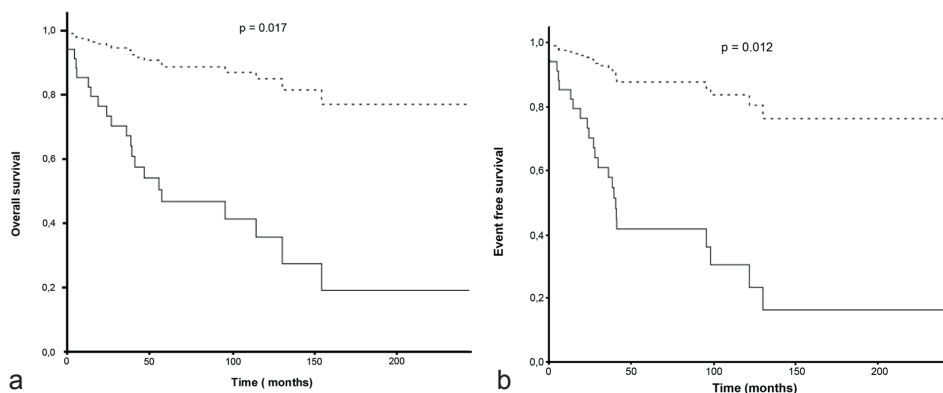


Fig. 3. Overall survival curve ($P = 0.017$) (a) and event-free survival curve ($P = 0.012$) (b) showing the effects of complete ($n = 7$, dotted line) and incomplete ($n = 33$, solid line) microscopic tumour resection in 40 retinoblastoma patients with second primary cranio-facial tumours.

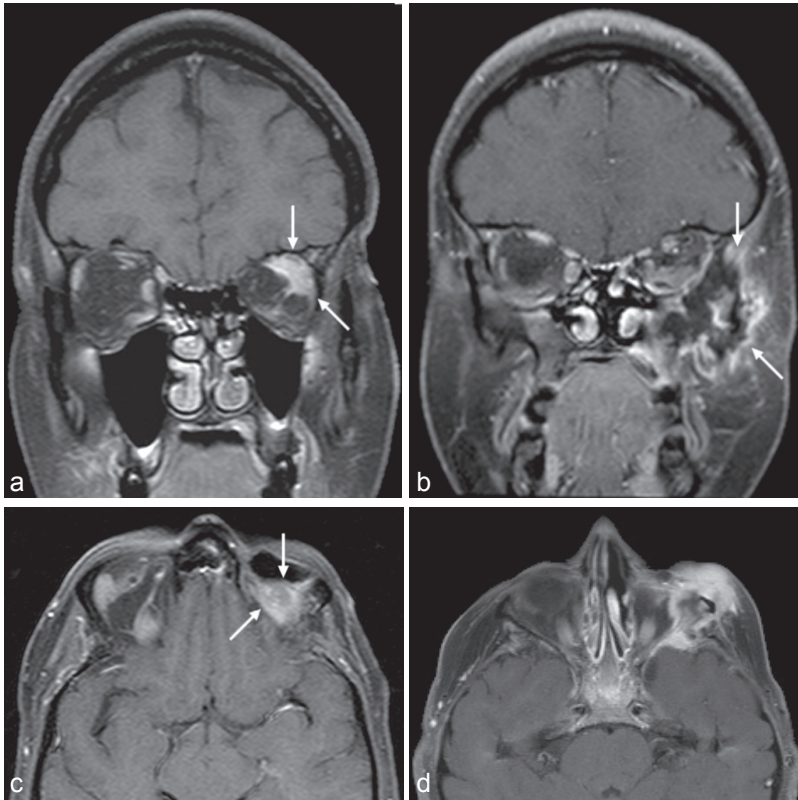


Fig. 4. Second primary tumours with complete (a and c) versus incomplete (b and d) microscopic tumour resection in the orbital region. Sebaceous gland carcinoma (a and c) in a 38 year old woman with invasion in intra-orbital fat treated with surgery and still under complete remission. Liposarcoma (b and d) in a 28 year old woman treated with chemotherapy and radiation therapy with tumour progression and death 3 years after diagnosis.

DISCUSSION

Osteosarcoma and rhabdomyosarcoma are the most common histopathological subtypes of craniofacial SPTs in irradiated hereditary retinoblastoma patients, accounting for 64% of all SPTs in our study. Most osteosarcomas are primarily located in the orbit or temporal fossa and rhabdomyosarcomas in the ethmoid sinus or temporal fossa. Hereditary Rb-patients irradiated in their first year-of-life have a higher risk of SPTs since 79% of osteosarcomas, 89% of rhabdomyosarcomas and 63% of the other sarcomas develop in this group of children (21).

In our study, the majority of the patients complained about a local swelling, sometimes combined with local pain as previously described (20). Physicians should realise that otherwise innocent symptoms, such as a combination of chronic headache and sinus symptoms, may be potentially indicative for craniofacial SPTs (8). These (chronic) symptoms in irradiated hereditary

Rb-patients should alert physicians to perform imaging without delay in order to detect SPTs at a potentially curative stage.

Radiologists should realise that cranio-facial SPTs in these patients occur in specific predilection sites. Most SPTs develop in the temporal fossa (39%), especially in patients treated with EBRT before 1 year-of-age. In the subgroup of 14 patients treated with a combination of EBRT and chemotherapy, no significant correlation was observed regarding histopathology, age at presentation or predilection sites of SPTs compared to patients treated for Rb with EBRT alone. Osteosarcomas frequently originated from the orbit and rhabdomyosarcomas from the ethmoid. Signal intensity or density are nonspecific for a specific histological type, although calcifications are present in at least 50% of osteosarcomas. Tateishi et al. (16) reported imaging characteristics (MRI or CT) of SPTs in the irradiated field in 15 patients, and only for osteosarcomas central calcification was found as important finding on CT. Therefore, any solid tissue mass should prompt to perform a biopsy for tumor identification without delay.

Prognosis of Rb patients with SPTs depends on possible treatment strategies. SPTs in the irradiated area, treated by a radical surgical approach in combination with chemotherapy and/or re-irradiation, show a better survival compared to cases without combined aggressive treatment (22). Re-irradiation however, has an increased risk of complications due to post-radiation effects and might further increase the risk for a third or fourth primary tumor (23). Therefore, in cases of small and resectable tumors in a previously irradiated area, surgery remains the modality of choice (24) and complete resection is important for an optimal outcome (25). In some cases however, it is difficult to achieve clear surgical margins in this region (20). Our study confirmed a significant better 5-year EFS (83%) and OS (80%) in patients treated with complete microscopic tumor resection. In this group, we saw significantly more patients with complete disease remission with a mean interval of 82 months. This stresses the need of early detection of SPTs in a stage where complete resection is possible. Additional pre-operative chemotherapy in combination with radical resection may increase the survival rate of patients treated for SPTs occurring after hereditary retinoblastoma (20).

A diagnostic protocol based on clinical symptoms is important in Rb patients previously irradiated and specific information regarding these symptoms should be provided as warning signs for the patient of interest. However, symptoms are usually nonspecific and the most common is soft tissue swelling which may occur quite late in tumor development. For the same reason, a clinical depiction based on regular ENT examination would also probably be insufficient. In order to detect SPTs at an early and potentially resectable stage, an imaging screening program could be suggested. According to our data, we would recommend to screen the population of all retinoblastoma patients treated with EBRT from an age of 5 years to approximately 20 years. Frequency of imaging is dependent of different factors including age and associated treatments, growth-rate of sarcomas, patients comfort and costs of imaging examinations. Although there is currently no consensus about the repetition time, a one year interval could be suggested. Because

hereditary retinoblastoma patients are extra vulnerable for radiation damage to the DNA, CT-scans should be avoided, and MRI should be preferred.

The benefit of such an MR depiction program in terms of survival is currently not evidence-based. Early diagnosis of SPTs should be balanced against patients' discomfort and anxiety related to repeated MRI examinations, and against potential false positive MR findings leading to unnecessary biopsies. Such a screening should only be performed through a scientific multi-center research protocol including informed consent and should assess screenings-intervals, exact radiation dose at the tumor site, survival, and the accuracy, benefit, costs and tolerability of the method.

Precise comparison of the SPT location with the radiation fields was not possible in this study with the consequence that the exact dose at the tumor site could not be calculated. Furthermore, the small size of our patient cohort was a study limitation for statistical issues.

In conclusion, osteosarcomas and rhabdomyosarcomas are the major cranio-facial SPTs in irradiated retinoblastoma patients developing in specific locations, particularly in patients with EBRT in their first year-of-life. As complete surgical resection is a major prognostic factor, the diagnosis of SPT should be obtained as early as possible. Therefore, awareness about the risk factors and associated revealing symptoms, typical location and radiological patterns is important. An MRI-based screening program could also prove value in detecting these tumors in an early and resectable stage to improve survival.

REFERENCES

1. Moll AC, Kuik DJ, Bouter LM, Den OW, Bezemer PD, Koten JW et al. Incidence and survival of retinoblastoma in The Netherlands: a register based study 1862-1995. *Br.J.Ophthalmol.* 1997;81:559-62.
2. Eng C, Li FP, Abramson DH, Ellsworth RM, Wong FL, Goldman MB et al. Mortality from second tumors among long-term survivors of retinoblastoma. *J.Natl.Cancer Inst.* 1993;85:1121-8.
3. Kleinerman RA, Tucker MA, Tarone RE, Abramson DH, Seddon JM, Stovall M et al. Risk of new cancers after radiotherapy in long-term survivors of retinoblastoma: an extended follow-up. *J.Clin.Oncol.* 2005;23:2272-9.
4. Marees T, Moll AC, Imhof SM, de Boer MR, Ringens PJ, van Leeuwen FE. Risk of second malignancies in survivors of retinoblastoma: more than 40 years of follow-up. *J.Natl.Cancer Inst.* 2008;100:1771-9.
5. Marees T, van Leeuwen FE, de Boer MR, Imhof SM, Ringens PJ, Moll AC. Cancer mortality in long-term survivors of retinoblastoma. *Eur.J.Cancer* 2009;45:3245-53.
6. Moll AC, Imhof SM, Bouter LM, Kuik DJ, Den OW, Bezemer PD et al. Second primary tumors in patients with hereditary retinoblastoma: a register-based follow-up study, 1945-1994. *Int.J.Cancer* 1996;67:515-9.
7. Draper GJ, Sanders BM, Kingston JE. Second primary neoplasms in patients with retinoblastoma. *Br.J.Cancer* 1986;53:661-71.
8. Bhagia P, Colanta AB, Abramson DH, Carlson DL, Kleinerman RA, Kraus D et al. Sinonasal adenocarcinoma: A rare second malignancy in long term retinoblastoma survivors. *Pediatr.Blood Cancer* 2011.
9. Draff C, Schaberg MR, Anand VK, Nyquist G, Hoda S. Radiation induced malignancy in retinoblastoma: new pathology in a case report. *Laryngoscope* 2010;120 Suppl 4:S238.
10. Soloway HB. Radiation-induced neoplasms following curative therapy for retinoblastoma. *Cancer* 1966;19:1984-8.
11. Imhof SM, Moll AC, Hofman P, Mourits MP, Schipper J, Tan KE. Second primary tumours in hereditary- and nonhereditary retinoblastoma patients treated with megavoltage external beam irradiation. *Doc.Ophthalmol.* 1997;93:337-44.
12. Schlienger P, Campana F, Vilcoq JR, Asselain B, Dendale R, Desjardins L et al. Nonocular second primary tumors after retinoblastoma: retrospective study of 111 patients treated by electron beam radiotherapy with or without TEM. *Am.J.Clin.Oncol.* 2004;27:411-9.
13. Abramson DH, Ellsworth RM, Kitchin FD, Tung G. Second nonocular tumors in retinoblastoma survivors. Are they radiation-induced? *Ophthalmology* 1984;91:1351-5.
14. Maes P, Brichard B, Vermeylen C, Cornu G, Ninane J. Primary and secondary osteosarcoma of the face: a rare childhood malignancy. *Med.Pediatr.Oncol.* 1998;30:170-4.
15. Abramson DH, Scheffer AC. Update on retinoblastoma. *Retina* 2004;24:828-48.
16. Abramson DH, Servodidio CA. Retinoblastoma in the first year of life. *Ophthalmic Paediatr.Genet.* 1992;13:191-203.
17. Moll AC, Imhof SM, Schouten-Van Meeteren AY, Kuik DJ, Hofman P, Boers M. Second primary tumors in hereditary retinoblastoma: a register-based study, 1945-1997: is there an age effect on radiation-related risk? *Ophthalmology* 2001;108:1109-14.
18. Kleinerman RA, Tucker MA, Abramson DH, Seddon JM, Tarone RE, Fraumeni JF, Jr. Risk of soft tissue sarcomas by individual subtype in survivors of hereditary retinoblastoma. *J.Natl.Cancer Inst.* 2007;99:24-31.
19. Tateishi U, Hasegawa T, Miyakawa K, Sumi M, Moriyama N. CT and MRI features of recurrent tumors and second primary neoplasms in pediatric patients with retinoblastoma. *AJR Am.J.Roentgenol.* 2003;181:879-84.
20. Aerts I, Pacquement H, Doz F, Mosseri V, Desjardins L, Sastre X et al. Outcome of second malignancies after retinoblastoma: a retrospective analysis of 25 patients treated at the Institut Curie. *Eur.J.Cancer* 2004;40:1522-9.

21. Abramson DH. Retinoblastoma in the 20th century: past success and future challenges the Weisenfeld lecture. *Invest Ophthalmol. Vis. Sci.* 2005;46:2683-91.
22. Smith LM, Donaldson SS, Egbert PR, Link MP, Bagshaw MA. Aggressive management of second primary tumors in survivors of hereditary retinoblastoma. *Int. J. Radiat. Oncol. Biol. Phys.* 1989;17:499-505.
23. de Bree R, Moll AC, Imhof SM, Buter J, Leemans CR. Subsequent tumors in retinoblastoma survivors: the role of the head and neck surgeon. *Oral Oncol.* 2008;44:982-5.
24. Kasperts N, Slotman B, Leemans CR, Langendijk JA. A review on re-irradiation for recurrent and second primary head and neck cancer. *Oral Oncol.* 2005;41:225-43.
25. Ottaviani G, Jaffe N. The epidemiology of osteosarcoma. *Cancer Treat. Res.* 2009;152:3-13.

Chapter 8

General discussion and future perspectives

Retinoblastoma has evolved from a deadly childhood cancer to a largely curable disease within the past 100 years. Current treatment strategies are firstly focused on survival and secondly on salvaging the eye, providing the best visual outcome as possible. Despite the clear advantages, the drawback of this development is that histopathological confirmation of diagnosis and analysis of prognostic factors will be decreasingly available in the future. Histopathology is the golden standard in evaluating tumor spread and therefore in predicting disease dissemination and prognosis of retinoblastoma. These parameters influence treatment options of a child with retinoblastoma. Therefore, non-invasive evaluation of prognostic risk factors and treatment response become increasingly important.

Hereditary retinoblastoma survivors have a greater risk to develop associated neoplasms. Hereditary retinoblastoma is associated with trilateral retinoblastoma (TRB) and second primary tumors (SPT). These co-morbidities have great consequences as most patients have a poor prognosis. It is important to understand the pattern of development of both TRB and SPT in retinoblastoma patients to detect these tumors in an early and potentially curable stage.

The first part of this thesis reports on novel diagnostic imaging techniques applied for ocular MR imaging to differentiate between retinoblastoma and simulating lesions. The capability of advanced imaging techniques to evaluate prognostic factors and treatment response such as angiogenesis and tumor necrosis are studied. The second part of this thesis focuses on imaging patterns of associated abnormalities and more specifically TRB and cranio-facial second primary tumors in irradiated hereditary retinoblastoma survivors.

Minimal required protocol for retinoblastoma imaging

Chapter 2 presents an overview of the minimum requirements for diagnostic evaluation of retinoblastoma or mimicking lesions according to the consensus reached among members of the European Retinoblastoma Imaging Collaboration (ERIC)¹. The value of MRI is mostly reliant on the protocol used². The combination of ultrasound with high resolution MRI is recommended as most useful imaging modalities. Together with funduscopy, ultrasound is mainly responsible for diagnosis of retinoblastoma and detects the specific calcifications in retinoblastoma. High resolution MRI is mainly necessary for determination of tumor extent (optic nerve, choroid, sclera and anterior eye segment) and associated morbidity as TRB and (during follow-up) SPT. Only in complicated eyes MRI may play a role in tumor diagnosis itself. The minimal required protocol explicitly excludes CT scans because it poses a significant radiation risk to (especially hereditary) retinoblastoma patients. The main advantage of MRI compared to CT includes the lack of radiation exposure, better soft tissue discrimination and higher soft tissue contrast. Standardization of imaging protocols world-wide is necessary to perform multicenter international studies for further tumor characterization and implementation of novel imaging techniques in retinoblastoma. New non-invasive imaging parameters to assess tumor response and prognostic factors are essential in the future of retinoblastoma treatment.

Value of novel techniques for ocular MRI in retinoblastoma diagnosis

Ultrasound remains the most economical, rapid and safest imaging modality for confirmation of diagnosis and has a high diagnostic accuracy. Even in difficult cases ultrasound is able to differentiate between benign and malignant intraocular childhood lesions by analysis of tumor morphology and by depicting calcifications which are characteristic for retinoblastoma¹. If clinical diagnosis is uncertain, the combination of ultrasound and MRI is necessary to differentiate between intraocular abnormalities. Confusion in diagnosis sometimes may be the case when persistent hyperplastic primary vitreous and Coats disease are considered in the differential diagnosis. These diseases have a close resemblance with retinoblastoma and can be differentiated by subtle additional MRI information such as eye size, morphology of mass-lesions and enhancement patterns. Because of the increasing use of conservative strategies in treatment of retinoblastoma, novel imaging techniques become more important for noninvasive diagnosis. Especially in complicated eyes, for example in cases when opaque media occurs such as cataract or bleeding in the anterior segment or vitreous, ultrasound and even the standard MRI techniques could become insufficient to confirm the diagnosis of retinoblastoma. Worldwide CT has been the method of choice to detect calcifications and confirm retinoblastoma diagnosis for years^{3,4}.

In chapter 3 we show that retinoblastoma imaging nowadays can be safer and more valuable without exposing the patients to the radiation hazards of CT. The use of T2*WI in depicting calcifications in retinoblastoma demonstrated to be as good as ex-vivo high resolution and high dosis CT-scans. Diagnostic value of T2*WI thereby surpasses the commonly used in vivo standard pediatric orbital CT, which is usually acquired with lower resolution and lower dosis. We were able to confirm and reproduce a study of Galluzzi et al which showed a good correlation between calcifications on CT and signal intensity voids on T2* weighted imaging⁵. In addition we showed MRI characteristics which could differentiate between other causes of signal intensity void spots on T2*WI and calcifications. In ocular MR imaging these additional void spots could indicate intratumoral hemorrhage, which mainly has a smooth and linear aspect and is predominantly located in the tumor periphery. Linear signal intensity voids could also be the effect of susceptibility artifacts causing magnetic field inhomogeneities at the air-tissue interface, such as under the eye lid and is primarily located close to the anterior eye segment. At last we described signal intensity voids due to venous congestion, which is a result of susceptibility effects in venous blood caused by the presence of deoxyhemoglobin, increased intravascular space and slow flowing venous blood. Another promising MRI technique we used to detect calcifications and differentiate them between intratumoral hemorrhage, necrosis and artifacts is susceptibility weighted imaging. Our study suggest that this technique has the potential to be more sensitive than T2*WI.

Value of novel MRI techniques in evaluation of prognostic factors and treatment response

In chapter 4 we describe the potential of dynamic contrast enhanced MRI (DCE-MRI) for assessment of tumor angiogenesis and tumor vitality in retinoblastoma. Microvessel density is an important parameter for tumor angiogenesis in vitro and is associated with local invasive growth and hematogenous metastases in retinoblastoma⁶.

In DCE-MRI, non-invasive evaluation of tumor angiogenesis is acquired by analysis of a set of T1W images, which are obtained consecutively before, during and after injection of a bolus of gadolinium contrast material. This technique supplies information on the uptake and eventually washout of gadolinium from the tissue in the first few minutes after injection. Highly vascularized tissue with a high MVD typically shows rapid signal enhancement after contrast injection, corresponding to a DCE-MRI curve with a steep slope. This curve provides information about blood flow, capillary leakage and related physiological parameters. This technique is increasingly being used in improving clinical diagnostic imaging and in assessing microvascular changes after treatment⁷. A variety of quantitative values associated with DCE-MRI has been analyzed in previous literature in which the same quantities appear with a different name or symbol so that comparison of work from different groups is difficult⁸. K_{trans} for example is a frequently used parameter representing the volume transfer constant but requires determination of both an arterial input function (AIF) and adequate precontrast datasets to calculate the baseline T1 relaxation time. In retinoblastoma imaging however this parameter is not easily applicable because of several reasons. First, in retinoblastoma imaging the estimation of an AIF for sampling is difficult because the lack of a large arterial vessel near the tumor. Secondly, a baseline T1 measurement is usually required for generating the contrast concentration curve from the signal curve. This T1 measurement requires additional acquisition time, and has not yet been applied and validated in orbital imaging⁹. In our study we used the parameter κ obtained with curve pattern analysis. We showed that the early phase of the curve $\kappa(5\text{min})$, which represents the initial phase of the curve, is positively correlated with tumor MVD ($p = 0.008$)¹⁰. This parameter could be a predictor of tumor extent since MVD as a marker correlates with both local invasive growth and the presence of metastasis in retinoblastoma. It could also be a useful follow-up parameter for evaluation of angiogenesis in tumors treated with vascular targeting (antiangiogenic) drugs (anti-VEGF drugs). Although, we observed no significant correlation between DCE-MRI parameters and VEGF in our small study population, it would be interesting to evaluate this in a large retinoblastoma population in the future.

The parameter obtained from the full time series, $\kappa(17\text{min})$, negatively correlated with the degree of tumor necrosis ($p = 0.002$). The $\kappa(17\text{min})$ could be a predictor for the success of conservative treatment of retinoblastoma because severe hypoxia, which is present in necrotic tumors, has a negative influence on the outcome of radiation and chemotherapy. A limitation of our study is the lack of clear landmarks to obtain the same cross section between MRI and the histopathology slice which is especially difficult in heterogenous tumors. We used the classical

region of interest (ROI) approach where the time intensity curves in a ROI are averaged. These curves reflect the status of the tissue and capillary integrity. In breast cancer it has been used as indicator of suspected malignancy^{11;12}. There is however still no general consensus on the real ability of this analysis to correctly grade tumors or exclude malignancy^{13;14}. Although we included the most enhancing part of the tumor, in heterogeneous tumors this technique is not accurate enough. In the future, pixel-by-pixel analysis could optimize DCE-MRI parameters by considering the heterogeneity of the tumor. Previous literature demonstrated that where the ROI approach fails to show the presence of highly vascularized areas, the pixel-by-pixel approach reveals co-existence of a heterogeneous pattern of signal intensity curves¹⁵. This technique could be valuable in the future for response prediction in conservative treatment strategies for retinoblastoma.

Follow-up imaging of associated morbidity

Hereditary retinoblastoma is associated with both malignant and benign brain abnormalities. First, the midline primitive neuroectodermal tumor in the pineal and suprasellar region (known as trilateral retinoblastoma [TRB]) occurs in 5-15% of this population^{16;17}. Structural brain abnormalities are reported in retinoblastoma patients with 13q deletion syndrome¹⁸. In chapter 5 we provide an overview of brain abnormalities that were found in a large group of 168 retinoblastoma patients of which 7 patients were diagnosed with 13q deletion syndrome. In this study population, structural brain abnormalities occurred only in combination with a 13q deletion syndrome. One patient showed a corpus callosum agenesis and another patient a Dandy-walker variant with dilated ventricles which has been described once before in literature¹⁹. In 5.5% of the hereditary retinoblastoma patients pineoblastoma was detected on MRI in accordance with previous literature^{16;17}. The total incidence of pineal cysts in our study was 5.4%, with an incidence of 9.0% in the non-hereditary group and 2.2% in the hereditary group. The incidence in the group of hereditary retinoblastoma is similar to that in healthy younger children and is therefore not associated with retinoblastoma. However, radiologists should realize that small pineoblastomas can have a cystic appearance which could be confusing when analyzing the pineal gland in hereditary retinoblastoma patients. This issue is further discussed in chapter 6. Some studies indicate that in the future the incidence of pineoblastoma may decrease due to the protective effect of chemoreduction therapy and/or the lack of external beam radiation therapy (EBRT)²⁰⁻²². It is likely that this decrease is a consequence of the latter because the vast majority of pineoblastomas are detected at baseline, even before intravenous chemoreduction therapy could have been applied. Furthermore, in the future it will be of interest to know if incidence of pineoblastoma remains the same after the introduction of selective intra-arterial chemotherapy applied to the affected eye via the ophthalmic artery.

In chapter 6 imaging parameters of TRB are further characterized. These intracranial primitive neuroectodermal tumors are most commonly located in the pineal gland (77% of the cases)²³.

Pineoblastomas and suprasellar tumors present as typically well-defined lesions with relatively isointense signal intensity on T1W images compared to gray matter, in agreement with previous literature¹⁷, and isointense signal intensity on T2-W images. These tumors show heterogeneous contrast enhancement because of cystic components or tumor necrosis. A possible association between benign pineal cysts and retinoblastoma which could be an indication for pineoblastoma development is also suggested²⁴. The majority of the pineoblastomas in our study are partially cystic with a solid part (29%) or totally cystic (29%). Benign pineal cysts occur in 0.4% - 2.2% of the general pediatric population in accordance with the incidence of pineal cysts in hereditary retinoblastoma^{25,26}. In hereditary retinoblastoma patients it is important that these cystic pineal glands based on early stage pineoblastomas are detected in time and not misinterpreted with benign pineal lesions so that treatment can be focused on curative. Benign pineal cysts are defined as (1) the presence of an enlarged pineal gland, (2) with a hypointense central region with respect to white matter on T1W images and isointense with respect to cerebral spinal fluid on T2W images, and (3) a thin wall of 2 mm or less with discrete rim enhancement after gadolinium injection²⁷. Despite these criteria, pineal lesions in retinoblastoma causes dilemmas, especially if the cyst wall is irregularly thickened (> 2mm) or shows a fine nodular aspect of the wall²⁸. Therefore identification of imaging criteria concerning early stage (cystic) pineoblastoma and follow-up of suspicious cystic pineal lesions are necessary in future prospective multicenter studies. In the meantime we recommend to classify cystic pineal lesions into three categories (1- “probably benign pineal cyst”, 2- “obvious cystic pineoblastoma”, or 3- “suspicious pineal cyst”) with different clinical approaches to detect pineoblastoma at an early stage. If the lesion follows the criteria regarding benign pineal cysts (category 1), we recommend repeating MRI after 6 months, if stable no further follow-up imaging will be necessary. The third category however needs close MR follow-up after three months. Screening of the pineal gland in retinoblastoma patients could be achieved by a post-contrast 3D T1W sequence with 1 mm slice thickness. If a cystic lesion is detected in the pineal gland, an additional 2 mm T2W sequence or thin slice 3D T2/CISS can be performed to characterize the lesion.

Primitive neuroectodermal tumors in the pineal gland or suprasellar location associated with retinoblastoma (known as trilateral retinoblastoma) has been lethal in virtually all cases previously reported. However, intensive treatment with high-dose chemotherapy protocols and stem cell reinfusion possibly combined with surgery may potentially be curative²⁹. This thesis demonstrates that TRB detected synchronous with retinoblastoma on first MRI examination (baseline brain imaging, BBI) are significantly smaller than metachronous tumors (18mm versus 35mm, P= 0.002). Patients with BBI also have lesser symptoms and tend to have a better prognosis compared with TRB detected after retinoblastoma diagnosis (metachronous tumors). Previous literature suggests that the occurrence of retinoblastoma and a simultaneous intracranial tumor is rare³⁰. However this incidence is probably underestimated as in most reported cases of TRB BBI is not present. The majority of our patients who did not survive TRB, presented usually

with large and mainly metachronous tumors. Kivela detected that mainly children with tumors that were 15 mm or less in size had a better prognosis than children with larger ones ($p = .020$). Screening should be focused on detection of these small tumors. The incidence of synchronous tumors is increased since the year 2000 when brain imaging was routinely performed in the ERIC-centers. Only in patients with BBI there is a possibility to detect these small tumors and potentially cure the patient. Therefore standard BBI in retinoblastoma is important in every newly diagnosed retinoblastoma patient and is therefore recommended in the ERIC guidelines. Although in this thesis the value of BBI is stressed, standard follow-up brain MRI screening in hereditary retinoblastoma patients is not recommended. In a previous study, screening led to a longer median survival time, but the age of TRB detection was earlier while the age of death did not differ. This means that screening led to lead time bias with more risk for severe treatment related morbidity and distress in children.

Second primary tumors (SPT) are responsible for a significant proportion of the mortality in hereditary retinoblastoma survivors^{31;32}. External beam radiation therapy (EBRT) increases the risk for (radiation induced) bone cancers and soft tissue sarcomas. Seventy percent of these sarcomas develop within the head and face³². Our study shows that craniofacial SPTs in irradiated retinoblastoma patients are diagnosed at a median age of 13 years (range 3 – 38 years) and a median time-interval between EBRT to SPT development of 15 years (range: 3–37). Age of EBRT is a risk factor for SPT development in retinoblastoma with development of considerably more SPTs in patients irradiated during their first year of life compared to irradiation after one year^{33;34}. This might in part be explained by the fact that hereditary retinoblastoma patients develop their disease at a younger age and therefore treated earlier. SPTs are usually symptomatic at diagnosis with local swelling (60%), local pain (14%), headache (19%), epistaxis (7%), persistent rhinorrhea (5%), not-fitting ocular prosthesis (10 %), symptoms of intracranial hypertension (5%), and ptosis (5%) as most frequent symptoms. These symptoms appear innocent, but when persistent it could indicate the presence of an SPT. When SPTs present with late stage disease with a bulky tumor mass, a complete resection is not possible anymore, which diminishes the chance of survival. Histopathological subtypes of SPT predominantly include osteosarcomas and rhabdomyosarcomas (together 64% of all cranio-facial second primary tumors in irradiated retinoblastoma patients) and with a lower prevalence leiomyosarcoma, undifferentiated sarcomas, meningiomas, and carcinomas. Predilection sites for SPT development in irradiated retinoblastoma survivors are the ipsilateral irradiated orbit and temporal fossa for osteosarcomas, and the ethmoid and temporal fossa for rhabdomyosarcomas. The overall prognosis of SPTs in the craniofacial area in previously irradiated retinoblastoma patients is generally poor, despite intensive treatment based on chemotherapy and surgery.^{35;36} Prognosis depends on feasibility of complete microscopic tumor resection of the SPT which has a significantly better overall and event free survival compared to incomplete resection.

CLINICAL IMPLICATIONS AND FUTURE PERSPECTIVE

Retinoblastoma diagnosis

In daily clinic practice, the combination of fundoscopy, ultrasound and MRI detects retinoblastoma in almost all cases⁵. Presence of calcifications is critical for retinoblastoma diagnosis and is difficult to evaluate by fundoscopy if unclear ocular medium is present. The most common mimickers of retinoblastoma in eyes with leukocoria include persistent hyperplastic primary vitreous and Coats disease. In contrast to retinoblastoma, both of these do not show calcifications. T2*WI shows to be a feasible technique to detect calcifications. It is possible to distinguish between calcifications and other causes of signal intensity void spots on MR (hemorrhage, venous congestion) by analyzing the shape and location of signal intensity voids. In patients with still confusion regarding diagnosis after fundoscopy and ultrasound, T2*WI could be added to the imaging protocol for further differentiation. Susceptibility weighted imaging has the potential to differentiate between hemorrhage and calcifications by using the phase information in the phase image, and could therefore be an even more specific technique for retinoblastoma diagnosis. Future research should focus on diagnostic accuracy of susceptibility weighted imaging in detection of calcifications and secondarily, the accuracy to differentiate between retinoblastoma and simulating lesions.

Conservative treatment and response evaluation

Super-selective administration of chemotherapy to the affected eye (i.e. intra-arterial and intra-vitreous chemotherapy) leads to globe salvage in more and more patients by avoiding enucleation or EBRT and minimizing side effects of systemic intravenous chemotherapy and late sequelae of EBRT. These conservative treatment strategies require an accurate pretreatment non-invasive staging of the disease. Furthermore, functional MRI techniques might provide parameters to support the ophthalmologists in treatment selection and early prediction of response to conservative treatment. Dynamic contrast enhanced MRI can be a feasible technique to non-invasively characterize the intraocular mass for tumor angiogenesis and tumor necrosis, which respectively is considered as a risk factor for disseminated disease and treatment response. This technique could even become more accurate with pixel-by-pixel analysis identifying separate regions of high vascularization and necrosis in one tumor. With increasing technical options for DCE-MRI, future applications of T1 relaxation time calculations and AIF measurements for quantitative modeling might further enhance the options for tumor characterization and treatment response prediction. Before this technique can be applied in daily clinical practice, prospective studies for response evaluation and standardization of imaging analysis methods between retinoblastoma centers should be achieved.

Imaging of associated morbidity

In every retinoblastoma patient the brain should be imaged during the first MRI examination as most trilateral retinoblastomas are detected at BBI. It is important that complex cystic lesions in the pineal gland are discovered in time, since small pineoblastomas can present as cystic lesions. If the lesion resembles a benign pineal cyst MRI should be repeated after 6 months, and if stable no further follow-up imaging will be necessary. In cases of irregularly thickened or fine nodular aspect of the wall occurs, close MR follow-up after three months should be performed. Larger prospective multicenter studies are necessary to evaluate the benefits of screening.

Most common cause of death in retinoblastoma survivors are development of second primary tumors, especially after external beam radiation therapy for retinoblastoma. Detection of these tumors in an early stage is crucial and therefore a screening program for craniofacial SPTs in hereditary retinoblastoma patients who were initially treated with EBRT could be beneficial. In the future a prospective non-invasive study (preferably part of a larger multicenter study) is necessary to investigate whether screening for SPTs in irradiated hereditary retinoblastoma survivors with MRI is effective for early tumor detection and results in a reduction of mortality. Screening could potentially be related to associated anxiety, but also to reassurance. Besides evaluation of the ability of MRI to detect these tumors in time, a future study should also focus on psychological burden.

REFERENCES

1. de Graaf P, Goricke S, Rodjan F, et al. Guidelines for imaging retinoblastoma: imaging principles and MRI standardization. *Pediatr Radiol* 2011;
2. Brisse HJ. Retinoblastoma imaging. *Ophthalmology* 2010;117:1051
3. Davis PC, Hopkins KL. Imaging of the pediatric orbit and visual pathways: computed tomography and magnetic resonance imaging. *Neuroimaging Clin N Am* 1999;9:93-114
4. Ettl A, Kramer J, Daxer A, et al. High resolution magnetic resonance imaging of neurovascular orbital anatomy. *Ophthalmology* 1997;104:869-77
5. Galluzzi P, Hadjistilianou T, Cerase A, et al. Is CT still useful in the study protocol of retinoblastoma? *AJNR Am J Neuroradiol* 2009;30:1760-65
6. Rossler J, Dietrich T, Pavlakovic H, et al. Higher vessel densities in retinoblastoma with local invasive growth and metastasis. *Am J Pathol* 2004;164:391-94
7. Galbraith SM, Lodge MA, Taylor NJ, et al. Reproducibility of dynamic contrast-enhanced MRI in human muscle and tumours: comparison of quantitative and semi-quantitative analysis. *NMR Biomed* 2002;15:132-42
8. Tofts PS, Brix G, Buckley DL, et al. Estimating kinetic parameters from dynamic contrast-enhanced T(1)-weighted MRI of a diffusible tracer: standardized quantities and symbols. *J Magn Reson Imaging* 1999;10:223-32
9. Guo JY, Reddick WE. DCE-MRI pixel-by-pixel quantitative curve pattern analysis and its application to osteosarcoma. *J Magn Reson Imaging* 2009;30:177-84
10. Rodjan F, de Graaf P, van der Valk P, et al. Retinoblastoma: value of dynamic contrast-enhanced MR imaging and correlation with tumor angiogenesis. *AJNR Am J Neuroradiol* 2012;33:2129-35
11. Hayes C, Padhani AR, Leach MO. Assessing changes in tumour vascular function using dynamic contrast-enhanced magnetic resonance imaging. *NMR Biomed* 2002;15:154-63
12. Padhani AR. Dynamic contrast-enhanced MRI in clinical oncology: current status and future directions. *J Magn Reson Imaging* 2002;16:407-22
13. Hawighorst H, Libicher M, Knopp MV, et al. Evaluation of angiogenesis and perfusion of bone marrow lesions: role of semiquantitative and quantitative dynamic MRI. *J Magn Reson Imaging* 1999;10:286-94
14. Tuncbilek N, Karakas HM, Okten OO. Dynamic contrast enhanced MRI in the differential diagnosis of soft tissue tumors. *Eur J Radiol* 2005;53:500-05
15. Lavini C, Pikaart BP, de Jonge MC, et al. Region of interest and pixel-by-pixel analysis of dynamic contrast enhanced magnetic resonance imaging parameters and time-intensity curve shapes: a comparison in chondroid tumors. *Magn Reson Imaging* 2009;27:62-68
16. Kivela T. Trilateral retinoblastoma: a meta-analysis of hereditary retinoblastoma associated with primary ectopic intracranial retinoblastoma. *J Clin Oncol* 1999;17:1829-37
17. Provenzale JM, Gururangan S, Klintworth G. Trilateral retinoblastoma: clinical and radiologic progression. *AJR Am J Roentgenol* 2004;183:505-11
18. Baud O, Cormier-Daire V, Lyonnet S, et al. Dysmorphic phenotype and neurological impairment in 22 retinoblastoma patients with constitutional cytogenetic 13q deletion. *Clin Genet* 1999;55:478-82
19. Alanay Y, Aktas D, Utine E, et al. Is Dandy-Walker malformation associated with "distal 13q deletion syndrome"? Findings in a fetus supporting previous observations. *Am J Med Genet A* 2005;136:265-68
20. Abramson DH, Frank CM. Second nonocular tumors in survivors of bilateral retinoblastoma: a possible age effect on radiation-related risk. *Ophthalmology* 1998;105:573-79
21. Marees T, Moll AC, Imhof SM, et al. Re: More about second cancers after retinoblastoma. *J Natl Cancer Inst* 2010;102:831-32
22. Ramasubramanian A, Kytasty C, Meadows AT, et al. Incidence of pineal gland cyst and pineoblastoma in children with retinoblastoma during the chemoreduction era. *Am J Ophthalmol* 2013;156:825-29
23. Rodjan F, de Graaf P, Brisse HJ, et al. Trilateral retinoblastoma: neuroimaging characteristics and value of routine brain screening on admission. *J Neurooncol* 2012;109:535-44

24. Popovic MB, Diezi M, Kuchler H, et al. Trilateral retinoblastoma with suprasellar tumor and associated pineal cyst. *J Pediatr Hematol Oncol* 2007;29:53-56
25. Al Holou WN, Garton HJ, Muraszko KM, et al. Prevalence of pineal cysts in children and young adults. Clinical article. *J Neurosurg Pediatr* 2009;4:230-36
26. Rodjan F, de Graaf P, Moll AC, et al. Brain abnormalities on MR imaging in patients with retinoblastoma. *AJNR Am J Neuroradiol* 2010;31:1385-89
27. Beck Popovic M, Balmer A, Maeder P, et al. Benign pineal cysts in children with bilateral retinoblastoma: a new variant of trilateral retinoblastoma? *Pediatr Blood Cancer* 2006;46:755-61
28. Jurkiewicz E, Pakula-Kosciesza I, Rutynowska O, et al. Trilateral retinoblastoma: an institutional experience and review of the literature. *Childs Nerv Syst* 2010;26:129-32
29. Dunkel IJ, Jubran RF, Gururangan S, et al. Trilateral retinoblastoma: potentially curable with intensive chemotherapy. *Pediatr Blood Cancer* 2010;54:384-87
30. Wright KD, Qaddoumi I, Patay Z, et al. Successful treatment of early detected trilateral retinoblastoma using standard infant brain tumor therapy. *Pediatr Blood Cancer* 2010;55:570-72
31. Eng C, Li FP, Abramson DH, et al. Mortality from second tumors among long-term survivors of retinoblastoma. *J Natl Cancer Inst* 1993;85:1121-28
32. Kleinerman RA, Tucker MA, Tarone RE, et al. Risk of new cancers after radiotherapy in long-term survivors of retinoblastoma: an extended follow-up. *J Clin Oncol* 2005;23:2272-79
33. Abramson DH, Beaverson KL, Chang ST, et al. Outcome following initial external beam radiotherapy in patients with Reese-Ellsworth group Vb retinoblastoma. *Arch Ophthalmol* 2004;122:1316-23
34. Moll AC, Kuik DJ, Bouter LM, et al. Incidence and survival of retinoblastoma in The Netherlands: a register based study 1862-1995. *Br J Ophthalmol* 1997;81:559-62
35. Draf C, Schaberg MR, Anand VK, et al. Radiation induced malignancy in retinoblastoma: new pathology in a case report. *Laryngoscope* 2010;120 Suppl 4:S238
36. Tabone MD, Terrier P, Pacquement H, et al. Outcome of radiation-related osteosarcoma after treatment of childhood and adolescent cancer: a study of 23 cases. *J Clin Oncol* 1999;17:2789-95

Chapter 9

Summary in Dutch/Nederlandse samenvatting

NEDERLANDSE SAMENVATTING

Retinoblastoom is in de afgelopen 100 jaar veranderd van een fatale vorm van kinderkanker tot een grotendeels geneesbare ziekte. De huidige behandelstrategieën zijn in de eerste plaats gericht op overleving en daarnaast behoud van het oog met optimale visus. Door deze ontwikkelingen zal er in de toekomst steeds minder vaak weefsel beschikbaar zijn waardoor histopathologische bevestiging van de diagnose en analyse van histopathologisch prognostische factoren beperkt wordt. Histopathologie is de gouden standaard in de evaluatie van tumor uitbreiding en prognose van retinoblastoom. In de toekomst wordt het daarom belangrijk om technieken te ontwikkelen die een niet-invasieve evaluatie van prognostische risicofactoren en behandelrespons mogelijk maken.

Patiënten met de erfelijke vorm van retinoblastoom hebben een groter risico op het ontwikkelen van geassocieerde vormen van kanker, zoals het trilaterale retinoblastoom (TRB) en tweede primaire tumoren (TPT), met een slechte prognose tot gevolg. Het is belangrijk om het ontwikkelingspatroon van deze tumoren in kaart te brengen, zodat behandeling in een vroeg en mogelijk curabel stadium kan plaatsvinden.

Het eerste deel van dit proefschrift richt zich op nieuwe beeldvormende technieken die worden toegepast bij MRI van het oog om onderscheid te maken tussen retinoblastoom en simulerende laesies. Tevens worden de mogelijkheden van geavanceerde beeldvormende technieken geanalyseerd om factoren die de prognose en respons op behandeling beïnvloeden, zoals angiogenese en tumor necrose, te identificeren. Het tweede deel van dit proefschrift richt zich op MRI karakteristieken van geassocieerde afwijkingen in het hoofd en aangezicht, in het bijzonder TRB en TPT.

Beeldvormend onderzoek bij retinoblastoom

Wereldwijd worden verschillende MRI technieken gebruikt voor de diagnostiek van retinoblastoom. Hoofdstuk 2 geeft een overzicht van de huidige toepassingen en beperkingen van beeldvormende technieken voor retinoblastoom en bevat een MRI protocol voor een hoogwaardige diagnostische evaluatie van retinoblastoompatiënten volgens consensus van de European Retinoblastoma Imaging Collaboration (ERIC), een samenwerkingsverband tussen radiologen uit Europese retinoblastoom-gespecialiseerde centra. Hoge resolutie MRI is noodzakelijk voor nauwkeurige evaluatie van tumoruitbreiding en daarnaast screening op geassocieerde maligniteiten zoals TRB en (tijdens de follow-up) TPT. Slechts in gecompliceerde gevallen speelt MRI een rol bij de diagnostiek van de primaire tumor. CT scans worden in dit protocol afgeraden vanwege de hoge stralingsbelasting in deze reeds erfelijk belaste groep patiënten. Afgezien hiervan is er bij MRI een beter onderscheid tussen weke delen doordat er een hoger weke-delen contrast is. Standaardisatie van MRI protocollen wereldwijd is belangrijk om internationale multicentrische studies uit te voeren voor verdere toepassing van nieuwe beeldvormende technieken bij retinoblastoom en daarmee een hoog niveau van beeldvorming na te streven.

Waarde van MRI voor differentiaal diagnose

Echografie blijft de meest praktische beeldvormende techniek voor bevestiging van de diagnose retinoblastoom en heeft een hoge diagnostische nauwkeurigheid. Zelfs in gecompliceerde gevallen is echografie in staat om onderscheid te maken tussen goedaardige en kwaadaardige intraoculaire laesies bij kinderen. Bij twijfel is de combinatie van MRI en echografie aangewezen om te differentiëren tussen maligne en benigne intraoculaire afwijkingen, zoals persisterende foetale vasculatuur en de ziekte van Coats. In gevallen met opake media zoals bij cataract of een bloeding in het voorste segment of glasvocht, kunnen echografie en zelfs de standaard MRI-technieken onvoldoende zijn om de diagnose retinoblastoom te bevestigen.

In hoofdstuk 3 wordt een T2* gewogen MRI techniek in de diagnostiek van retinoblastoom besproken. Het gebruik van T2* gewogen opnamen om karakteristieke verkalkingen in retinoblastoom aan te tonen bleek net zo nauwkeurig te zijn als ex-vivo hoge resolutie CT-scans. De MRI techniek is echter veiliger vanwege de afwezigheid van additionele stralingsrisico's zoals die bij CT wel aanwezig zijn. In vergelijking met de doorgaans lage resolutie CT scans die standaard bij kinderen wordt verricht, blijkt de diagnostische waarde van T2* gewogen beeldvorming beter. In onze studie bevestigen wij de goede correlatie tussen verkalkingen aangetoond op CT en hypointense laesies op de T2* gewogen opnames zoals eerder aangetoond door Galluzzi. Daarnaast formuleerden wij MRI kenmerken die kunnen differentiëren tussen verkalkingen en andere oorzaken van hypointense laesies op T2* gewogen beeldvorming bij retinoblastoom. Een bloeding in het oog kan zich bijvoorbeeld presenteren als een hypointense laesie. Het kan worden onderscheiden van verkalkingen door het aspect van de bloeding, namelijk glad met een lineair aspect en voornamelijk gelegen in de periferie van de tumor. Lineaire hypointense laesies kunnen echter ook het gevolg zijn van artefacten. Ook veneuze stuwning veroorzaakt hypointense laesies op T2* gewogen opnames door de aanwezigheid van deoxyhemoglobine, een gedilateerde veneuze vaten en langzaam stromend veneus bloed. Susceptibility weighted imaging lijkt een andere veelbelovende MRI techniek om verkalkingen te differentiëren van bloedingen, necrose en artefacten. Uit onze studie blijkt dat deze techniek mogelijk gevoeliger is dan T2* gewogen beeldvorming.

Waarde van dynamische MRI voor prognostische factoren en respons op behandeling

In hoofdstuk 4 beschrijven we de mogelijkheden van dynamische MRI (DMRI) voor de beoordeling van vaatnieuwgroei (angiogenese) in de tumor en vitaliteit van het tumor weefsel in een groep van 15 retinoblastoom patiënten. Dynamische MRI is een techniek waarbij een serie MRI beelden voor, tijdens en na contrasttoediening wordt vervaardigd. Deze techniek biedt de mogelijkheid van kwantitatieve evaluatie van de fysiologische eigenschappen van tumorweefsel. Analyse van contrastaankeuring van de tumor wordt gedaan met behulp van de "curve pattern analysis" methode. Microvasculaire dichtheid is een belangrijke histopathologische parameter voor tumorangiogenese in vitro en is gecorreleerd met invasieve groei en hematogene metastasen.

Karakteristiek voor zeer gevasculariseerd weefsel met een hoge microvasculaire dichtheid is snelle signaalversterking na contrastinjectie, overeenkomend met een DMRI curve met een steile helling. Deze curve geeft informatie over de doorbloeding, capillaire lekkage en gerelateerde fysiologische parameters. Deze techniek wordt steeds vaker gebruikt bij het verbeteren van klinisch diagnostische beeldvorming en bij de beoordeling van microvasculaire veranderingen na behandeling. In onze studie hebben we de fysiologische parameter κ gebruikt, verkregen met curve pattern analyse. We toonden aan dat de vroege fase van de curve $\kappa(5 \text{ min})$, welke representatief is voor de eerste fase, positief gecorreleerd is met de microvasculaire dichtheid van retinoblastoom ($p = 0.008$). Dit kan mogelijk in de toekomst een belangrijke parameter vormen bij de follow-up van retinoblastoom patiënten die behandeld worden met anti-angiogene geneesmiddelen. De $\kappa(17\text{min})$ vertegenwoordigd de volledige tijdscurve en is negatief gecorreleerd met de mate van tumornecrose ($p = 0.002$). De $\kappa(17\text{min})$ zou een geschikte parameter kunnen zijn om het succes van conservatieve behandeling van retinoblastoom te evalueren. In necrotische tumoren is namelijk sprake van ernstige hypoxie, wat het effect van behandeling middels bestraling en chemotherapie negatief beïnvloedt. Er bleek geen significante relatie te bestaan tussen kinetische gegevens van DMRI en de aanwezigheid van risicofactoren voor het optreden van metastasen (oogzenuw en choroidea invasie) of de aanwezigheid van groeifactoren voor vaatnieuwgroei (vascular endothelial growth factor; VEGF) in de tumor.

Follow- up beeldvorming van geassocieerde hersenafwijkingen of maligniteiten

Erfelijk retinoblastoom is geassocieerd met zowel kwaadaardige als goedaardige hersenafwijkingen. De meest bekende is het trilaterale retinoblastoom (ontogenetisch ontstaan uit hetzelfde weefsel als de retina, met lokalisatie in de pijnappelklier [pineoblastoom] en supra- of parasellaire regio) bij 5-15% van de retinoblastoom patiënten. Daarnaast zijn er ook structurele hersenafwijkingen gerapporteerd bij kinderen met het 13q deletie syndroom. In hoofdstuk 5 geven we een overzicht van de hersenen afwijkingen die werden gevonden in een grote groep van 168 retinoblastoom patiënten waarvan 7 patiënten werden gediagnosticeerd met het 13q deletie syndroom. In onze studie werden structurele hersenafwijkingen alleen in combinatie met dit syndroom gevonden. Eén patiënt toonde een corpus callosum agenesie en een andere patiënt een Dandy-Walker variant met verwijde ventrikels. Daarnaast vonden wij in 5.5% van de erfelijke retinoblastoom patiënten een trilateraal retinoblastoom, in overeenstemming met eerdere literatuur. De totale incidentie van pinealiscysten was 5.4 % (9.0 % in de niet-erfelijke groep en 2.2 % in de erfelijke groep). De incidentie in de groep van erfelijk retinoblastoom is gelijk aan die bij gezonde jonge kinderen en derhalve niet geassocieerd met retinoblastoom. Belangrijk voor radiologen is dat kleine pineoblastomen een cysteus aspect kunnen hebben wat verwarring kan veroorzaken in de differentiatie met benigne pinealis cysten. Dit wordt besproken in hoofdstuk 6. Sommige studies geven aan dat de incidentie van het trilateraal retinoblastoom in de toekomst zal afnemen als gevolg van de beschermende werking van chemoreductie therapie en/of het ontbreken van

uiterwijdige bestraling voor de behandeling van het retinoblastoom. Het is het meest aannemelijk dat deze afname het gevolg zal zijn van dit laatste aspect, omdat de overgrote meerderheid van pineoblastomen wordt gedetecteerd reeds vóór intraveneuze chemoreductie behandeling. Verder is het interessant om te evalueren of in de toekomst de incidentie van het pineoblastoom hetzelfde blijft na de invoering van selectieve intra-arteriële chemotherapie via lokale toediening in de arteria ophthalmica van het getroffen oog.

In hoofdstuk 6 worden karakteristieke MRI parameters van TRB vastgesteld. Deze intracraniele tumoren zijn meestal gelokaliseerd in de glandula pinealis (77% van de gevallen) of in de suprasellaire regio. Pineoblastomen en suprasellaire tumoren hebben een relatief isointense signaalintensiteit op T1-gewogen beelden ten opzichte van grijze stof en isointense signaalintensiteit op T2-gewogen beelden. Deze tumoren hebben een heterogeen aankleuringspatroon na contrasttoediening door met name cysteuze componenten in de tumor of tumornecrose. In de literatuur wordt een mogelijk verband gesuggereerd tussen goedaardige pinealiscysten en retinoblastoom, welke zich zouden kunnen ontwikkelen tot een pineoblastoom. De meeste pineoblastomen in onze studie zijn gedeeltelijk cysteus met een solide deel (29 %) of helemaal cysteus (29 %). Goedaardige pinealiscysten treden op in 0.4% - 2.2% van de algehele pediatrische populatie overeenkomend met de incidentie van pinealiscysten in erfelijke retinoblastoom patiënten. Bij erfelijke retinoblastoompatiënten is het belangrijk om de cysteuze glandula pinealis die gebaseerd is op een pineoblastoom vroegtijdig te herkennen, zodat behandeling, gericht op curatie, zo vroeg mogelijk ingezet kan worden. Goedaardige pinealiscysten worden gedefinieerd als (1) de aanwezigheid van een vergrote glandula pinealis, (2) met een hypointens centraal gebied in vergelijking met witte stof op T1 gewogen beelden en isointens ten opzichte van liquor op T2 -gewogen beelden en (3) een dunne wand van 2 mm of minder met discrete en regelmatige randaankleuring na contrasttoediening. Ondanks deze criteria kunnen laesies in de glandula pinealis dilemma's veroorzaken, vooral als de wand van de cyste onregelmatig verdikt is (> 2 mm) of een fijn nodulair aspect heeft. In de toekomst is het van belang om prospectieve multicenter studies op te zetten om beeldvormende criteria te formuleren gericht op het identificeren van pineoblastoom in een vroeg stadium (mogelijk cysteus) en follow-up van verdachte pinealiscysten. In de tussentijd raden we aan om pinealiscysten in te delen in drie categorieën (1 - "waarschijnlijk goedaardige pinealiscyste", 2 - "duidelijk cysteus pineoblastoom", of 3 - "verdachte pinealiscyste") met verschillende klinische benaderingen. Indien er duidelijk sprake is van een goedaardige pinealiscyste (categorie 1), dan raden wij aan de MRI na 6 maanden te herhalen. Indien de cyste stabiel blijft is er geen verdere follow-up beeldvorming noodzakelijk. In de derde categorie is echter strikte follow-up na drie maanden noodzakelijk. Screening van de glandula pinealis in retinoblastoom patiënten dient plaats te vinden middels een post-contrast 3D T1 gewogen sequentie met 1 mm plakdikte. Als er tevens sprake is van een cysteuze laesie in de glandula pinealis, dan dient er additioneel een 2 mm T2 - gewogen sequentie of 3D T2/CISS sequentie uitgevoerd te worden om de laesie (met name de wand) te karakteriseren.

Trilateraal retinoblastoom was dodelijk in vrijwel alle eerder gerapporteerde gevallen in de literatuur. Intensieve behandeling met hoge doses chemotherapie en stamceltransplantatie, eventueel in combinatie met chirurgie blijken potentieel curatief. Dit proefschrift toont aan dat als het TRB synchroon met retinoblastoom (hersentumor tegelijkertijd met de oogtumor) tijdens het eerste MRI-onderzoek vastgesteld wordt (baseline beeldvorming van de hersenen, BBI), de grootte aanzienlijk kleiner is dan metachrone (hersentumor vastgesteld na BBI) tumoren (18mm versus 35mm, $P = 0.002$). Patiënten met BBI hebben tevens minder symptomen en neigen tot een betere prognose in vergelijking met TRB ontdekt na retinoblastoom diagnose (metachrone tumoren). In de ERIC richtlijn wordt geadviseerd om BBI bij iedere nieuw gediagnosticeerde retinoblastoom patiënt te verrichten. Hoewel in dit proefschrift de waarde van BBI wordt benadrukt, wordt standaard herhaaldelijke follow-up van de hersenen middels MRI bij erfelijk retinoblastoom patiënten niet aanbevolen. In een eerdere studie bleek screening namelijk te leiden tot een langere mediane overlevingstijd doordat de leeftijd van TRB detectie eerder was, terwijl de leeftijd van overlijden niet verschilde. Dit betekent dat het onderzoek leidde tot lead time bias en snellere behandeling, waardoor meer kans op ernstige behandelrisico's en gerelateerde morbiditeit en stress bij kinderen.

Erfelijk retinoblastoom patiënten hebben een verhoogd risico op het ontstaan van tumoren elders in het lichaam. Deze zogenaamde tweede primaire tumoren (TPT) zijn verantwoordelijk voor een aanzienlijk deel van de sterfte van erfelijk retinoblastoom patiënten. Uitwendige bestraling geeft een verdere verhoging van het bestaande risico op botkanker en weke delen sarcomen. Daarvan ontwikkelt zich 70% in het hoofd en aangezicht; voormalig bestralingsveld voor de oogtumoren. Onze Europese studie toont aan dat craniofaciale tweede primaire tumoren in bestraalde retinoblastoom patiënten worden gediagnosticeerd op een mediane leeftijd van 13 jaar (range 3-38 jaar). De mediane tijd tussen bestraling en ontwikkeling van SPT is 15 jaar (range 3-37). Leeftijd van bestraling is een risicofactor voor de ontwikkeling van TPT in retinoblastoompatiënten. Patiënten bestraald tijdens hun eerste levensjaar ontwikkelen aanzienlijk meer TPT in vergelijking met bestraling na het eerste levensjaar. Dit zou deels verklaard kunnen worden door het feit dat erfelijk retinoblastoom patiënten hun ziekte op een jongere leeftijd ontwikkelen en dus eerder behandeld worden. TPT presenteren zich bij diagnose met de volgende klachten; plaatselijke zwelling (60 %), lokale pijn (14 %), hoofdpijn (19 %), epistaxis (7 %), persistente rhinorroe (5 %), niet-passend oculaire prothese (10 %), symptomen van intracraniale hypertensie (5 %) en ptosis (5%). Sommige van deze symptomen lijken onschuldig en aspecifiek, maar bij aanhoudende klachten kunnen deze symptomen duiden op een TPT. Wanneer TPT zich presenteren in een laat stadium van de ziekte met een grote tumormassa, is er vaak geen complete tumorresectie meer mogelijk wat de kans op uiteindelijke overleving verkleint. Histopathologische subtypen van TPT bestaan voornamelijk uit osteosarcomen en rhabdomyosarcomen (samen 64 % van alle craniofaciale tweede primaire tumoren bij bestraalde retinoblastoom patiënten) en in mindere mate leiomyosarcomen, ongedifferentieerde sarcomen,

meningiomen, en carcinomen. Voorkeurslokalisaties voor TPT in bestraalde retinoblastoom patiënten bestaan uit de ipsilateraal bestraalde orbita en fossa temporalis voor het osteosarcoom; en het ethmoid en fossa temporalis voor het rhabdomyosarcoom. De algehele prognose van bestraalde retinoblastoom patiënten met TPT in het craniofaciale gebied is over het algemeen slecht, ondanks intensieve behandeling op basis van chemotherapie en chirurgie. De prognose is afhankelijk van de haalbaarheid van een volledige microscopische tumor resectie van de TPT. Dit heeft een significant betere overall en event-free overleving in vergelijking met incomplete tumorresectie.

Klinische implicaties en toekomstperspectief

Selectieve toediening van chemotherapie aan het aangetaste oog (d.w.z. intra-arteriële en intra-vitreale chemotherapie) leidt tot behoud van het oog en voorkomt enucleatie en bestraling in de meerderheid van de patiënten. Dit heeft als gevolg dat bijwerkingen door systemische intraveneuze chemotherapie en tevens late gevolgen van bestraling voorkomen worden. Deze conservatieve behandelingsstrategieën vereisen een nauwkeurige niet-invasieve evaluatie van het retinoblastoom voordat er gestart wordt met therapie voor verdere vervolg van de ziekte. Met behulp van functionele MRI-technieken kunnen ook parameters vastgesteld worden die de oogarts in een vroeg stadium kunnen helpen in het voorspellen van respons op conservatieve behandeling. Door middel van dynamische MRI kan niet-invasief de tumor angiogenese activiteit en necrose van de tumor in het oog geëvalueerd worden, wat respectievelijk beschouwd wordt als een risicofactor voor gedissemineerde ziekte en behandelrespons. In de toekomst kan deze techniek geoptimaliseerd worden door “pixel-by-pixel analyse” waarbij afzonderlijke gebieden van hoge vascularisatie en necrose in een tumor vastgesteld kan worden. Voordat de DMRI in de dagelijkse klinische praktijk kan worden toegepast, dienen toekomstige studies voor standaardisatie van analysemethoden te zorgen tussen retinoblastoom expertise centra.

Beeldvorming van morbiditeit

Bij elke retinoblastoom patiënt moeten de hersenen worden afgebeeld in het eerste MRI-onderzoek, omdat de meeste trilaterale retinoblastomen worden vastgesteld bij BBI. Omdat kleine pineoblastomen zich als cysteuze laesies kunnen presenteren, is het belangrijk dat complexe cysteuze laesies in de pijnappelklier tijdig worden ontdekt. Indien de laesie een goedaardige pinealiscyste op MRI lijkt te zijn, dan wordt de MRI herhaald na 6 maanden en is er indien stabiel, geen verdere follow-up beeldvorming noodzakelijk. Indien er sprake is van een onregelmatig verdikte fijn nodulair aspect van de wand, dan is follow-up beeldvorming middels MRI na drie maanden aanbevolen. In de toekomst is multicentrisch onderzoek in een grote patiëntenpopulatie nodig om de voordelen van screening te evalueren.

De meeste voorkomende oorzaak waaraan retinoblastoom overlevenden sterven is de ontwikkeling van een tweede primaire tumor, vooral als de patiënt uitwendig is bestraald voor het

retinoblastoom. Het vaststellen van deze tumoren in een vroeg stadium is derhalve cruciaal. Een screeningsprogramma voor craniofaciale TPT in erfelijk retinoblastoom patiënten die aanvankelijk werden behandeld met bestraling kan gunstig zijn. In de toekomst is een multicentrische studie noodzakelijk om te evalueren of screening middels MRI op TPT in bestraalde erfelijke retinoblastoom overlevenden effectief is om vroegtijdige tumoren te ontdekken en met name of door het eerder vaststellen van de TPT de mortaliteit ook afneemt. Screening zou kunnen leiden tot angst, maar ook geruststelling. Een toekomstige studie zou zich daarom ook moeten richten op psychische belasting.

Chapter 10

Dankwoord

List of Publications

Curriculum Vitae

DANKWOORD

Heerlijk, het is zover! De periode dat ik aan dit proefschrift heb gewerkt, eindigt met dit dankwoord. Zonder de betrokkenheid van velen was dit proefschrift niet tot stand gekomen. Ik wil daarom graag op deze manier iedereen bedanken die direct of indirect heeft bijgedragen aan mijn onderzoek.

Allereerst wil ik mijn bewondering uitspreken voor alle kinderen met retinoblastoom en hun ouders die samen zo ongelofelijk dapper omgaan met deze ziekte en de MRI onderzoeken onder narcose ondergaan. Respect hiervoor!

Mijn promotoren Prof. dr. J.A. Castelijns en Prof. dr. A. C. Moll en co-promotor dr. P. de Graaf wil ik graag bedanken voor hun begeleiding in alle fasen van het onderzoek. In de praktijk bleek de combinatie van jullie kwaliteiten goed te werken.

Beste Jonas. Bedankt voor de geboden ruimte en het vertrouwen dat je mij gaf om als onderzoeker onder jouw begeleiding te promoveren en het inmiddels succesvolle Europese retinoblastoom-netwerk (ERIC) te coördineren. Hieruit zijn een aantal mooie multicentrische studies voortgevloeid. Het begon tijdens mijn wetenschappelijke stage waarbij jij veel tijd en energie hebt geïnvesteerd in het mij wegwijs maken in de wereld van de hoofdhals MRI. Dit heeft mijn enthousiasme aangewakkerd om meer onderzoek te doen onder jouw supervisie. Met name je persoonlijke begeleiding en betrokkenheid heb ik zeer gewaardeerd. Jouw deur stond altijd open voor overleg. Tijdens mijn promotie heb ik een grote persoonlijke tegenslag moeten verwerken. Hierbij kon ik voor 100% op jou rekenen. Ik zal jou hiervoor altijd dankbaar blijven!

Beste Annette. Dank voor de regelmatige gesprekken over mijn onderzoek, waarbij jouw blik vanuit de kliniek een verrijking was. Hierdoor is de inhoud van mijn proefschrift enorm verbeterd. Als je promoveert binnen een vakgebied waarin met name naar beelden wordt gekeken, dan schuilt het gevaar om het contact met patiënten te verliezen. Ik vond het fijn dat je mij de mogelijkheid gaf om met het retinoblastoomspreekuur mee te lopen om zo een goede indruk te krijgen van de impact die deze ziekte heeft. Fijn dat je mijn tweede promotor bent geworden!

Beste Pim, ik ben jou heel veel dank verschuldigd voor de tijd en energie die je hebt gestoken in dit proefschrift, ondanks je drukke werkzaamheden (afronding promotie, ERIC, opleiding tot radioloog, begeleiding promovendi, gezin). Ik heb hier veel bewondering voor! Jij tilde elk artikel naar een hoger niveau door jouw zeer kritische en verhelderende feedback. Op inhoudelijk vlak kon ik mij geen betere begeleider wensen. En zonder jou was dit proefschrift er zeker niet geweest! Het onderzoek naar beeldvorming van retinoblastoom is bij jou in zeer goede handen.

The members of the European retinoblastoma imaging collaboration, dr. H. Brisse, dr. P. Galluzzi, dr. P. Maeder and dr. S. Göricke, thank you for your co-operation in the “marathon” MRI examination sessions. This collaboration resulted in some great articles. I was very grateful for your hospitality and the opportunity to visit your hospital for data collection and I enjoyed your company during the ERIC dinners!

Ik wil alle co-auteurs bedanken voor hun onmiskenbare bijdrage op verschillende gebieden.

I would like to express special thanks to dr. Brisse. Dear Hervé. I really enjoyed working with you. Thank you for your always quick and constructive feedback regarding our European studies. It is an honour that you agreed to join the reading committee. I loved to visit your beautiful Paris!

Dr. P.J.W. Pouwels, beste Petra, dank voor je intensieve begeleiding en hulp bij het testen, implementeren en analyseren van data m.b.t. de dynamische MRI studie. Zonder jouw duidelijke uitleg en bereidheid om dit enkele keren te herhalen, was ik waarschijnlijk verdrongen in deze materie. Je was mijn rots in de branding!

Dr. D. L. Knol, beste Dirk, voor de statistiek van mijn onderzoeken kon ik volledig op jou bouwen. Dank voor de heldere uitleg en de tijd die je voor mij uitgetrokken hebt.

Prof. dr. P van der Valk, beste Paul, dank dat je ondanks jouw drukke agenda altijd wel tijd kon vrijmaken voor het tijdrovende werk van het vinden (!) en daarna het beoordelen van alle histopathologische coupes voor de MRI/CT- PA correlatiestudies.

Prof. dr. S. Imhof, beste Saskia, ik voel mij vereerd dat jij deel wilt uitmaken van mijn leescommissie. Ondanks het feit dat we slechts kort met elkaar hebben samengewerkt, voordat jij hoogleraar werd in Utrecht, heb ik onze samenwerking altijd erg prettig gevonden. Dank voor je enthousiasme en deskundigheid!

Drs. E. Sanchez en drs. J.I.L.M. Verbeke, beste Ester en Jonathan. Dank dat jullie bereid waren om de vele MRI beelden te beoordelen. Dankzij jullie was dit gezellig en leerzaam.

De betrokken verpleegkundigen, artsen en onderzoekers van het multidisciplinaire retinoblastoom team van het VUmc wil ik bedanken voor hun samenwerking en gezelligheid tijdens mijn promotietraject. Jennifer en Tamara, dank jullie wel voor de fijne gesprekken waarbij we het wel en wee van onderzoek doen met elkaar konden delen.

Graag wil ik de leden van de leescommissie bedanken voor het zorgvuldig lezen van mijn proefschrift en de bereidheid om hierover van gedachten te wisselen tijdens de verdediging: mw. prof. dr. S. M. Imhof, prof. dr. F. Barkhof, dr. H. Brisse, prof. dr. P. van der Valk, prof. dr. G. J. L. Kaspers en prof. dr. G. P. M. Luyten.

Mijn ex-kamergenoten Iris Kilsdonk en Wolter de Graaf wil ik bedanken voor de ontzettend gezellige tijd waarin we veel lief en leed hebben gedeeld. Iris, dank voor alle momenten dat ik me kapot heb gelachen met jou en ook voor je steun tijdens de moeilijke periodes. Aan deze promotie heb ik een goede vriendin overgehouden en ik zou dan ook niemand anders als paranimf naast mij willen op deze belangrijke dag! Ik ben blij dat jij je plek hebt gevonden bij de radiologie. Met jouw skills wordt je een fantastische radioloog en wetenschapper. Wolter, dank dat jij als een soort redder in nood altijd klaar stond om mij uit de brand te helpen (met name de computerproblemen en de muizen...!). Fijn dat je inmiddels je plek hebt gevonden.

Maja en Milou wil ik danken voor de koffiemomenten waarbij de belangrijkste actualiteiten de revu passeerden. Jammer dat deze intervisiemomenten nu schaars zijn geworden, maar we gaan hier zeker verandering in brengen als we zometeen alle 3 gepromoveerd zijn.

Martijn, jou wil ik in het bijzonder bedanken voor het prachtige coverdesign van mijn boekje! En dit was slechts een van de vele momenten waarop je mij en ook anderen geholpen hebt. Tijdens mijn promotie kwam ik regelmatig buurten in de kamer die jij deelde met Gijs en Veronica. Jullie waren een hilarisch trio!

Alle mede-onderzoekers van verschillende afdelingen wil ik bedanken voor hun collegialiteit: Veronica, Gijs, Oliver, Bastiaan, Ivo, Stefan, Jasper, Marieke, Marcus en Daan. In het bijzonder Marloes, mijn beste studiemaatje!

De ondersteuning van de secretaresses was goud waard. Sandra, Angélique, Karlijn, Letty, Regina en Lydia, dank jullie wel!

Bij het opzetten van multicentrische studies, waarbij veel data verstuurd en opgeslagen moet worden, is de ICT essentieel! Dennis en Freek, dank dat jullie hierbij een belangrijke rol hebben gespeeld.

Hesdy zonder jou had ik geen enkele MRI kunnen beoordelen of een letter digitaal “op papier” kunnen krijgen, aangezien mijn computer op de een of andere manier regelmatig crashte. Bedankt dat je hier altijd een oplossing voor wist te vinden. Kees, dank voor je ondersteuning hierbij ;).

Van het ene warme bad naar het andere. Ik wil graag al mijn collega arts-assistenten en specialisten van het Slotervaartziekenhuis bedanken voor de gezelligheid en collegialiteit die ik tot op de dag van vandaag enorm waardeer. Prof. Dr. D. Brandjes en dr. J. W. Mulder, dank voor de kans die ik heb gekregen om in opleiding tot internist te komen. Ik voel me helemaal op mijn plek bij de interne geneeskunde!

Lieve vrienden en (schoon)familie, dank voor jullie interesse in mijn onderzoek en alle gezelligheid naast het harde werken!

Mijn broer en zusjes wil ik bedanken voor het feit dat we altijd op elkaar kunnen rekenen. Als het er echt op aankomt, dan staan we voor elkaar klaar. Ashwad, fijn dat jij door je rust en kalmte vaak de relativerende factor bent in ons kippenhok. Soheilah, dank voor jouw eeuwige enthousiasme en gezelligheid. Ik ben blij dat jij mijn paranimf bent. Zonder jou zou ik hier niet rustig kunnen staan. Faaïzah, ik bewonder jouw standvastigheid en idealen. Onze gesprekken zijn altijd erg motiverend voor mij geweest. Mijn baby-zusje Sadia, ik ben trots op de vrouw die jij geworden bent! Dank dat je ons gezinnetje het afgelopen jaar geholpen hebt om de ballen in de lucht te houden waardoor het mede mogelijk is geworden dit proefschrift af te ronden.

Mijn nanie (oma) wil ik bedanken voor het feit dat haar deur altijd voor ons open staat. De weg naar Zwolle weten we ook zeker te vinden!

Dan de twee grootste liefdes in mijn leven (de echte mannen!). Daniël Jorna, mijn allerliefste Ziaul, jij staat altijd voor mij klaar en geeft mij de kans om mijn dromen te realiseren. Ik had dit nooit voor elkaar kunnen krijgen zonder jouw onbeperkte liefde, steun en geduld. Met jou aan mijn zijde weet ik dat ik de hele wereld aan kan. Ik hou van jou!

Lieve Kamiel, hemaar baby, jij bent het allermooiste wat me ooit is overkomen! Mijn grootste motivatie om dit boekje af te ronden, ben jij. Met jouw lachebekkie sleep jij me door alle moeilijke momenten heen en breng jij ongelofelijk veel blijdschap in mijn leven.

Tenslotte wil ik mijn moeder bedanken. Helaas ben je niet meer bij ons, een gemis wat ik nog steeds elke dag voel. Alles wat ik in mijn leven bereikt heb, komt door jouw onvoorwaardelijke liefde, vertrouwen en de kansen die jij voor mij gecreëerd hebt! Mama, dit proefschrift draag ik op aan jou.

LIST OF PUBLICATIONS

Rodjan F, Graaf de P, van der Valk P, Hadjistilianou T, Cerase A, Toti P, Jong de M.C, Moll A.C, Castelijns J.A, Galluzzi P, on behalf of the European Retinoblastoma Imaging Collaboration (ERIC). Detection of calcifications in retinoblastoma using gradient-echo MR imaging sequences: comparative study between in-vivo MR imaging and ex-vivo high resolution CT. Accepted for publication: American Journal of Neuroradiology; February 2015.

Rodjan F, Graaf de P, Brisse H.J, Verbeke J.I. L. M, Sanchez E, Galluzzi P, Göricke S, Maeder P, Aerts I, Dendale R, Desjardin L, Francesco de S, Bornfeld N, Sauerwein W, Popovic MB, Knol D.L, Moll A.C, Castelijns J.A. Second cranio-facial malignancies in hereditary retinoblastoma survivors previously treated with radiation therapy: clinical and radiological characteristics and survival outcomes. European Journal of Cancer. 2013 May; 49(8); 1939-47.

Rodjan F, Graaf de P, Brisse H.J, Göricke S, Maeder P, Galluzzi P, Aerts I, Alapetite C, Desjardins L, Wieland R, Popovic MB, Diezi M, Munier F.L, Hadjistilianou T, Knol D.L, Moll A.C, Castelijns J.A. Trilateral retinoblastoma: neuroimaging characteristics and value of routine brain screening on admission.

Journal of Neurooncology. 2012 September; 109(3); 535-44.

Rodjan F, de Graaf P, van der Valk P, Moll A.C, Kuijer J.P, Knol D.L, Castelijns J.A, Pouwels P.J. Retinoblastoma: value of dynamic contrast-enhanced MR imaging and correlation with tumor angiogenesis. American Journal of Neuroradiology. 2012 December; 33(11); 2129-35.

de Graaf P, Pouwels P.J, **Rodjan F**, Moll A.C, Imhof S.M, Knol D.L, Sanchez E, van der Valk P, Castelijns J.A. Single-shot turbo spin-echo diffusion-weighted imaging and correlation with tumor angiogenesis. American Journal of Neuroradiology. 2012 January; 33(1); 110-8.

de Graaf P, Göricke S, **Rodjan F**, Galluzzi P, Maeder P, Castelijns J.A, Brisse H.J; European Retinoblastoma Imaging Collaboration (ERIC). Guidelines for imaging retinoblastoma: imaging principles and MRI standardization. Pediatric Radiology. 2012 January; 42(1): 2-14.

Rodjan F, de Bree R, Weijs J, Knol D.L, Leemans C.R, Castelijns J.A. Refinement of selection criteria to perform ultrasound guided aspiration cytology during follow-up in patients with early staged oral cavity carcinoma and initially cN0 necks. Oral Oncology. 2011 May; 47(5): 391-4.

Brisse HJ; European Retinoblastoma Imaging Collaboration. Retinoblastoma imaging. Ophthalmology. 2010 May; 117(5): 1051-1051.

Rodjan F, de Graaf P, Moll AC, Imhof SM, Verbeke JI, Sanchez E, Castelijns JA. Brain abnormalities on MR imaging in patients with retinoblastoma. *American Journal of Neuroradiology*. 2010 September; 31(8): 1385-9.

CURRICULUM VITAE

Firazia Rodjan was born on the 2nd of April 1983 in Zwolle, the Netherlands. From 1995 to 2001, she attended secondary school at the Thorbecke Scholengemeenschap in Zwolle.

After graduation, she studied Medicine at the VU University of Amsterdam from 2001 to 2008. During medical studies her special focus was on Oncology within the Head and Neck area at the department of Radiology (Prof. dr. J. A. Castelijns). After obtaining her medical degree in 2008 she started the research project that resulted in this thesis at the VU University medical center under the supervision of Prof. dr. J. A. Castelijns and Prof. dr. A. C. Moll. In april 2012 she worked for one year as resident Internal Medicine at the Slotervaart Hospital in Amsterdam. The following year in april 2013 she started her specialty training in Internal Medicine at the Slotervaart Hospital (Prof. dr. D. P. M. Brandjes and dr. J. W. Mulder) and Academical Medical Center in Amsterdam (dr. S. E. Geerlings).

